AN ABSTRACT OF THE DISSERTATION OF

José Antonio Martínez Alcalá for the degree of Doctor of Philosophy in Oceanography presented on March 22, 2002. Title: Modeling Studies of Mesoscale Circulation in the Gulf of California.

Abstract approved:

Redacted for privacy

John S. Allen

The mesoscale circulation in the Gulf of California is investigated using a numerical model (Princeton Ocean Model). Forced by satellite-derived winds, the circulation in the gulf shows a complex pattern dominated in the southern gulf by multiple eddies. Near the coast and in most of the north gulf, the circulation is wind-driven. Away from the coast, velocity fluctuations are poorly correlated with the wind. Positive relative vorticity at the surface seems to be produced along the west side and to extend into the interior in the vicinity of cyclonic eddies. Negative vorticity values are significant near anticyclonic eddies and seem to be connected to the east coast. Regions of relatively high values of turbulent kinetic energy $\frac{1}{2}q^2$ ($\approx 10^{-4} cm^2 s^{-2}$) are found in the interior away from the boundary layers at depths 350-500 m and are associated with low values of the Richardson number, negative relative vorticity and concentrations of near-inertial wave energy. In a separate set of experiments the

evolution of remotely forced coastal-trapped waves in the gulf is studied. In general, model-data sea level and velocity fluctuations are reasonably well correlated. Coastal-trapped waves propagate northward along the east side of the gulf with no significant changes south of the sill. Most of the wave energy is steered at the sill to the west side of the gulf where it propagates southward with decreased sea level amplitude. Just a small fraction of the wave energy enters the northern gulf and is dissipated. Some of the incident wave energy is lost into down-slope propagating disturbances generated as the CTWs pass resulting in relatively intense bottom currents. Wave disturbances exhibit nonlinear characteristics while propagating. Most of the dissipation of wave energy in the gulf takes place through bottom friction in the vicinity of the sill. On the east side, large amplitude elevation waves produce a down-gulf current adjacent to the coast such that the up-gulf currents associated with the wave separate from the coast. Eddies with a spatial scale of 50-80 km are generated by long time scale or large amplitude waves.

Modeling Studies of Mesoscale Circulation in the Gulf of California

By

José Antonio Martínez Alcalá

A DISSERTATION

Submitted to

Oregon State University

in partial fulfillment of
the requirements for the
degree of

Doctor of Philosophy

Presented March 22, 2002
Commencement June 2002

Doctor of Philosophy dissertation of José Antonio Martínez Alcalá presented on March 22, 2002

APPROVED:

Redacted for privacy

Major Professor, representing Oceanography

Redacted for privacy

Dean of the College of Oceanic and Atmospheric Sciences

Redacted for privacy

Dean of Graduate School

I understand that my dissertation will become part of the permanent collection of Oregon State University libraries. My signature below authorizes release of my dissertation to any reader upon request.

Redacted for privacy

José Antonio Martínez Alcalá, Author

ACKNOWLEDGMENTS

Special thanks to Dr. John Allen for his guidance and patience in accomplishing this work. I am glad for the opportunity of sharing his enthusiasm in discovering new ideas.

I thank my committee members Roland deSzoeke, Murray Levine, Ricardo Matano, Robert Smith, and William Warnes for their friendly advice. I would like to thank Priscilla Newberger for always willing to help.

This study required intense use of computer resources provided by COAS and the use of the CM500e's facilitated by ONR grant N00014-99-1-0040 and by NSF grant OCE-952095b to Andrew Bennett. The use of this supercomputer was indispensable for the completion of this work and I am gratefully acknowledged. I thank Curt Vandetta and Tom Leach for assistance with supercomputer and computer use and for keeping the systems alive.

The life in Corvallis was easier thanks to all the wonderful people I was lucky to meet here. I hope to see you all again. Friends in Ensenada always provided all kind of help, in particular I would like to thank Ruben Castro for all the support during this time.

Thanks to Gabriela for being always there for me and for all the moments we share together. Con todo mi amor.

CONTRIBUTION OF AUTHORS

Dr. John S. Allen was involved in the design and writing of all chapters .

TABLE OF CONTENTS

TABLE OF CONTENTS (Continued)

LIST OF FIGURES

LIST OF FIGURES (Continued)

LIST OF FIGURES (Continued)

LIST OF FIGURES (Continued)

LIST OF FIGURES (Continued)

LIST OF FIGURES (Continued)

LIST OF TABLES

I would like to dedicate this thesis to the memory of my good friend Pedro Ripa (1946-2001).

This research was supported by the Office of Naval Research (ONR) Coastal Dynamics Program through Grant N00014-93-1-1301, partially supported by the scholarship Fulbright-LASPAU and the Facultad de Ciencias Marinas UABC.

Modeling Studies of Mesoscale Circulation in the Gulf of California

Chapter 1

1. Introduction

The Gulf of California is a semi-closed basin (1100x150 km) with very irregular topography and coastline. It is shallow at the north with depth increasing southward through a series of basins and is open to the Pacific Ocean at the south (Fig. 2.1). The gulf dimensions and shape allow the existence of diverse oceanic features with varied time scales that differentiate the gulf from surrounding waters such as those on the Pacific side of the Baja California Peninsula and the tropical waters south of the entrance.

Geographically, physical oceanographic processes in the north and central gulf have received attention from both numerical studies (Beier and Ripa 1999) and field observations (Bray 1988 a,b; Merrifield and Winant 1989; Lavin et al 1997, Palacios-Hernandez et al 2002). Most of the effort has concentrated on the study of frequencies with a clear signature in sparse data sets, specifically variations on the seasonal (Castro et al 1994, Ripa 1997) and tidal (Hendershot and Speranza 1971, Grijalva 1972, Argote et al 1995) time scales.

All modeling wind-driven studies have been focused on the seasonal circulation and have assumed a spatially homogeneous wind. Carbajal (1993) assumed a wind constant in time. The wind in Ripa (1990, 1997) and Beier (1997) varied at the annual frequency. The specified wind forcing in those cases was northward up-gulf in summer and southward down-gulf during winter, with no contribution of the across-gulf component. Ripa (1997) and Beier (1997) used a linear two layer model and examined the relative roles of wind stress, surface heat flux and oceanographic input from the Pacific Ocean as forcing functions. They concluded that the dominant forcing on the annual time scale is associated with an annual baroclinic Kelvin wave that enters from the Pacific Ocean. The incident Kelvin wave accounted for approximately 65% of the sea level variability in the gulf. The contribution of the wind (spatially homogeneous) was much smaller (26%), while the surface heat flux had a yet weaker effect (9%).

Mesoscale circulation has received minor attention from observational and theoretical studies, and to our knowledge, no consideration from numerical modelers. The mesoscale response of the gulf to forcing is far from clear. Merrifield and Winant (1989) in an analysis of field observations from the central gulf, found low correlations of local wind with currents and temperature fluctuations on short several-day, time scales. They speculate about the relevance of remote forcing in the form of coastal trapped waves that propagate northward into the gulf along the mainland coast of Mexico and that could dominate or mask the wind forcing, developing a complex mesoscale circulation. Evidence for

energetic coastal-trapped waves entering the Gulf of California (Christensen et al 1983; Enfield and Allen 1983), and modified in the gulf (Spillane et al 1987) has been found from analysis of coastal sea level measurements. Somehow, these waves lose energy in the gulf, since they are not observed along the Pacific side of the Baja Peninsula. The role of CTW in forcing the mesoscale circulation in the gulf remains unknown. The nature of the wind-driven mesoscale circulation, however, is probably one of the most poorly known aspects of the physical oceanography of the gulf. This is in part due to the lack of buoy wind measurements representative of the marine environment, but also due to the limited number of wind measurements from coastal land stations.

Isolated eddies have been observed north of Angel de la Guarda island (AGI hereafter) at 29.4N, 246.7W in Fig. 2.1 (Lavin et al 1997, Palacios et al 2001), and in the south gulf offshore of La Paz at 24.2 N, 249.4W (Emilson and Alatorre 1997). With the advent of satellites, new mesoscale features have been revealed giving some insight into the complexity of the circulation. Based in infrared images, Badan et al, (1985) described thermal plumes moving across the gulf and vortex pairs of eddies in the central and north gulf. Pegau et al, (2002) using SeaWiFS ocean color satellite images, observed the generation of anticyclonic eddies along the east side of the gulf with spatial scales of ≈70 km and with high concentrations of chlorophyll.

Since the introduction of satellite scatterometers, valuable new wind measurements have become available for modelers. Model studies can now use

realistic spatially extensive wind measurements and model results can be compared with satellite observations such as SST, sea level, chlorophyll, etc. Our objective in chapter 1 of this study is to utilize numerical model experiments to investigate the atmospherically-forced mesoscale circulation in the Gulf of California using wind stress obtained from satellite scatterometer measurements (Milliff et al 1999) and a seasonal surface heat flux from Castro et al (1994).

Free coastal trapped waves (CTWs) generated by hurricanes along the Pacific coast of Mexico have been observed propagating northward and entering the Gulf of California (GOC) (Christensen et al, 1983; Enfield and Allen, 1983; Merrifield, 1992). These waves typically have periods of 4 to 20 days and sea level amplitudes at the coast of 20 to 30 cm. Inside the gulf the waves are modified, as they are not observed on the Pacific side of the Baja California peninsula (Spillane et al, 1987). Most of the properties of the CTWs entering the gulf have been derived using sea level observations from tide gauges along the coast (Christensen et al, 1983; Enfield and Allen, 1983).

Observation of sea level, bottom pressure, currents and temperature were collected in the central Gulf of California by the Scripps Institution of Oceanography and the Centro de Investigación Cientifíca y de Educación Superior de Ensenada (CICESE) during 1983-1984. From this data set, Merrifield and Winant (1989) found very low correlations between local winds and currents, sea level and temperature, suggesting the importance of remote forcing. Incident CTWs are clearly observed along the east side of the gulf, but are not as readily identified

on the west side. Dissipation in the shallow north has been the most common explanation for the disappearance of poleward propagating CTWs (Merrifield, 1992; Ramp et al. 1997). Breaking and generation of eddies have also been proposed as possible mechanisms able to dissipate incident CTWs (Christensen et al. 1983). In chapter 2 of this work, we use numerical model experiments to study the propagation of remotely forced CTWs inside the Gulf of California for 80 days during summer 1984 (July 5 to September 23). The model is forced by an incident mode 1 CTW with a time-dependent amplitude derived from sea level observations south of the gulf. The propagation of the incident CTW and the resulting behavior of mesoscale disturbances in the gulf are examined. The possible contribution of remote forcing to the overall mesoscale circulation in the gulf is also evaluated.

In chapter 2 (Martinez and Allen, 2002a) the evolution of remotely forced CTWs in the Gulf of California was studied using a hydrostatic primitive equation model (POM). The model was forced by an incident mode 1 coastal-trapped wave (CTW) with time dependent amplitude derived from sea level observations south of the gulf during the 80 day period July-5 to September 23 1984. It was found that the propagation and scattering of CTWs in the gulf are strongly affected by topography and coastline variations. In the southern gulf, incident CTWs (hereafter designated ICTWs) propagate with no appreciable change in properties, although some of the incident wave energy is lost. The possible mechanisms that can drain energy from the wave include bottom friction, breaking, scattering into higher modes, interactions with the local circulation, and generation of other features such

as eddies or residual currents. At present there are no detailed studies about the possible role of these mechanisms in association with CTW propagation in the gulf. In chapter 3 of this study we complement the experiment in chapter 2 by analysis of a set of experiments in which we vary the amplitude and the time scale of idealized incident wave pulses with single-signed displacements in coastal sea level. We study the behavior of the wave propagation in the gulf as a function of incident wave amplitude and time scale and attempt to identify the mechanisms by which energy is lost. An outline of the paper is as follows: the model formulation and the numerical experiments are described in section 2. Basic characteristics of the propagation and nonlinear effects are discussed in section 3 and 4, respectively. A summary is given in section 5.

Chapter 2

A Modeling Study of the Atmospherically-Forced Mesoscale Circulation in the Gulf of California

Antonio Martinez and John S. Allen

Submitted to *Journal of Physical Oceanography*

2.1 Abstract

The atmospherically-forced mesoscale circulation in the Gulf of California is investigated using a numerical model forced by satellite-derived winds. The circulation shows a complex pattern dominated by the presence of multiple eddies, both cyclonic and anticyclonic, in the southern gulf. The eddies have horizontal scales the order of the gulf width (≈100 km) and vertical scales of 1000 m. Near the coast along both sides and in most of the north gulf, the circulation is wind-driven and has high variability. Away from the coast in the interior, the velocity fluctuations are characterized by lower variability and are poorly correlated with the wind. The temporal mean surface circulation consists of southward down-gulf currents along the coast on both sides, with larger magnitude currents on the west side. In the temporal mean circulation, the cyclonic eddies generally include a northward up-gulf current that is 800 m deep along the east side and a southward down-gulf current with similar depth along the west side. In the vicinity of anticyclonic eddies, the circulation is more complex with southward down-gulf currents on both sides and a northward up-gulf current near the center of the gulf that has baroclinic vertical structure with southward flow at depth. The temporal mean across-gulf averaged along-gulf circulation can be described as a three layer system. The upper layer has a depth of about 60 m and flows southward down-gulf. An intermediate layer with a vertical extent that increases from 100 m in the north to 300 m in the south, flows northward up-gulf. Below the intermediate layer, the

lower layer extends to 1000 m depth with weak southward down-gulf flow. Positive relative vorticity at the surface seems to be produced along the west side and to extend into the interior in the vicinity of cyclonic eddies. Negative vorticity values are significant near anticyclonic eddies and seem to be connected to the east coast. An inverse relation is found in the along-gulf variations of the time mean, across-gulf averaged potential and kinetic energies in the neighborhood of the eddies. Regions of relatively high values of turbulent kinetic energy $\frac{1}{2}q^2$ ($\approx 10^{-4}$ cm^2s^{-2}) are found in the interior away from the boundary layers and from the coast near the center of the gulf at depths 350-500 m and are associated with low values of the Richardson number *Ri*. High values of q^2 typically occur where the vorticity is negative, and appear to be related to the concentration of near-inertial wave energy. The circulation in the gulf is sensitive to the specification of the Coriolis parameter f which in the main experiments here is assumed to vary as in a β-plane approximation. With a constant f, the circulation is more energetic than with a variable f. In contrast to the variable f case, there are no well-developed anticyclonic eddies in the central gulf and the scale of the cyclonic eddies is larger with constant f. These results demonstrate that even though the gulf is relatively narrow ($\approx$100 km) in the east-west direction, the variation of f has an important effect on the wind-driven circulation.

2.2. Introduction

The Gulf of California is a semi-closed basin (1100x150 km) with very irregular topography and coastline. It is shallow at the north with depth increasing southward through a series of basins and is open to the Pacific Ocean at the south (Fig. 2.1). The gulf dimensions and shape allow the existence of diverse oceanic features with varied time scales that differentiate the gulf from surrounding waters such as those on the Pacific side of the Baja California peninsula and the tropical waters south of the entrance.

Physical oceanographic processes in the north and central gulf have received attention from both numerical studies (Beier and Ripa 1999) and field observations (Bray 1988 a,b; Merrifield and Winant 1989; Lavin et al 1997, Palacios-Hernandez et al 2002). Most of the effort has concentrated on the study of frequencies with a clear signature in sparse data sets, specifically variations on the seasonal (Castro et al 1994, Ripa 1997) and tidal (Hendershott and Speranza 1971, Grijalva 1972, Argote et al 1995) time scales.

All modeling wind-driven studies have been focused on the seasonal circulation and have assumed a spatially homogeneous wind. Carbajal (1993) assumed a wind constant in time. The wind in Ripa (1990, 1997) and Beier (1997) varied at the annual frequency. The specified wind forcing in those cases was northward up-gulf in summer and southward down-gulf during winter, with no contribution of the across-gulf component. Ripa (1997) and Beier (1997) used a

linear two layer model and examined the relative roles of wind stress, surface heat flux and oceanographic input from the Pacific Ocean as forcing functions. They concluded that the dominant forcing on the annual time scale is associated with an annual baroclinic Kelvin wave that enters from the Pacific Ocean. The incident Kelvin wave accounted for approximately 65% of the sea level variability in the gulf. The contribution of the wind (spatially homogeneous) was much smaller (26%), while the surface heat flux had a yet weaker effect (9%).

Mesoscale circulation has received minor attention from observational and theoretical studies, and to our knowledge, no consideration from numerical modelers. The mesoscale response of the gulf to forcing is far from clear. Merrifield and Winant (1989) in an analysis of field observations from the central gulf, found low correlations of local wind with currents and temperature fluctuations on short several-day, time scales. They speculate about the relevance of remote forcing in the form of coastal trapped waves that propagate northward into the gulf along the mainland coast of Mexico and that could dominate or mask the wind forcing, developing a complex mesoscale circulation. Evidence for energetic coastal-trapped waves entering the Gulf of California (Christensen et al 1983; Enfield and Allen 1983), and modified in the gulf (Spillane et al 1987) has been found from analysis of coastal sea level measurements. Somehow, these waves lose energy in the gulf, since they are not observed along the Pacific side of the Baja Peninsula. The role of CTW in forcing the mesoscale circulation in the gulf remains unknown. The nature of the wind-driven mesoscale circulation,

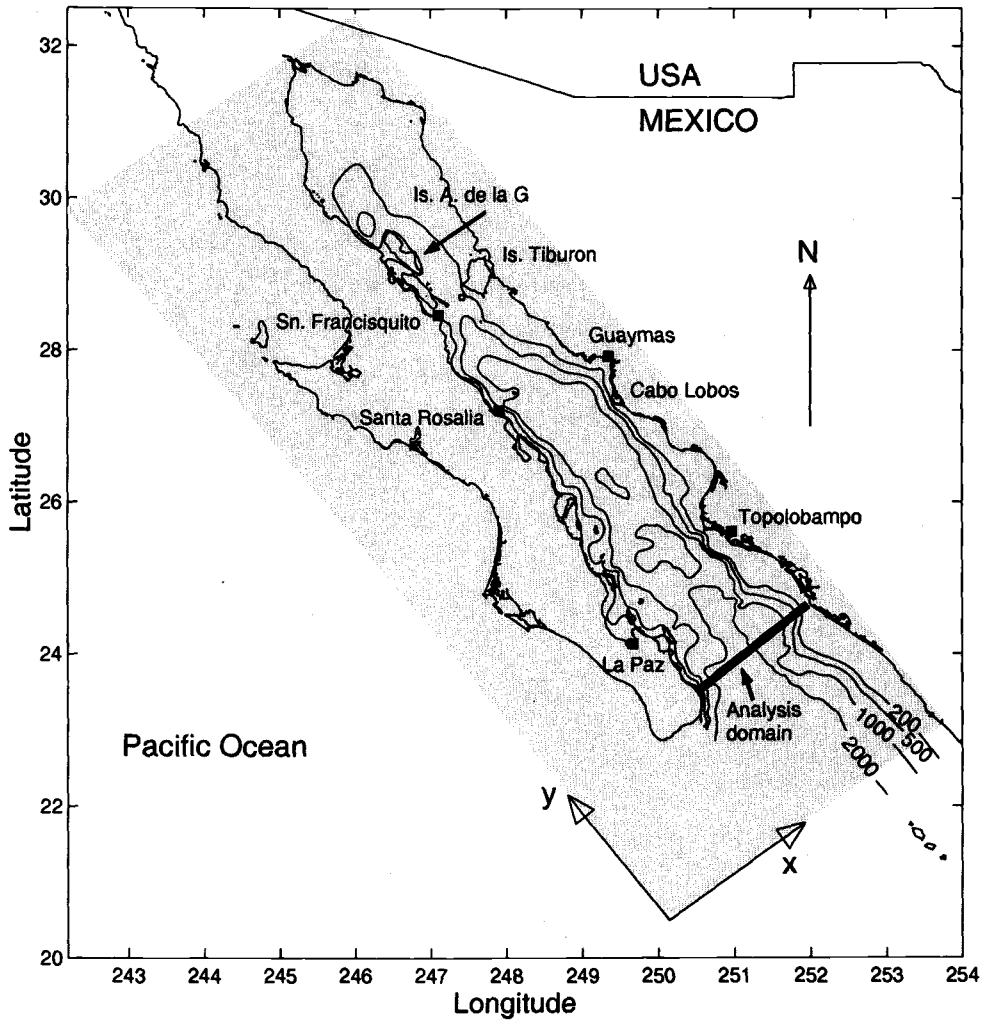

Figure 2.1: The Gulf of California and geometry of the numerical domain shaded in gray. Results presented are obtained primarily from analysis inside the gulf. The thick line across the gulf in the south at y= 300 km shows the southern extent of the analysis domain.

however, is probably one of the most poorly known aspects of the physical oceanography of the gulf. This is in part due to the lack of buoy wind measurements representative of the marine environment, but also due to the limited number of wind measurements from coastal land stations.

Isolated eddies have been observed north of Angel de la Guarda island (AGI hereafter) at 29.4N, 246.7W in Fig. 2.1 (Lavin et al 1997, Palacios et al 2001), and in the south gulf offshore of La Paz at 24.2 N, 249.4W (Emilsson and Alatorre 1997). With the advent of satellites, new mesoscale features have been revealed giving some insight into the complexity of the circulation. Based on infrared images, Badan et al, (1985) described thermal plumes moving across the gulf and vortex pairs of eddies in the central and north gulf. Pegau et al, (2002) using SeaWiFS ocean color satellite images, observed the generation of anticyclonic eddies along the east side of the gulf with spatial scales of ≈70 km and with high concentrations of chlorophyll.

Since the introduction of satellite scatterometers, valuable new wind measurements have become available for modelers. Model studies can now use realistic spatially extensive wind measurements and model results can be compared with satellite observations such as SST, sea level, chlorophyll, etc. Our objective in this study is to utilize numerical model experiments to investigate the atmospherically-forced mesoscale circulation in the Gulf of California using wind stress obtained from satellite scatterometer measurements (Milliff et al 1999) and a seasonal surface heat flux from Castro et al (1994).

2.3. Model

We use the Princeton Ocean Model (Blumberg and Mellor, 1987; Mellor, 1991). Potential density is utilized as a single variable in place of temperature and salinity as in Allen et al (1995). A horizontal rectangular grid with Cartesian coordinates (x,y) is used with 3 km horizontal resolution and 50 sigma levels in the vertical (Fig. 2.2). The y coordinate is aligned in the along-gulf direction and is oriented towards the northwest along the Baja California peninsula (Fig. 2.1). The x coordinate has an across-gulf orientation, directed towards the northeast. The velocity components in the (x,y) directions are (u,v). The numerical domain (Fig. 2.1) has open boundary conditions at the south, west, and at the north. At the north and south, we use standard Orlanski radiation conditions for both depth-averaged and internal velocity and sea level, and an advection condition for density (Petruncio, 1996). On the western boundary an auxiliary wall with no normal mass flux and with density fixed to the initial value is used. Several tests were performed to assure that the circulation inside the gulf was not affected by the position of the open boundaries at the south and west. The external and internal mode time steps are 3 s and 120 s, respectively. We use a constant horizontal viscosity coefficient of 15 m^2s^{-1}, which we consider an intermediate value (Oey 1996) able to preserve mesoscale features. In every experiment we start from rest, with horizontally homogeneous depth-dependent stratification (Fig. 2.2). The initial density field is determined from hydrographic measurements in the gulf (Bray, 1988a).

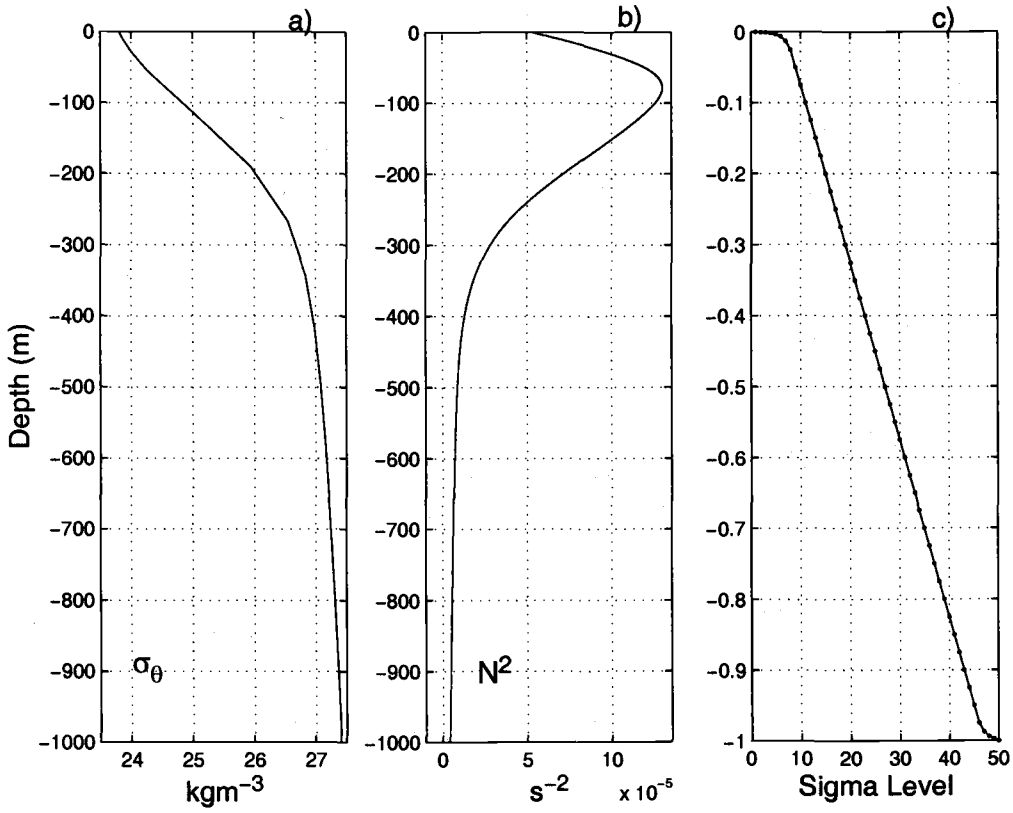

Figure 2.2: (a) Initial density profile, (b) initial N^2 profile and (c) vertical coordinate sigma level distribution

Experiments are run for a total of 8 months. The first 4 months (Aug-Nov), are considered as spin-up time. The results are based on analysis of the last 4 months (Dec-Mar) characterized by more intense winter winds. Four different experiments were completed for this study (Table 2.1). In the basic case (EXP1), the model is

Table 2.1. Description of the experiments conducted. Experiments 1 to 3 are forced by satellite-derived winds. Experiment 4 is forced by a constant in time and space wind. Experiment 1 is also forced by surface buoyancy flux. In experiments 1, 2, and 4 the Coriolis parameter is variable (β-plane). In experiment 3 the Coriolis parameter is constant

Exp.	Forcing	Coriolis
1	*Wind+BF**	*Variable*
2	*Wind*	*Variable*
3	*Wind*	*Constant*
4	*Wind*[c]	*Variable*

* BF=Buoyancy Flux
[c] Uniform constant wind

driven by wind stress and surface buoyancy fluxes (W+BF) with a variable Coriolis parameter that varies as in a β-plane approximation, linearly in the north-south direction. The second (EXP2) and third (EXP3) experiments are driven by the wind

stress only, with a variable Coriolis parameter and a constant Coriolis parameter, respectively. Wind stress fields derived from satellite measurements as described below are used for forcing in experiments 1-3. In experiment 4 (EXP4) with variable Coriolis parameter the wind is assumed uniform in space, constant in time, and directed down the gulf in the direction of the y coordinate with no across-gulf component.

2.4. Atmospheric forcing

The wind stress used to drive the model is obtained from Milliff et. al. (1999). It consists of blended wind data from satellite measurements, NSCAT/ERS-2, and from an atmospheric circulation model, NCEP (0.5 degree by 0.5 degree). A complete description of this product is given in (Milliff et. al. 1999). For use in model forcing, the wind data, supplied four times daily, are filtered with a 40 hr low pass filter and interpolated to the model grid. The surface heat flux is obtained from Castro et al. (1994) were it was derived from bulk formulae. The surface flux is a function of the along-gulf coordinate and has an annual time variability.

The satellite-derived winds exhibit some new features that have not been described previously. Some of these features are relevant to the wind-driven circulation of the Gulf of California. In this section we briefly describe the

temporal and spatial variability of the wind field. Time series of spatially-averaged wind stress components inside the Gulf of California for the period August 1996 to July 1997 are shown in Fig. 2.3. The strongest wind events occur from December through March. During this period, the across-gulf component of the wind stress changes sign, but the time mean is very small (-0.04 dyne cm^{-1}). The along-gulf component is dominantly southward, down-gulf, but it can reverse sign as well. The up-gulf events, however, are short and very weak. A relevant point, visible in Fig. 2.3, is the lack of a clear annual cycle. Winds blow predominantly from the northwest, with short periods of weak reversals, which occur mainly in the south gulf. It is important to notice that the across-gulf component has a significant amplitude. The spatial distribution of the annual mean (Fig. 2.4) shows that there is a significant gradient in the magnitude of the wind stress across the gulf, with 25% stronger winds along the Baja California Peninsula side. For our numerical studies we choose to analyze the stronger wind stress period corresponding to 120 days during the winter months of Dec 1996-March 1997 (Fig. 2.3). The time mean and rms values of the wind stress in the gulf for Dec-Mar are shown in Fig. 2.5.

Empirical Orthogonal Functions (EOFs) are calculated to synthesize the satellite winter wind stress information and to determine the principal patterns of variability. The EOF modes 1 and 2 account for 75.8 % of the total variance (Fig. 2.5). The dominant mode 1 (58.6 %) consists of along-gulf wind stress (τ_y) in most of the gulf with some across-gulf component (τ_x) in the north. The second mode (17 %) represents mostly an across-gulf component. The corresponding modal

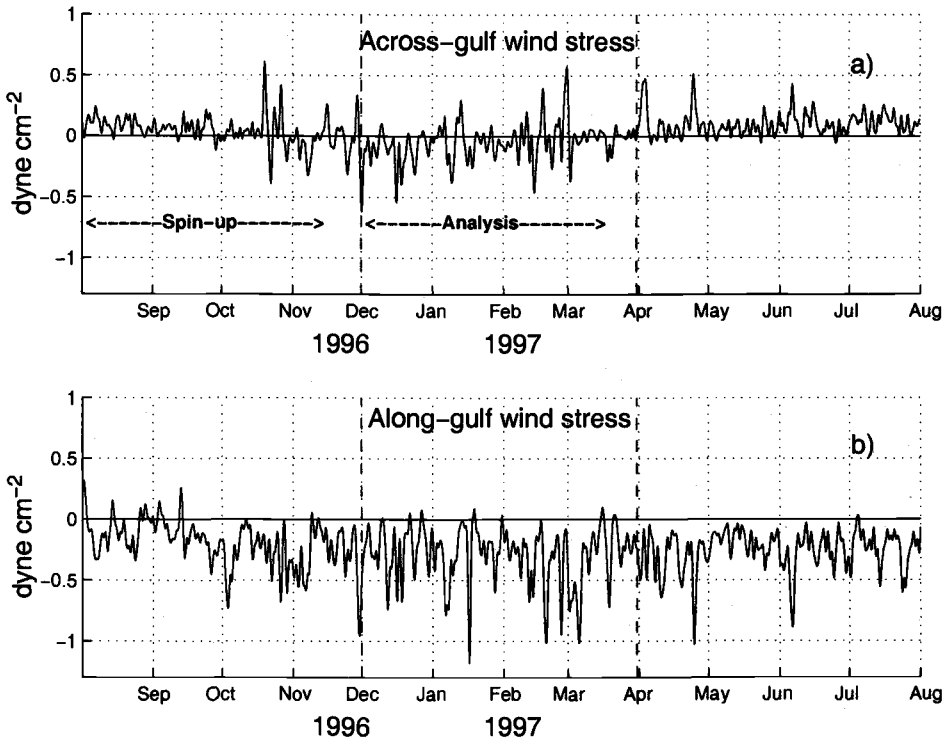

Figure 2.3: Time series of the spatially-averaged satellite-derived wind stress inside the gulf. a) across-gulf x component τ_x and b) along-gulf y component τ_y. The temporal mean and the rms values of (τ_x, τ_y) are (-.05,-0.3) and (0.08,0.2) dyne cm^{-2} respectively.

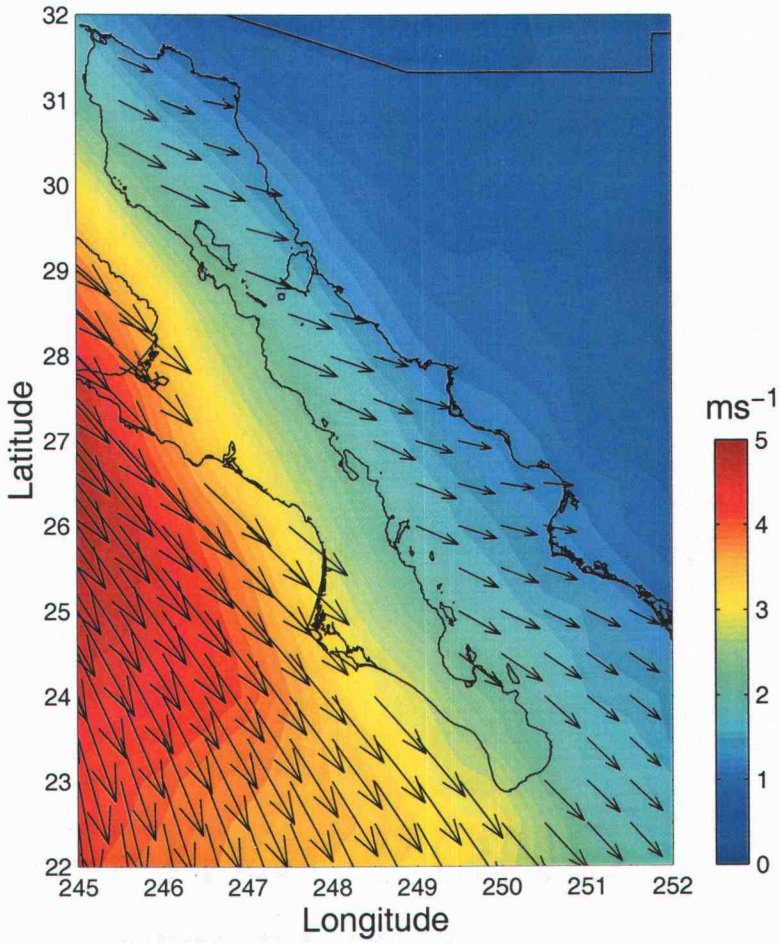

Figure 2.4: Annual mean satellite-derived wind velocity vectors. The color contours indicate the magnitude of the wind velocity vectors in m s^{-1}.

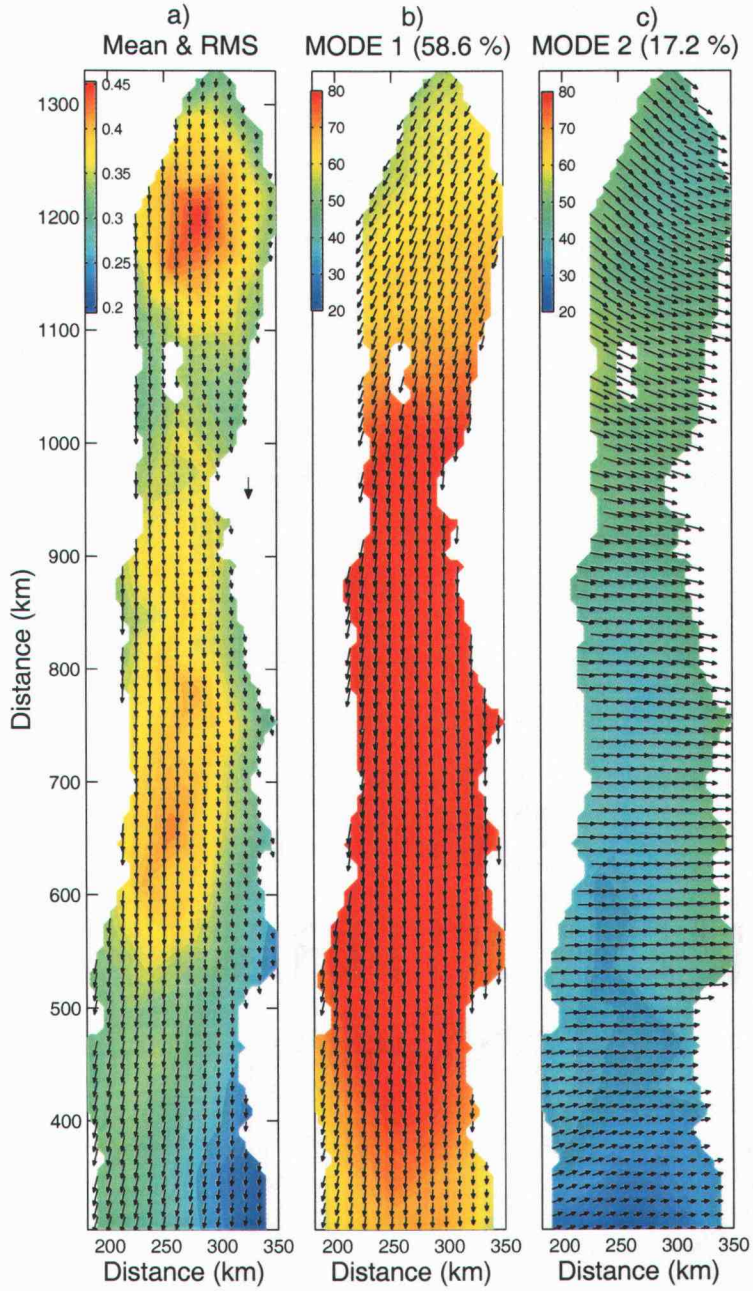

Figure 2.5: a) Temporal mean (arrows) and rms (color) wind stress fields for the period Dec-Mar. b) EOF mode 1, c) EOF mode 2. The color contours in b) and c) show the fraction of the local variance explained by that mode. The arrows to the right show the scale: 5 m s^{-1} for the mean velocity, and 1 for the normalized EOF modes.

amplitude time series (Fig. 2.6) show high variability for both modes on a several day time scale. The amplitudes frequently reverse signs in such a way that τ_y can reverse direction during short and weak events if the amplitude of the mode exceeds the mean. This is found, for example in mode 1 around days 18, 48, and 98.

2.5. Circulation.

Driven by realistic winds and influenced by very irregular topography and irregular coast lines along both sides, the mesoscale circulation in the gulf exhibits complex circulation patterns. In this section we describe the main characteristic of the circulation patterns.

Total kinetic energy density is defined as

$$\langle KED \rangle_{xyz} = \frac{1}{V} \int \frac{1}{2} \rho_o \left(u^2 + v^2 \right) dxdydz, \tag{2.5.1}$$

where V represents the volume. In a similar way the potential energy density is given by

$$\langle PED \rangle_{xyz} = \frac{1}{V} \int \frac{1}{2} \rho g z dxdydz. \tag{2.5.2}$$

Time series of those variables together with the spatially-averaged wind stress are shown in Fig. 2.7. After the spin-up period, kinetic energy density

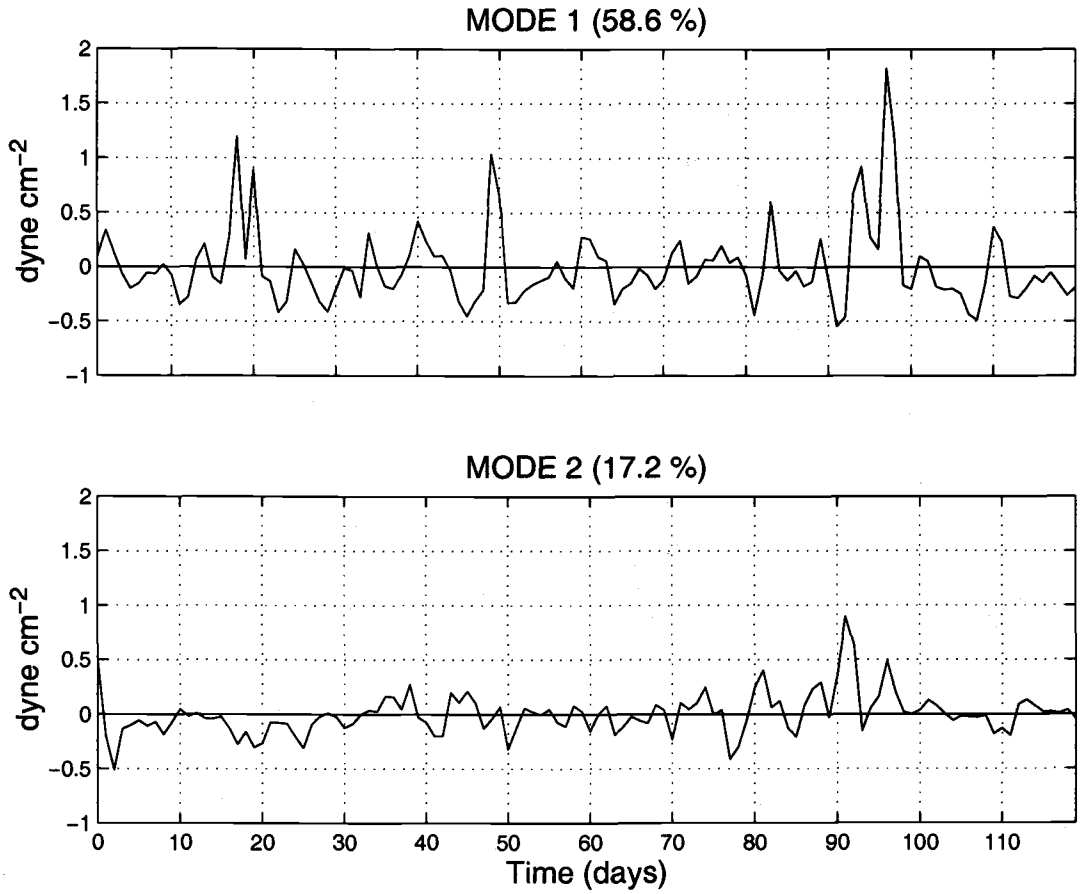

Figure 2.6. Time series of the amplitudes for the wind stress EOF modes 1 and 2. Time scale is days from 1 Dec 1996.

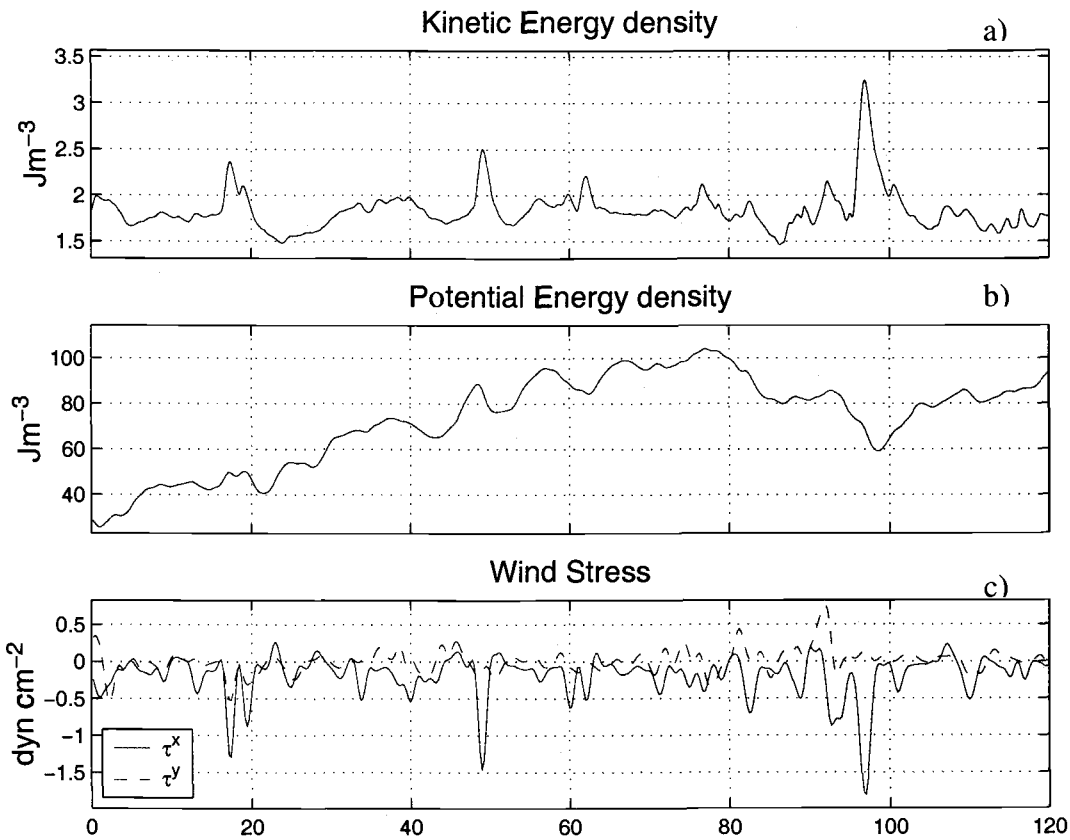

Figure 2.7. Time series of a) kinetic energy density (4.1), b) potential energy density (4.2), and spatially-averaged wind stress inside the gulf. Time scale is days from 1 Dec 1996.

remains at an approximately constant value, increasing only during stronger wind events. The potential energy density generally increases during this time period of strong wind stress. A comparison of the time-dependent behavior of the along-gulf component of the wind stress and the kinetic energy density shows a clear correspondence. Short strong wind events e.g., on days 18, 48 and 98 are followed by a similar time scale response involving a rapid increase of $\langle KED \rangle_{xyz}$. The fluctuations in $\langle PED \rangle_{xyz}$ appear to have a somewhat longer time scale than those in $\langle KED \rangle_{xyz}$ and to have much less of a direct relation to the wind stress.

2.5.1. Depth-averaged velocity

The temporal mean depth-averaged velocity vectors from EXP1 for December through March are plotted in Fig. 2.8. A striking feature is the presence of multiple eddies with horizontal scales the order of the gulf width (~100 km). These eddies are centered approximately at y=350, 450, 520, 610, 730, 800 and 1120 km. The eddies are stronger in the south and dominate the mean circulation of the gulf. Most of the gulf exhibits a cyclonic circulation. Along the west side, there is a well defined mean down-gulf current that is slower in the north. On the east side, there is a weak and narrow current with a down-gulf tendency. On both sides, the continuity of the currents along the coast is interrupted by the presence of the

eddies, mainly in the south gulf. Along the east side, the effect of the eddies is more evident causing the southward down-gulf current to reverse when interacting with the cyclonic eddies. The southward mean currents along the west side are not strongly affected by the presence of the smaller and weaker anticyclonic eddies, with exception of the eddy at the entrance of the gulf near y=350 km. Along the west side, mean currents flow continuously from the northern gulf to La Paz (y=400 km) where a strong anticyclonic eddy reverses the coastal current. The circulation in the shallow northern region is more complex. The mean currents seem to be controlled by the presence of several eddies with smaller spatial scales compared to the eddies in the south. Along the west coast, the down-gulf current is present, while the circulation along the east side is more irregular.

Also shown in Fig. 2.8 are the mean and rms fields of sea surface elevation. Mean sea level increases from north to south. It is generally lower on the east side than on the west side, with the difference decreasing to the north. The cyclonic eddies are associated with relative depressions in sea level near y=450, 600, 800 and 1100 km, consistent with geostrophic balance. The sea level expression of the weaker anticyclonic eddies is not as clear, although they are accompanied by small increases in elevation.

The spatial distribution of the rms variability in the depth-averaged velocity (Fig. 2.8) suggests two types of circulation: 1) wind-driven flow near the coast on both sides with high variability and 2) circulation in the interior off the coast with lower variability. Model velocity time series from different across-gulf locations at

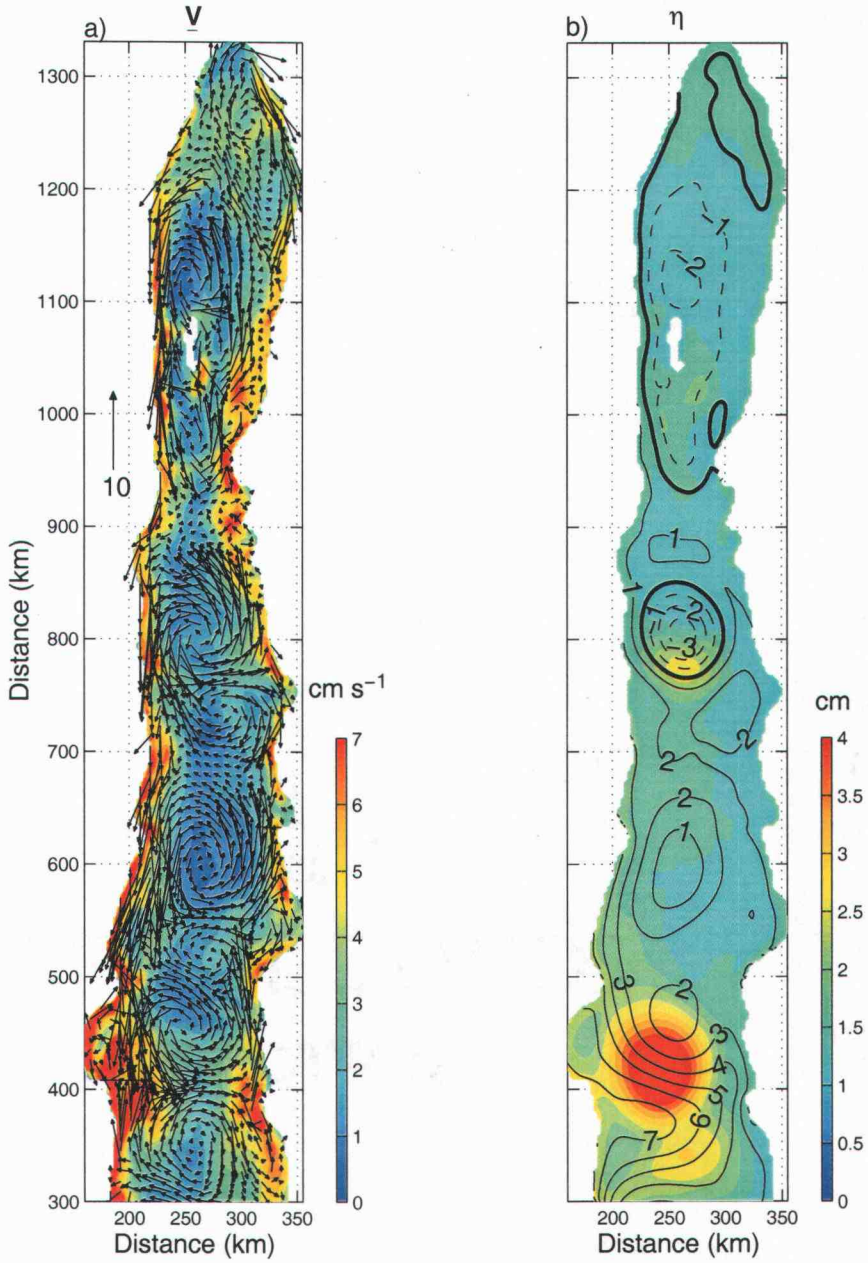

Figure 2.8. Temporal mean depth-averaged velocity (vectors) and rms (color), and temporal mean sea level (contours) and rms (color) for the period Dec-Mar from EXP1. The vector on the left shows the 10 cm s^{-1} scale. For sea level, the contour interval is 1 cm, dashed lines correspond to negative values, and the thick line is the zero contour.

y=564 km (Fig. 2.9) illustrate the spatial dependence of the variability. The velocities near either coast show high variability similar to that in the vector time series of wind stress (also shown in Figure 9). The velocity vectors from the western side of the gulf have a somewhat higher complex correlation coefficient (Kundu, 1976) (magnitude 0.54 at 1.2 days lag) with the wind stress vectors than those on the eastern side (0.45 at 1.2 days lag). In contrast, the velocity vectors from the interior (center) of the gulf exhibit fluctuations on relatively larger time scales and are poorly correlated with the wind stress. We obtain additional information about the spatial distribution of the time scales of the current variability by examining the autocorrelation function of the depth-averaged velocity vectors as a function of location in the gulf. The time lag required for the autocorrelation to decrease to an arbitrary 0.6 value is shown in Fig. 2.10. The lag is shorter (<1.5 days) along the coast and in the region to the north (y>1060 km), suggesting a wind-driven circulation with high variability. The interior is characterized by longer time scales (>6 days). Note that for $450 \leq y \leq 1100$ km the region characterized by short time scales extends farther from the coast on the eastern side while, except near y=600 km, the region of larger time scales associated with the interior flow exists closer to the western side.

Empirical orthogonal function decomposition provides an objective tool to synthesize the model information and to determine the dominant patterns of variability in the circulation. This analysis was applied to the depth-averaged velocity vectors from EXP1 for the period Dec-Mar. The first two modes together

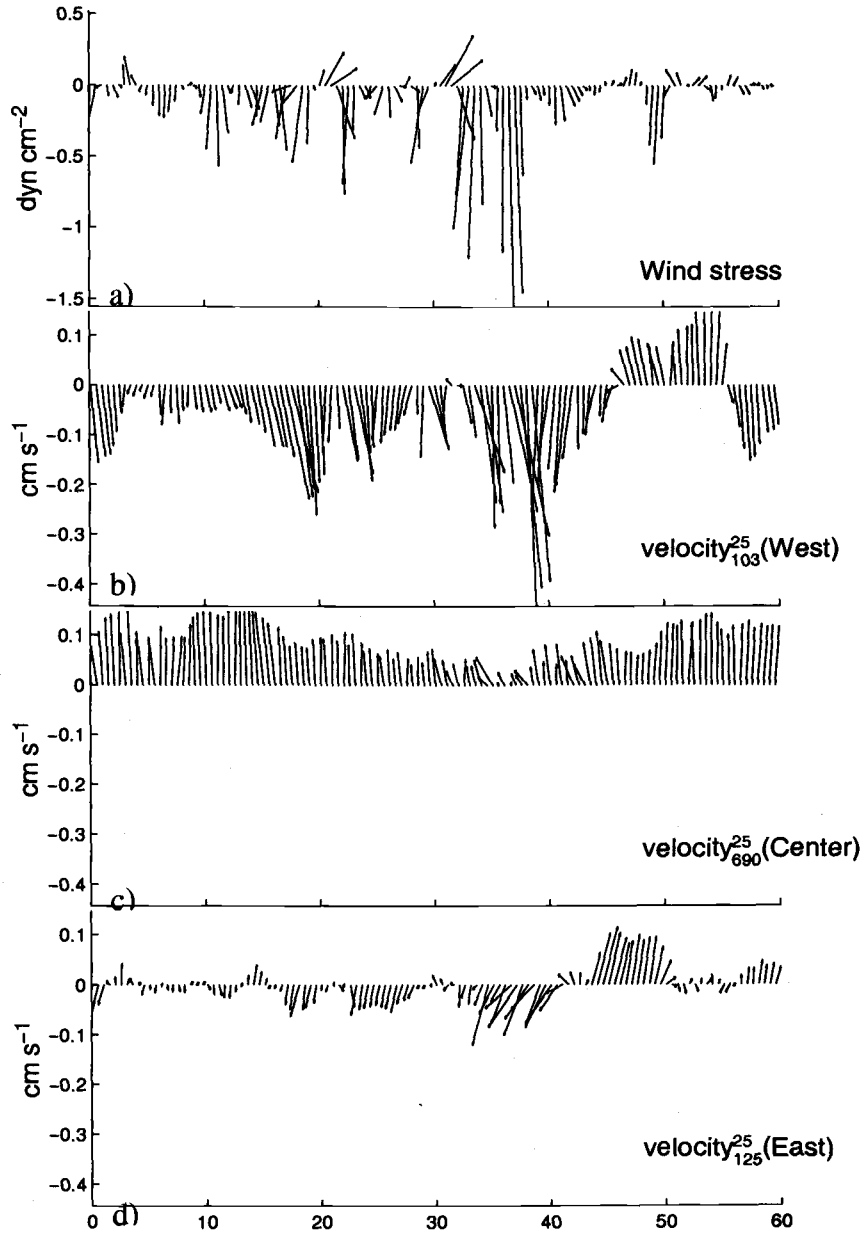

Figure 2.9. Vector time-series for Feb-Mar of wind stress and currents at y=564 km. a) The wind stress is the average across the section. The currents are sampled every 12 hrs. at a depth of 25 m, b) on the east side (water depth 103 m), c) center (water depth 690 m), and d) on the west side (water depth 125 m). Day 1 corresponds to 1 February 1997. A vector pointing vertically upward corresponds to up-gulf flow along the *y*-axis in Fig. 1.

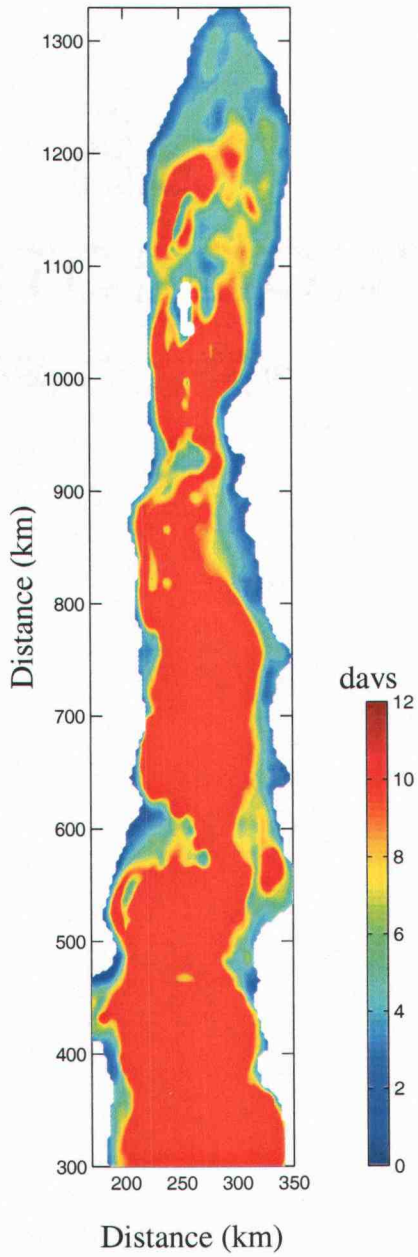

Figure 2.10. Time lag (days) at which the complex autocorrelations of the vertically-averaged velocities decreases to 0.6 for EXP 1.

represent 47% of the total variance of the currents (Fig. 2.11). The arrows correspond to the eigenvectors of the normalized mode and the color contours show the distribution of the fraction of the local variance explained. There is a dominant mode 1 with 29 % of the total variance that has a spatial circulation pattern that for days 0-50, when the amplitude function is positive (Fig. 2.12), is mostly cyclonic except at the entrance and at the northern end. The local variance explained is not spatially uniform but has larger values south of y=800 km along the west side and in the interior. The amplitude function of mode 1 (Fig. 2.12) reverses sign on day 52 (Jan 21 1997) and is poorly correlated at any lag with the amplitudes of the wind stress EOFs in Fig. 2.6. The general linear decrease of the mode 1 amplitude represents a continuous change in the circulation over these 120 days. Adding the mean values (Fig. 2.8) to mode 1 with the amplitudes at days 20 and 100 (Fig. 2.13) shows this change in circulation. On day 20, which is the beginning of the strong wind season (Fig. 2.3), the circulation is characterized by four strong cyclonic eddies, with very weak anticyclonic activity (except at the entrance to the gulf). By day 100, the scale of the cyclonic eddies is reduced and the strength of the anticyclonic eddies is increased. The presence of strong anticyclonic eddies has a clear effect on the shelf circulation on the west side, as they generally weaken the southward alongshore currents and actually result in northward coastal currents, e.g., near $y \approx 400$ km and $y \approx 700$ km. In the north, the transition produces a weaker circulation north of AGI and a separation of the up-gulf current along the east side south of AGI at $y \approx 1000$ km.

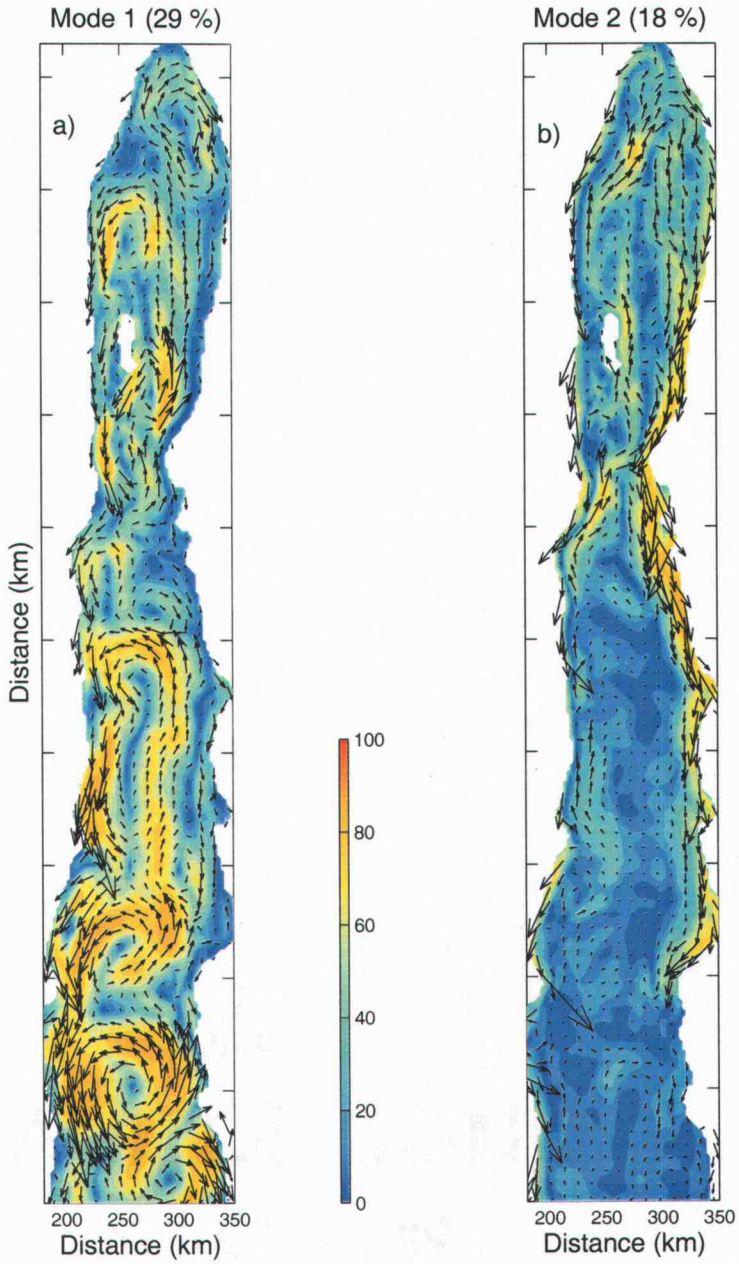

Figure 2.11. Depth-averaged velocity EOF mode 1 and mode 2. The color contours show the fraction of the local variance explained by that mode.

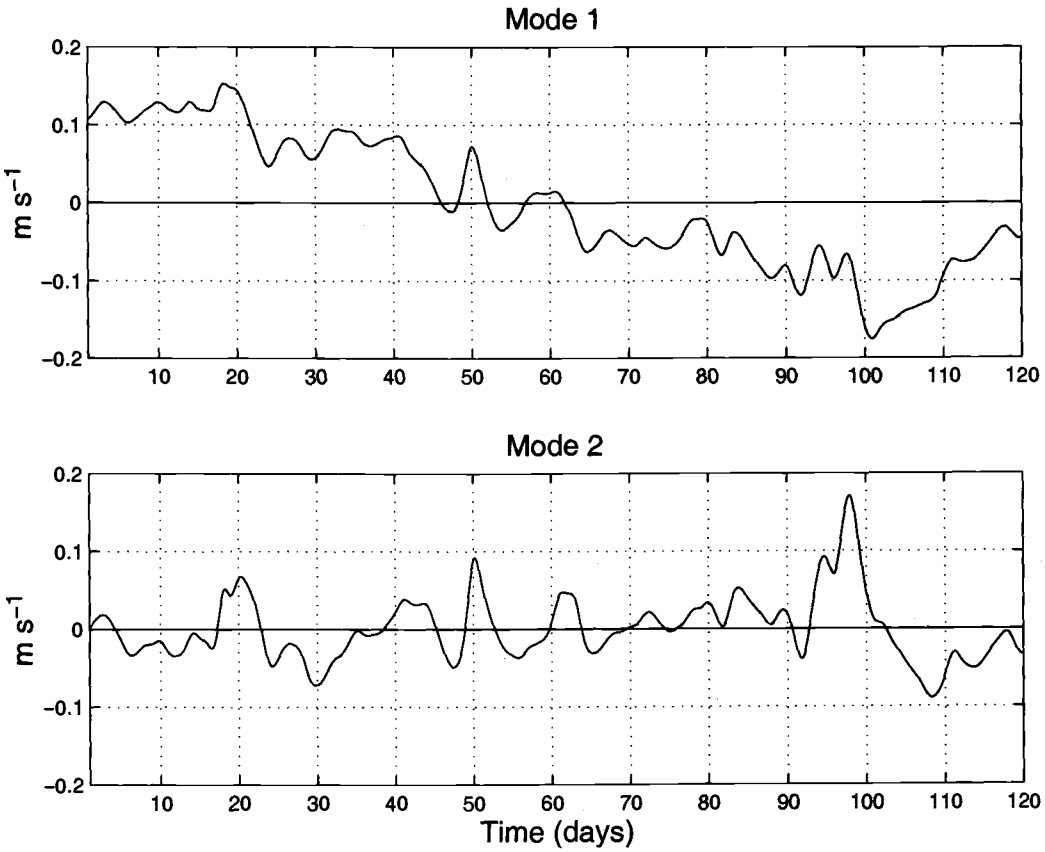

Figure 2.12. Time series of the amplitudes for the depth-averaged velocity EOF modes 1 and 2 in Fig. 11.

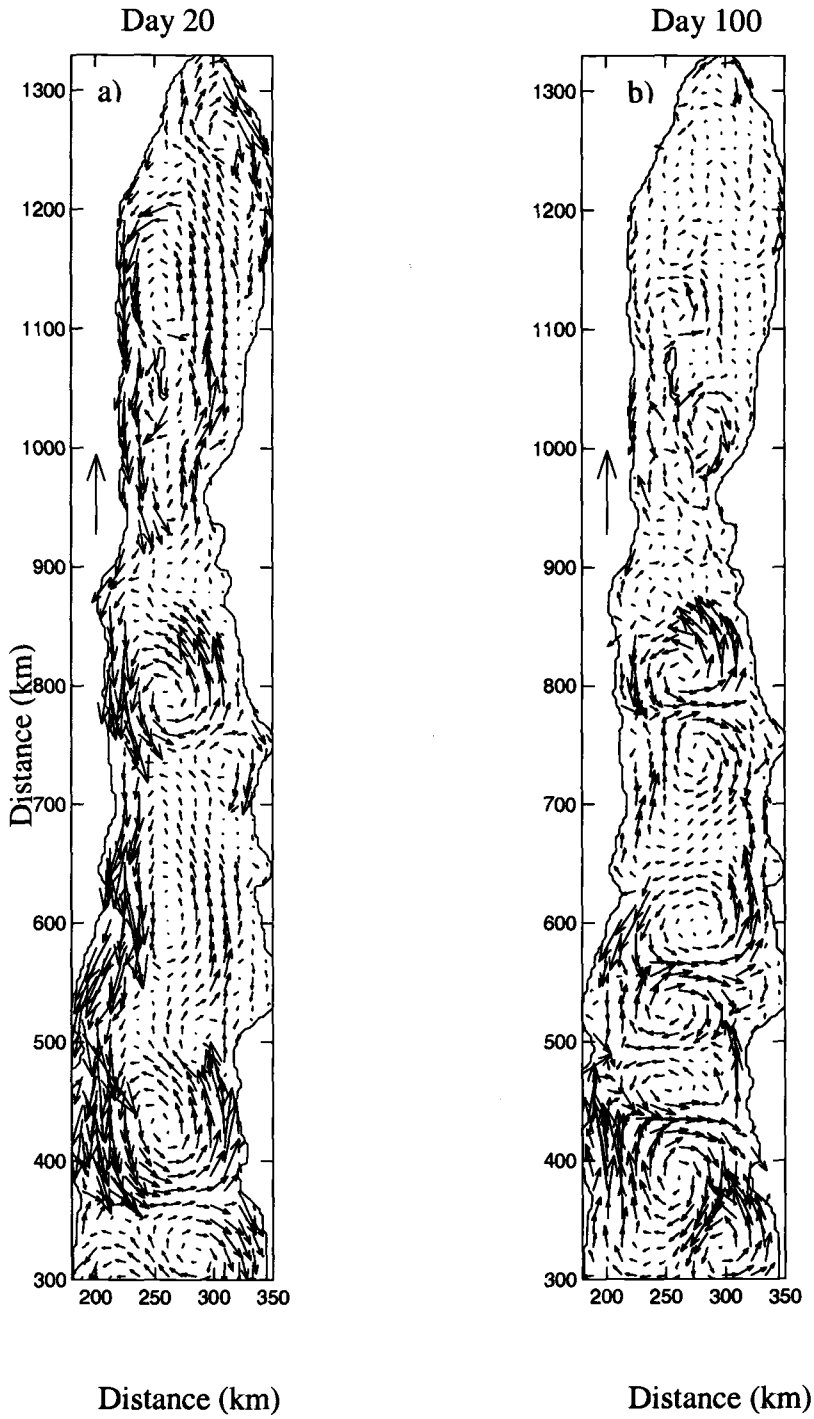

Figure 2.13. Temporal mean depth-averaged velocity vectors with mode 1 added at day 20 and at day 100. The vector on the left shows the 10 cm s^{-1} scale.

The second mode (Fig. 2.11) explains 18% of the total variance and is highly correlated (0.8 at 1 day lag) with the mode 1 wind amplitude (Fig. 2.6). The spatial pattern consists of a wind driven coastal current along the east side indicated clearly by the high fraction of local variance explained in that location. The spatial distribution of the local fraction of the variance explained for mode 2 fills much of the region where mode 1 has low local variance. The mode 2 amplitude (Fig. 2.12) is mostly positive from day 17 to day 103, corresponding to down-gulf (southward) coastal currents on the east side.

2.5.2. Surface velocity.

Surface currents include both frictionally influenced flow in the Ekman layer and the surface expression of the flow below. A comparison of the mean and rms surface (Fig. 2.14) and depth-averaged (Fig. 2.8) velocities reveals different patterns. Surface currents show a tendency to flow continuously down-gulf along both sides and to flow westward in most of the interior, except in the neighborhood of the cyclonic eddy centered at y=800 km and near the eddy-like structures at y=450 and 560 km. Surface currents along the west side are more intense than on the east side. The surface velocity rms shows higher variability in the south gulf close to y=400 km and does not show maximum variability along the coast as exhibited by the depth-averaged velocity. Instead, the rms surface velocity

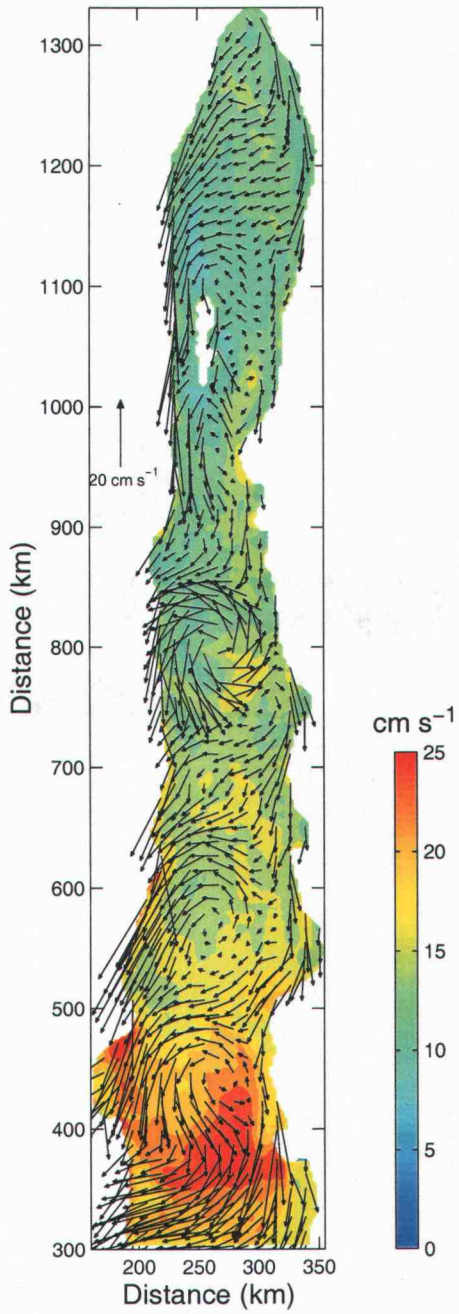

Figure 2.14. Temporal mean surface velocity (arrows) and rms (color) for EXP 1. The vector on the left shows the 20 cm s^{-1} scale.

variability seems to increase from north to south with a continuous narrow fringe of high variability along the west side.

It is interesting to notice the absence of anticyclonic eddies in the surface velocity field. Due to stronger winds directed down gulf on the west side the wind stress curl is positive and thus a positive source of relative vorticity at the surface. The wind-driven circulation response is characterized by down-gulf southward surface currents along both sides of the gulf (Fig. 2.14). In that circulation, positive vorticity (cyclonic) results along the west side and negative (anticyclonic) vorticity along the east side as shown in the mean relative vorticity calculated from the surface currents and shown in Fig. 2.15. The relative vorticity has been divided by the Coriolis parameter, so that its absolute value is a measure of the local Rossby number. Spots of positive vorticity emanate from the coast on the west side to the interior, close to the cyclonic eddies at y=450, 600 and 800 km. Negative vorticity values are significant near anticyclonic eddies and seem to be connected to the coast on the east side at y=370, 540, and 760 km. The rms field of the surface relative vorticity has a very irregular distribution, but it is in general higher south of y=800 km, where the most energetic eddies are located. In many locations, the rms values are higher than the mean. In the northern gulf, AGI is surrounded by relatively large positive mean vorticity. The largest mean vorticity values and significant variability is found in the northern gulf between AGI and the west coast, near y=1050 km. Overall, in the gulf the mean local Rossby number is appreciable (0.2) with large peak variations (0.4) along the coast on both sides and close to the

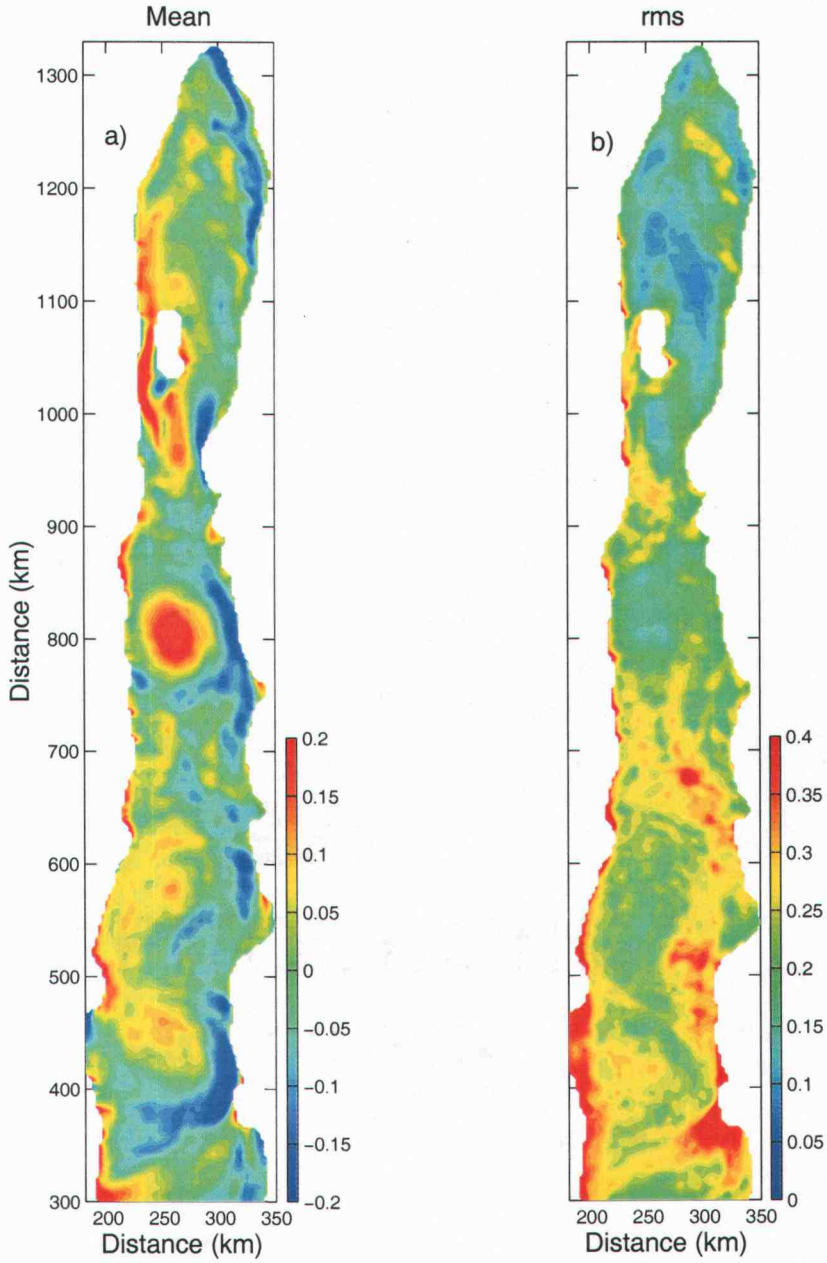

Figure 2.15. Temporal mean and rms fields of surface vorticity divided by *f*.

position of the eddies, indicating that nonlinear advective effects are important in those locations.

2.5.3. Vertical structure.

The vertical and across-gulf structure of the time mean and rms values of the along-gulf velocity in the upper 1000 m at different values of y is shown in Fig. 2.16 for EXP 1 and EXP 2. The along-gulf positions of the sections are chosen to include across-gulf sections through both cyclonic eddies (y=600, 801 km) and anticyclonic eddies (y=528, 747 km). Looking first at EXP1, we see that on both sides there is typically a down-gulf current, evident also in surface velocity field (Fig. 2.14). On the west side, the down-gulf current is relatively deep and well defined, showing that the anticyclonic eddies have little influence on the mean west side currents. On the east side, the down-gulf current in the vicinity of cyclonic eddies (y=600, 801 km) is weaker, confined near the surface, and very narrow. In the cyclonic eddies the vertical structure of velocity has a barotropic-like behavior on both sides, i.e. does not change sign in the vertical, whereas in the anticyclonic eddies the northward up-gulf velocity near the center of the gulf has a baroclinic-like structure with considerable vertical shear and southward flow at depth. Without surface buoyancy flux (SBF) in EXP2, the currents weaken. The circulation patterns, however, remain similar. The contribution of SBF is more

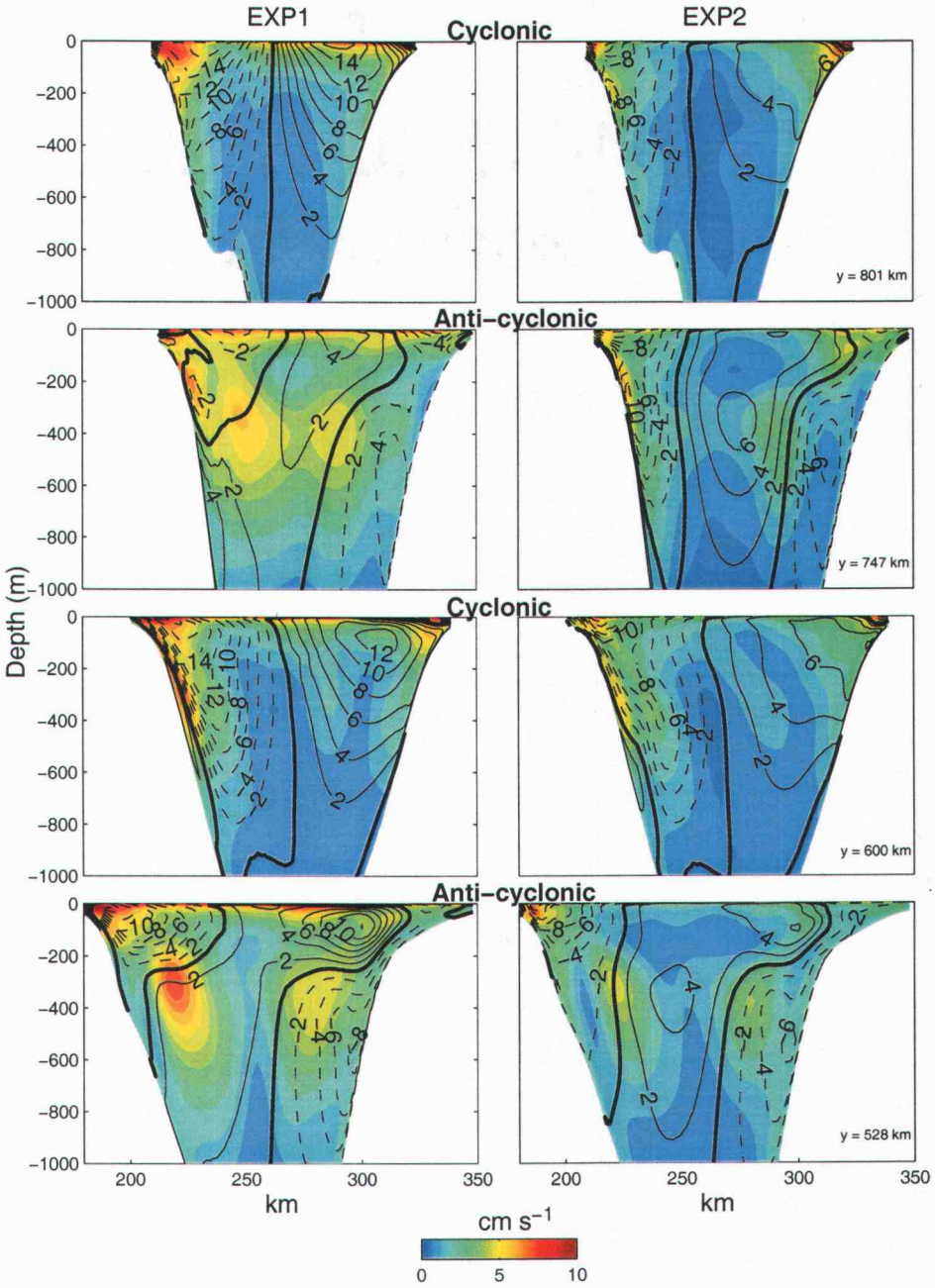

Figure 2.16. Vertical across-gulf sections of the temporal mean (contours) and rms (color) along-gulf velocity for EXP 1 (left) and EXP 2 (right). Contour interval is 2 cm s^{-1}. Dashed lines represent negative values (down-gulf), and the thick line is the zero contour. Sections at y=600 and 800 km are across the center of cyclonic eddies and sections at y=528 and 747 km are across anticyclonic eddies (see Fig. 8).

evident in the cyclonic eddies where the mean velocities in EXP2 are 50 % weaker than in EXP1. The anticyclonic eddies exhibit similar vertical structure on the east side in both experiments, with weaker surface circulation in EXP2. In both experiments, the rms variability is higher in the upper 100 m and on the west side. Deep high variance spots in the anticyclonic eddies have a maximum where the mean velocity changes signs around depths of 300-350 m. At those spots, the rms velocity is higher than the mean values with substantial fluctuations reaching depths of 800 m on both sides.

The temporal mean and rms values of the velocity components (u,v) averaged across the gulf, $(T^{-1}L(y)^{-1}\iint(u,v)dxdt)$ where T is 120 days, and $L(y)$ is the width of the gulf) are plotted as a function y and z in Fig. 2.17 to illustrate the vertical and along-gulf distribution of the velocity fields. A similar plot of the density anomaly field (difference from initial value) is also included in Fig. 2.17. The mean across-gulf component is dominated by the eddies south of the sill (y<900 km). The eddy-like structures extend to 800 m depth and in some cases deeper to 1000 m (e.g. at y=770 km). The variance has largest values near the surface and decreases with depth, having a spatial distribution similar to the temporal mean. The mean across-gulf average along-gulf circulation can be qualitatively described as a three layer system. The upper layer has a depth of about 60 m, and flows southward in the direction of the mean wind consistent with the impression from Fig. 2.14. Below the upper layer an intermediate layer, with a vertical extent of about 100 m in the north that increases to more than 300 m at the

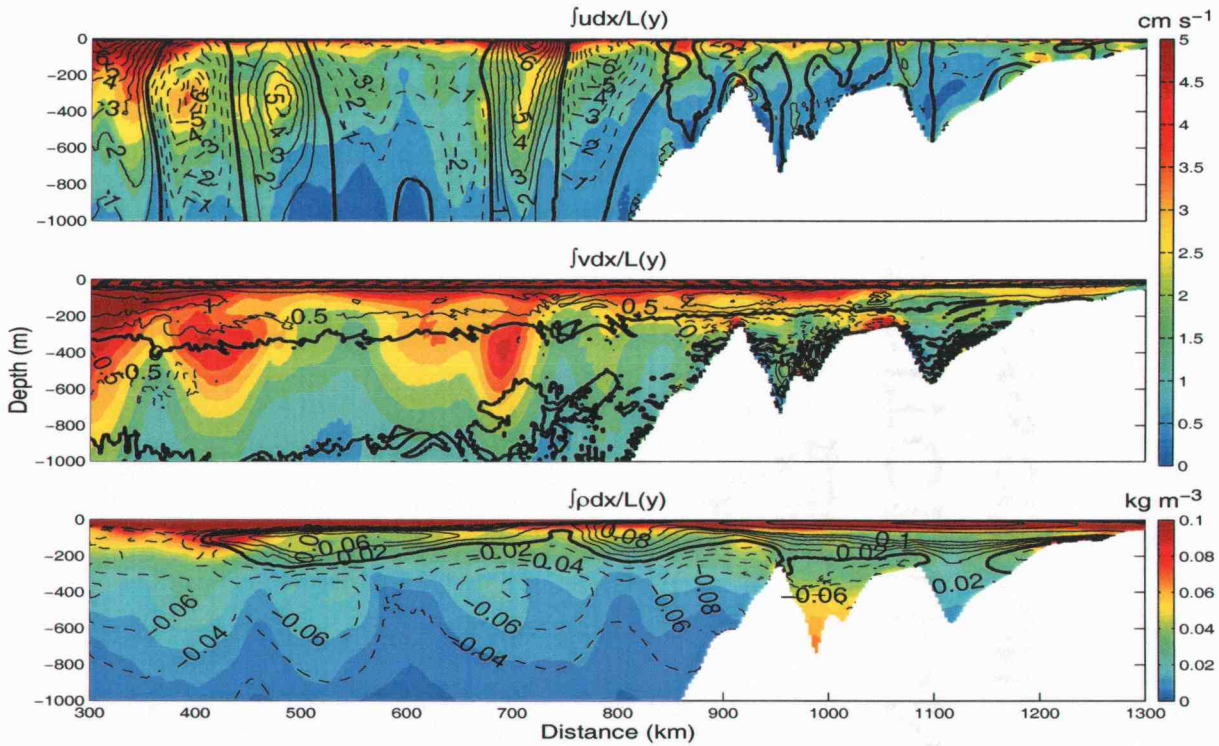

Figure 2.17. Time and across-gulf average velocity components and density anomaly from EXP 1. a) across-gulf component u, b) along-gulf component v, and c) density anomaly. The thick line is the zero velocity contour. The contour intervals are 1 cm s^{-1} for the across-gulf velocity u, 0.5 cm s^{-1} for the along-gulf velocity v, and 0.02 kg m^{-3} for density anomaly.

entrance, is characterized by small northward up-gulf velocities. Below the intermediate layer, a lower layer that extends down to almost 1000 m depth includes small velocities with a southward down-gulf tendency. There is no evidence of the eddies in the along-gulf velocity after averaging across the gulf, which suggests that the eddies have little effect on the mean along-gulf transport. The rms variability of the along-gulf velocity is higher near the surface, but deep patches (depths of order 400 m) of high variability exist at y=400, 500, 700, and 750 km and seem to be associated with the boundaries between eddies (see Figs. 8 and 17).

From hydrographic data, Bray (1988a) described the mean along-gulf circulation in the northern gulf as a three layer system with southward wind-driven flow in a surface layer 50 m thick, northward inflow from 50 to 250 m, and southward outflow below to 500m, qualitatively similar to the circulation shown in Fig. 2.17. This circulation pattern was attributed to a net heat gain in the annual mean from the atmosphere into the gulf (Bray, 1988a) and the absence of a Mediterranean circulation (Bray, 1988b). In our numerical experiments, if SBF is not included (EXP 2), the same circulation pattern as shown in Fig. 2.17 is obtained, with a slower and thicker southward flowing upper layer. The circulation, with the upper layer moving southward in the direction of the mean wind, produces a continuous cooling of the gulf as the surface warm layer moves out of the gulf and is compensated by subsurface colder water moving into the gulf.

2.5.4. Density

The distribution of surface temperature in the gulf and its modification by coastal upwelling is influenced by the fact that the Gulf of California is a semi-closed basin with free connection to the Pacific Ocean through the mouth. Monthly composite sea surface temperatures from satellite images (Fig. 2.18) shows some persistent features such as the relatively cold water across the gulf in the region near the sill (y=900 km) and the cold upwelled water along the gulf on the east side. There is some evidence of eddies with spatial scale similar to the eddies in Fig. 2.7. In the south, the SST gradient across the gulf is enhanced by upwelling on the east side and the influence of the warm Pacific water on the west side. North of the sill, the across-gulf SST gradient is weaker. The upwelling region on the east coast north of AGI is very narrow, increasing in width at the northern end.

The mean surface density anomaly (difference from initial value) field obtained from the model results in EXP1 (Fig. 2.19) has a spatial distribution that is similar to the satellite derived SST in Fig. 2.18. High density (low temperature) values are common along the east side, with a low density warm spot toward the east of La Paz (y=440 km). The influence of Pacific waters extends 350 km north of the mouth to y=650. The across-gulf density gradient is smaller for y>800 km similar to the measured across-gulf SST gradient in Fig. 2.18.

The surface density anomaly in EXP1 (Fig. 2.19) is produced by a combination of surface buoyancy flux, coastal upwelling along the east coast, and

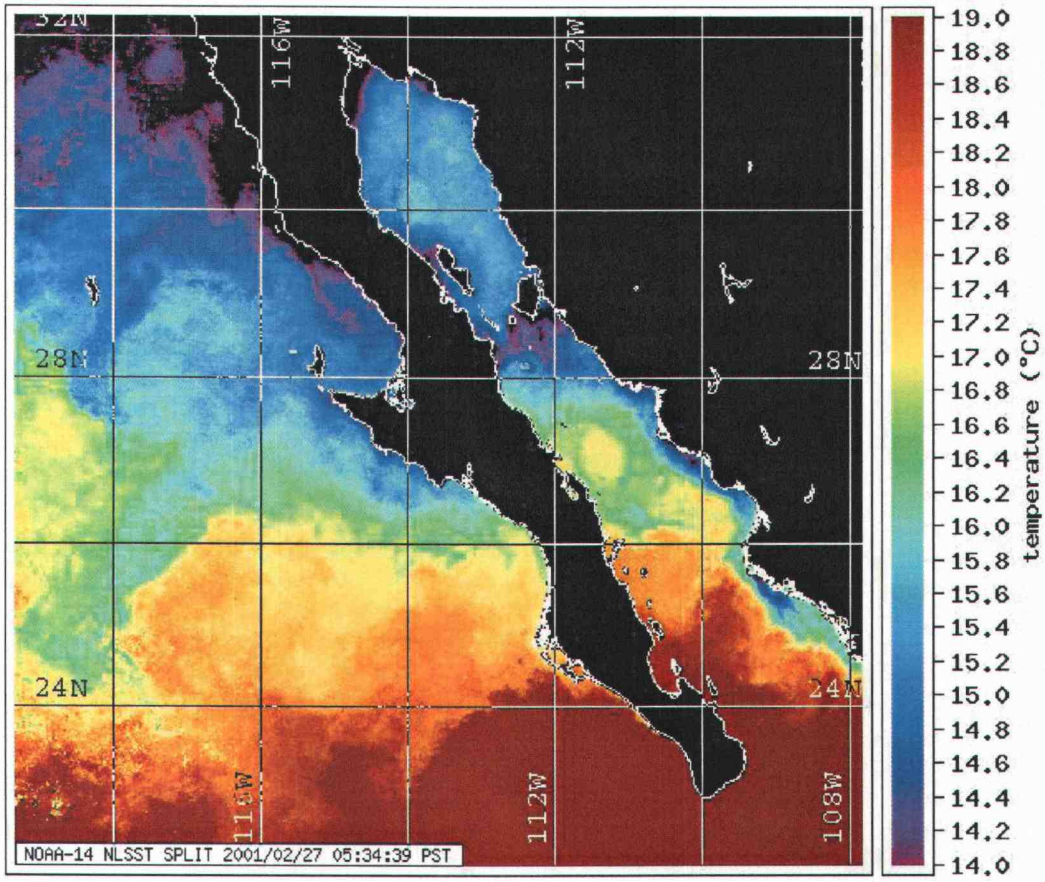

Figure 2.18. Sea surface temperature February 2001 monthly composite. (From NOAA-CoastWatch).

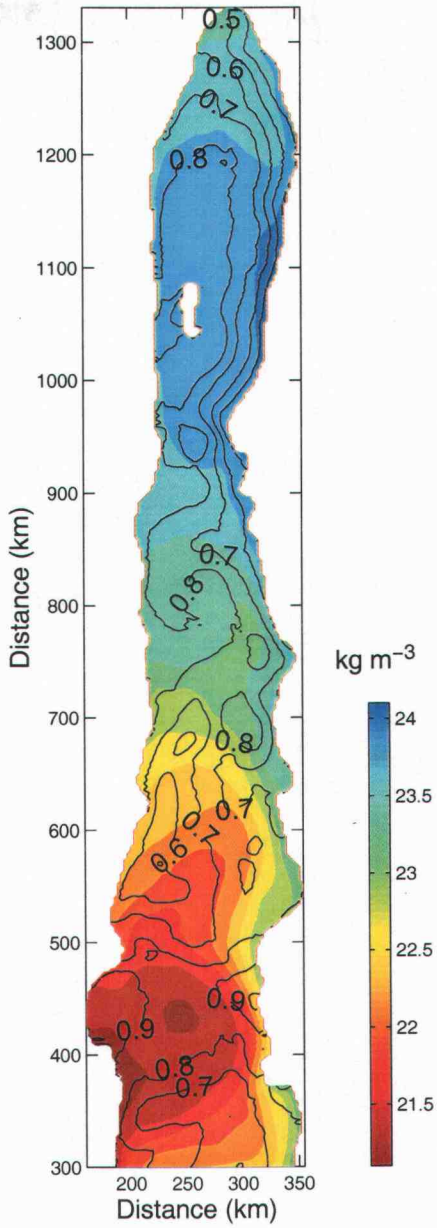

Figure 2.19. Temporal mean surface density anomaly (difference from initial value) (color) and rms (contour lines) for the period Dec-Mar from EXP 1. The color scale has been inverted for easier comparison with Fig. 18.

advection southward by surface currents of upwelled water from the north gulf, mainly along the west coast. The equation for the evolution of the density may be written as

$$\frac{\partial \rho}{\partial t} + \nabla \bullet \rho \underline{v} = \nabla_H \left(A_H \bullet \nabla_H \rho \right) + \frac{\partial}{\partial z} \left[K_H \frac{\partial \rho}{\partial z} \right], \tag{2.5.3}$$

where A_H and K_H are the horizontal and vertical diffusion coefficients, $\underline{v}=u\underline{i}+v\underline{j}+w\underline{k}$ (and $\nabla_H = (\mathbf{i}\partial_x + \mathbf{j}\partial_y)$. Fig. 2.20 shows the time mean of the terms in (4.3) integrated in the across-gulf direction and in depth (e.g., $T^{1}\Delta y\int(\rho)_t dtdxdz$) as a function of y. The local density balance in Fig. 2.20 shows that, north of the sill (y>900 km), the average density is increased over the initial values. This is accomplished mostly by a negative northward mass flux that also balances a small positive contribution from the surface buoyancy flux (vertical diffusion term). South of the sill, the average density is decreased. Although there is a negative mass flux, the positive surface buoyancy flux is strong enough to decrease the density. The contribution of horizontal diffusion (dotted line) is negligible in the northern gulf. In the south, its contribution is non-negligible only at the boundaries of some of the eddies (y=400, 500, and 630 km) and at some other isolated points.

2.5.5. Eddies.

One of the most robust features of the wind-driven circulation in our simulations is the presence of energetic eddies south of the sill with horizontal scales generally of order of the gulf width and with alternating sense of rotation

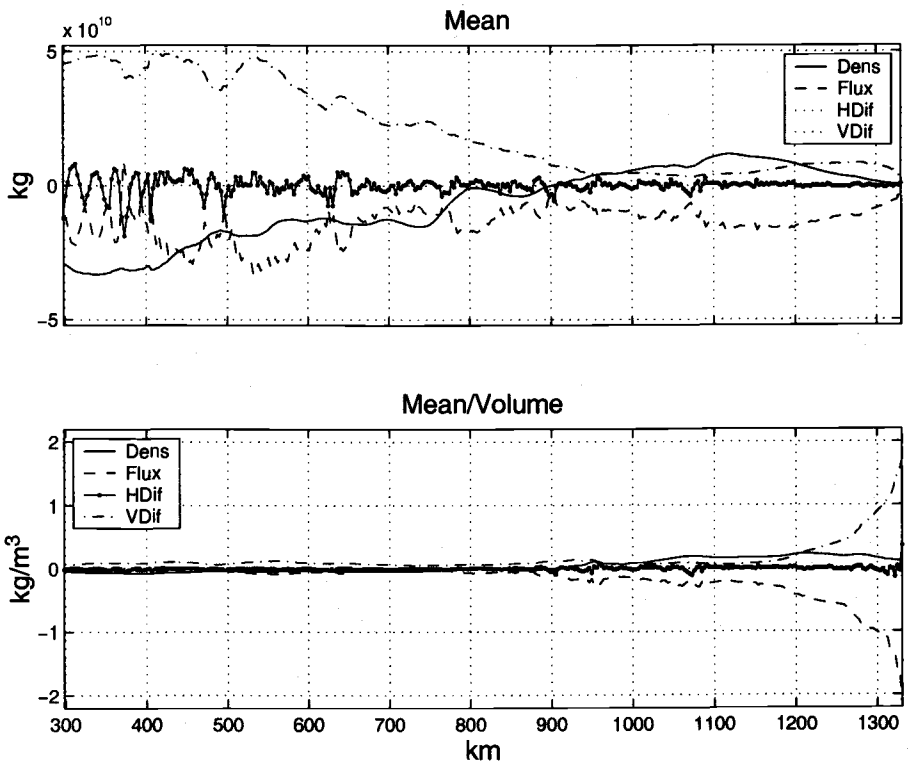

Figure 2.20. Along-gulf distribution of the density balance for EXP1. The terms in the density equation are labeled: Dens=density, Flux=advective flux of density, HDif=horizontal diffusion, and VDif=vertical diffusion. In the top plot, every term in the density equation is averaged in time and integrated across-gulf and in the vertical ($T^{-1}\Delta y\int dxdzdt$). In the bottom plot the same terms are divided by the volume ($\Delta y\int dxdz$) of the across-gulf section.

(Fig. 2.8). In this subsection, we describe the eddies and some of their main dynamical characteristics.

Isolated eddies have been reported from drifters and mooring observations in the northern gulf (Lavin, et al. 1995) and in the south (Emilson and Alatorre, 1997). In the north gulf, Lavin et al. (1995) and Palacios et al. (2001) observed a persistent eddy north of AGI, cyclonic in summer and anticyclonic in winter. Using satellite infrared images, Badan et al (1985) described vortex pairs and accompanying plumes of upwelled water that develop in the central gulf and that move offshore westward from the east side. Previous numerical studies of the wind-driven circulation in the Gulf of California have assumed a spatially uniform wind. Carbajal (1993) used a three-dimensional model forced by a wind stress constant in time. Beier (1997) studied the wind-driven circulation using a linear two-layer model driven by a wind-stress with only an along-gulf component that varies sinusoidally at the annual frequency. The circulations obtained by Carbajal, (1993) and Beier, (1997) include an anticyclonic eddy north of AGI if the wind blows from the northwest aligned along the gulf. During summer simulations, with the wind assumed to be from the south (Carbajal, 1993) or from the southeast (Beier, 1997) a cyclonic eddy is formed in the northern gulf. No wind-driven eddies have been reported south of the sill.

The spatial and temporal variability of the wind field seems to be an important factor in the generation of eddies. In EXP4 using a constant in time and spatially uniform 5 m s^{-1} wind from the northwest, assumed representative of

winter, with no contribution of the across-gulf wind stress component as in Carbajal (1993) and Beier (1997), we obtained an anticyclonic circulation pattern similar to the one obtained by Beier (1997). However, using the more realistic satellite-derived space-and time-dependent wind stress in EXP 1, the mean circulation in the north is found to be cyclonic with a cyclonic tendency also in the central and south gulf (Fig. 2.8). This difference suggests that the observed anticyclonic northern eddy is not just driven by wind, but by a combination of local atmospheric forcing and remote forcing from the Pacific Ocean. The wind in the Gulf of California has been described as blowing northward up-gulf in summer and southward down-gulf the rest of the year (Beier, 1997, Lavin et al 1995, Bray, 1988a), but there is no evidence in the satellite-derived winds in Fig. 2.3 of this reversal of direction occurring over the entire gulf for long time periods. Reversing events are common, but they are very weak and short-lived. In addition, they occur locally with no dominant annual harmonic. A persistent and seasonally reversing eddy such as the one described by Lavin et al. (1995) requires a driving force with a strong seasonal signal. Strong tides in the north (~8m range), coastal trapped waves, and mass fluxes are introduced into the gulf from the Pacific Ocean, and combined with the local wind forcing, may be partially responsible for such a feature.

In our experiments, cyclonic eddies are more energetic and have larger spatial scales, except at the entrance of the gulf, where the biggest anticyclonic eddy is found. There are two main sources of vorticity in the gulf. One is the curl of

the wind stress. During the analysis period (Dec-Mar) the curl is positive inside the gulf with no change of sign and thus forces positive cyclonic vorticity at the surface of the gulf. The other source is the flow adjustment to the coastal boundaries, as mentioned before, where intensified southward coastal currents result in positive vorticity along the west side and negative vorticity along the east side (Fig. 2.15). The generation of vorticity with opposite sign on each side of the gulf might provide an explanation for observed anticyclonic and cyclonic eddies with high and low chlorophyll concentrations respectively. Using SeaWiFS ocean color satellite images, Pegau et al (2002) observed a five day evolution of two anticyclonic eddies generated on the east side and one cyclonic eddy on the opposite side. Even though those images were from summer, the upwelling observed along the east side of the gulf suggests a wind pattern blowing down-gulf from the northwest similar to, but probably weaker than, our winter simulations. Negative vorticity generation is expected along the east side with the above wind pattern, where upwelled nutrient rich water can sustain high primary production. In contrast, the cyclonic eddies draw downwelled water from the west side, poor in nutrients with resulting low chlorophyll concentrations. The position of the observed eddies in Pegau et al (2002) corresponds well with our model results. Anticyclonic eddies are observed there to form close to Cabo Lobos, north of Topolobampo and near the entrance of the gulf (y~730, 520, and 340 km in Fig. 2.8).

It is evident from the mean fields (Fig. 2.8) that the presence of eddies dominates the mean wind-driven mesoscale circulation in the gulf. Holland et al

(1983) has characterized the origin of mesoscale variability by energy transformations (integrated over the model domain) able to maintain the eddy kinetic energy. In addition to flow-topography interactions, possible explanations for the formation of eddies are barotropic instability, if the mean flow transfers energy into the fluctuating velocity field, baroclinic instability, if there is conversion of potential energy into kinetic, or a mixed instability if there is not a dominant process.

The temporal mean kinetic energy density ($\overline{\langle KED \rangle}_{xz}$) and potential energy density ($\overline{\langle PED \rangle}_{xz}$) for EXP 1 are plotted in Fig. 2.21, where $\langle\ \rangle$ indicates averages over the sub-indexed directions, as in (3.1) and (3.2), and the overbar represent time average. The distribution of $\overline{\langle KED \rangle}_{xz}$ along the gulf reflects the presence of the eddies, with local maximum values close to the center of cyclonic eddies at y=460, 600, and 800 km (Fig. 2.8). The $\overline{\langle PED \rangle}_{xz}$ has an irregular distribution along the gulf with higher values south of the sill (y<900 km) and it also shows evidence of the eddies, with local maximum close to the center of anticyclonic eddies at y=330, 520, and 730 km (Fig. 2.8). The relation of energy densities is such that a relatively high (low) value of $\overline{\langle KED \rangle}_{xz}$, is associated with a relative low (high) value of $\overline{\langle PED \rangle}_{xz}$ and vice-versa. The time correlation coefficients between $\overline{\langle KED \rangle}_{xz}$ and $\overline{\langle PED \rangle}_{xz}$ as well as the position of the center for anticyclonic (○) and cyclonic (+) eddies are also plotted in Fig. 2.21. The correlation is low near the

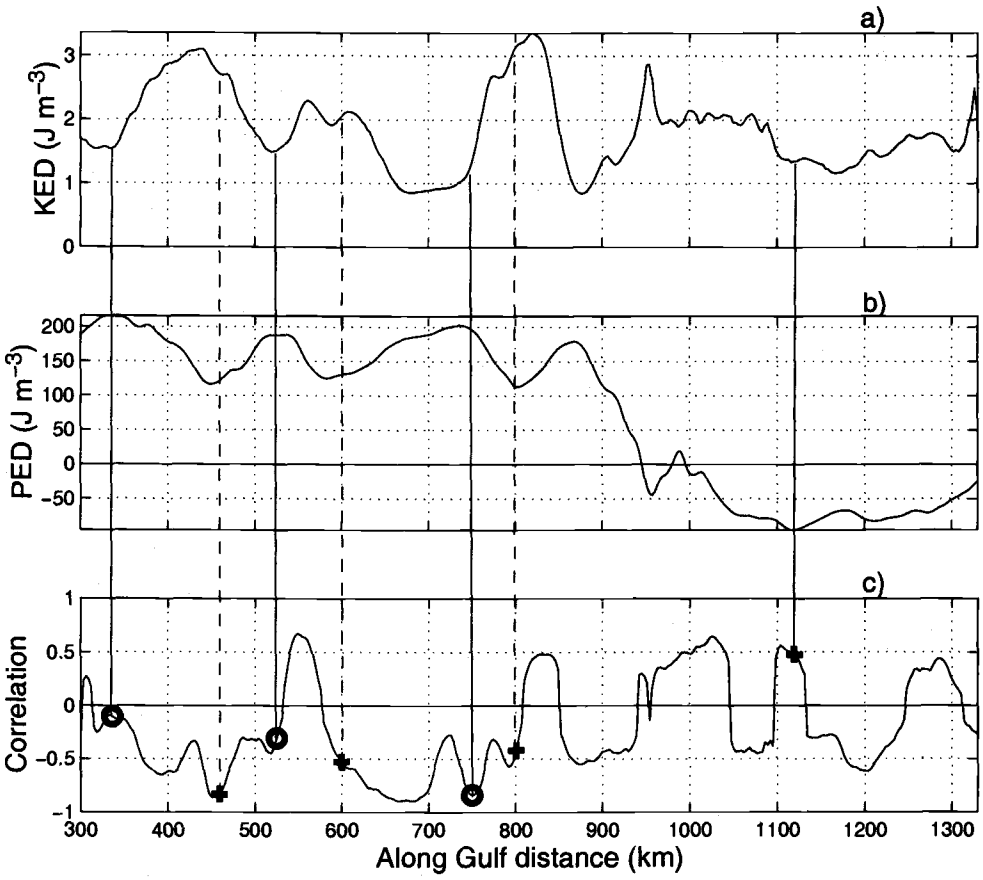

Figure 2.21. a) Temporal mean kinetic energy density $\overline{\langle KED \rangle}_{xz}$ integrated across the gulf and in the vertical, b) potential energy density $\overline{\langle PED \rangle}_{xz}$, and c) their time correlation coefficient. The symbols indicate the center of cyclonic (+) and anticyclonic (O) eddies.

anticyclonic eddy (○) at the entrance of the gulf (y=340 km) and is positive near the cyclonic eddy in the north gulf (y≈1120 km), but negative, consistent with energy conversion, for the rest of the eddies. Not all the maxima in Fig. 2.21 are associated with eddies, as is the case of the relative maximum in $\overline{\langle KED \rangle}_{xz}$ near the sill at y=950 km. At this location, there is a corresponding minimum of $\overline{\langle PED \rangle}_{xz}$, but no visible eddy and the time correlation coefficient is positive. With no eddy at this position, the relation between $\overline{\langle KED \rangle}_{xz}$ and $\overline{\langle PED \rangle}_{xz}$ suggests different processes take place here, probably related to topographic effects as the gulf narrows and the currents intensify.

Net conversion from potential energy into kinetic energy requires that the work done by buoyancy forces (integrated over the domain and over time) be negative. Fig. 2.22 shows the along-gulf distribution of the across-gulf and time-averaged conversion term

$$\overline{\langle gw\rho \rangle}_{xz} = A^{-1} \int \overline{gw\rho} dxdz, \tag{2.5.4}$$

where $A=A(y)$ is the (x,z) across gulf area. Most of the conversion takes place in the southern gulf and in the neighborhood of anticyclonic eddies at y= 520 and 750 km (see Fig. 2.8). The volume integral in the gulf of the conversion term $\overline{\langle gw\rho \rangle}_{xyz}$ is negative, -6.1×10^6 Js^{-1}, indicating that a net conversion of potential energy into kinetic energy takes place. Another instability mechanism is barotropic instability,

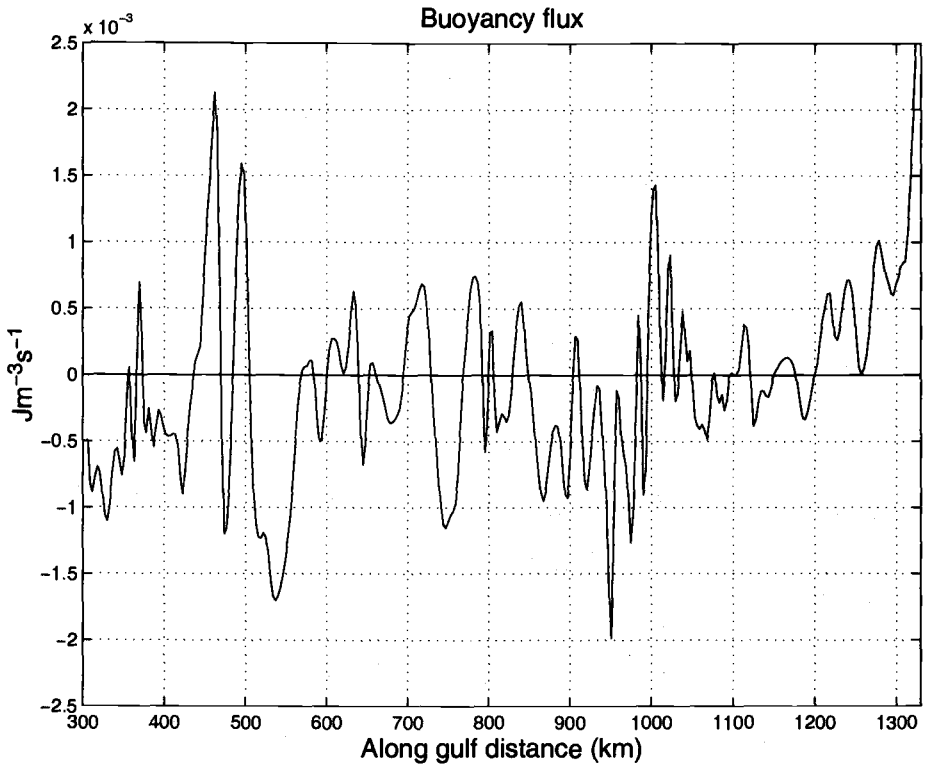

Figure 2.22. Time and across-gulf averaged conversion term $\overline{\langle gw\rho \rangle}_{xz}$ (4.4) as a function of distance y along the gulf.

but no significant conversion of mean kinetic energy into eddy kinetic energy, related to the presence of the eddies, is found.

2.6. Turbulent kinetic energy

The generation of turbulence in the ocean interior is usually attributed to breaking internal waves by mechanisms that are poorly understood (Gregg et al, 1992). It is clear that near-inertial frequency internal waves play an important role in the distribution of energy, particularly in the transport of energy from the mixed layer into the deep ocean (Pollard, 1970). Eddies and near-inertial wave activity seem to be closely related. High dissipation rates of kinetic energy near the edge of a Gulf Stream warm core ring were observed by Lueck and Osborn (1986), and additional evidence presented indicated the trapping of near-inertial waves by the geostrophic shear of the ring. Kunze and Sanford (1986) found energetic downward-propagating near-inertial waves at the base of an anticyclonic eddy. The presence of near-inertial waves is closely related to the distribution of relative vorticity and vertical shear. Theoretical work (Kunze, 1985) and numerical models (Wang, 1991) have shown that horizontal and vertical shear can result in near inertial wave trapping in negative vorticity regions of mesoscale flows. In a modeling study of near-inertial waves in flow over the Oregon continental shelf Frederiuk and Allen (1996) found that the negative relative vorticity field of a

southward coastal jet creates regions over the shelf favorable for inertial wave propagation. During upwelling conditions, they found high concentrations of near-inertial wave energy accompanied by relatively high values of turbulent kinetic energy $\frac{1}{2}q^2$ in these regions.

In EXP 1 we find regions with relatively high temporal mean values of q^2 ($\approx 10^{-4}\text{cm}^2\text{s}^2$) in the interior away from the top and bottom boundary layers near the center of the gulf between y=380 and y=450 km at depths around z=500 m (Fig. 2.23). Velocity shear is known to be effective for the generation of turbulence. If the Richardson number Ri is small (<0.25) shear flows are unstable and may produce turbulence. In our experiments, the spatial distribution of relatively high mean values of q^2 is closely related to high mean values of the inverse Richardson number Ri^{-1} (Fig. 2.23). Also plotted in Fig. 2.23 is the time averaged kinetic energy per unit mass $\overline{KE}_w$ in the superinertial frequency fluctuations, where

$$KE_w = \frac{1}{2}\left(\{u'^2\} + \{v'^2\}\right), \tag{2.6.1}$$

and $\{u'^2\} = \{(u - \{u\})^2\}$ is defined as the inertial-period averaged variance of the u velocity component about the inertial-period averaged u. Here brackets $\{\bullet\}$ indicate time-average over an inertial period, a similar definition holds for $\{v'^2\}$, and the overbar indicates time average over the 4 month experiment as before. The spatial distribution of $\overline{KE}_w$ (Fig. 2.23) shows relatively high values in the same general locations as the high q^2 values. The time-averaged relative vorticity v_x-u_y plotted in

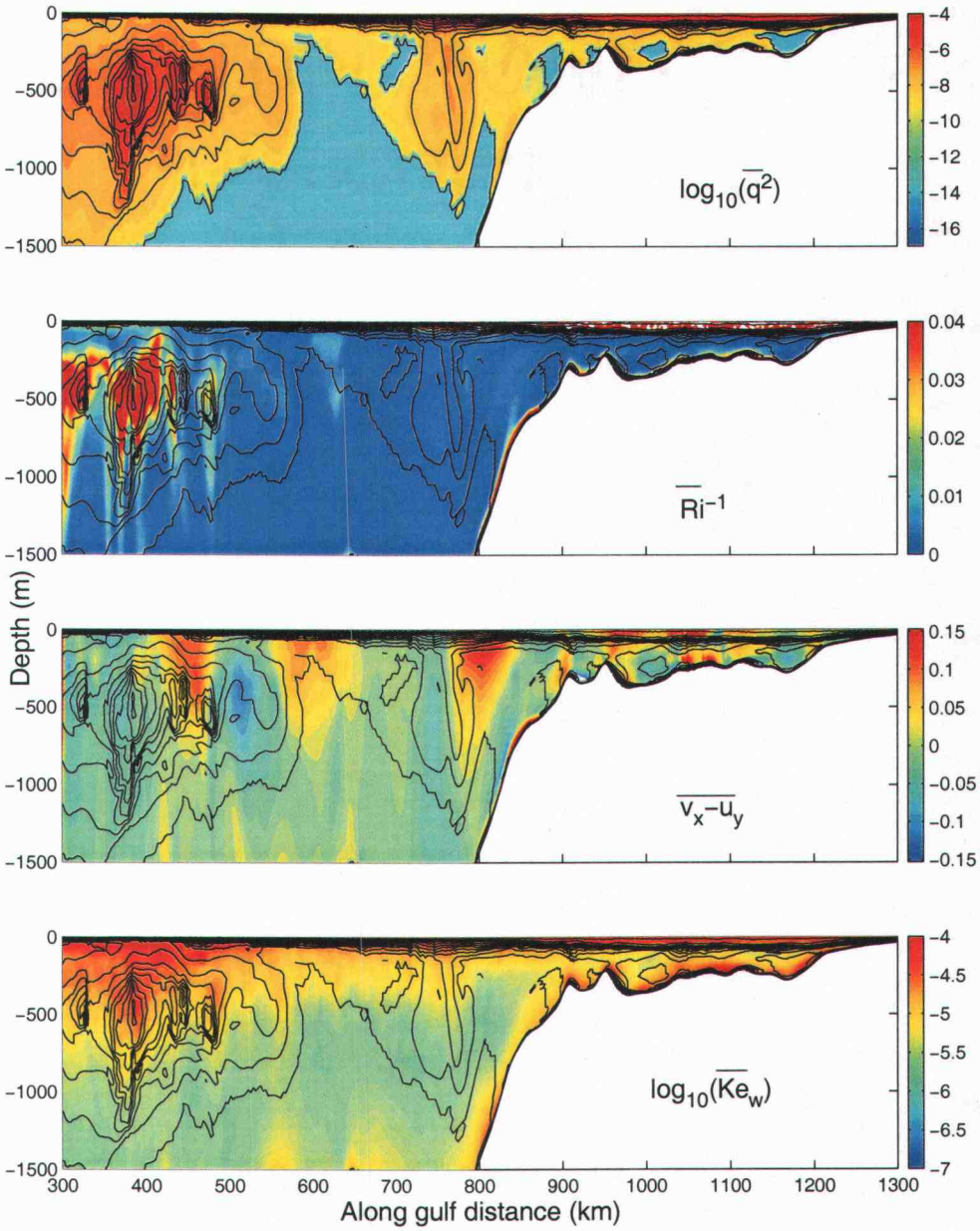

Figure 2.23. A vertical and along-gulf section at x=270 km of the time-averaged a) two times the turbulent kinetic energy q^2 ($\log_{10}$), (b) inverse Richardson number Ri^{-1}, c) relative vorticity v_x-u_y and d) wave kinetic energy KE_w ($\log_{10}$) (5.1).

the same along-gulf section (Fig. 2.23) shows generally negative values in the locations where q^2 and KE_w are relatively large.

Time series of q^2, u_z, v_z, N^2, Ri^{-1}, KE_w and relative vorticity v_x-u_y at x=270 km, y= 384 km, and z=-500 m are plotted in Fig. 2.24. High values of q^2 are observed during a 20 day period between days 34 and 54. During this time period, the vertical shear also increases and N^2 decreases resulting in high Ri^{-1} values (Fig. 2.24). The kinetic energy KE_w increases at about day 28. Six days later at day 34, the values of q^2 increase and the kinetic energy KE_w begins to decrease. Relatively large negative fluctuations in the relative vorticity also start around day 34 and persist through day 65. In general the occurrence of the high q^2 and Ri^{-1} values following the increase of KE_w and persisting during the subsequent gradual decay of KE_w is clear from the time series in Fig. 2.24. Examination of the time variability of the vertical shear shows that it is dominantly near-inertial period during days 30-60. Overall, the implication is that near-inertial waves are propagating to depths of 500-1000 m in regions of negative relative vorticity before being dissipated by small scale turbulence.

2.7. Effects of variations in the Coriolis parameter.

Although the gulf is characterized by a narrow average width of 170 km, its latitudinal dimension of about 1000 km (22° N to 32° N) represents a variation of

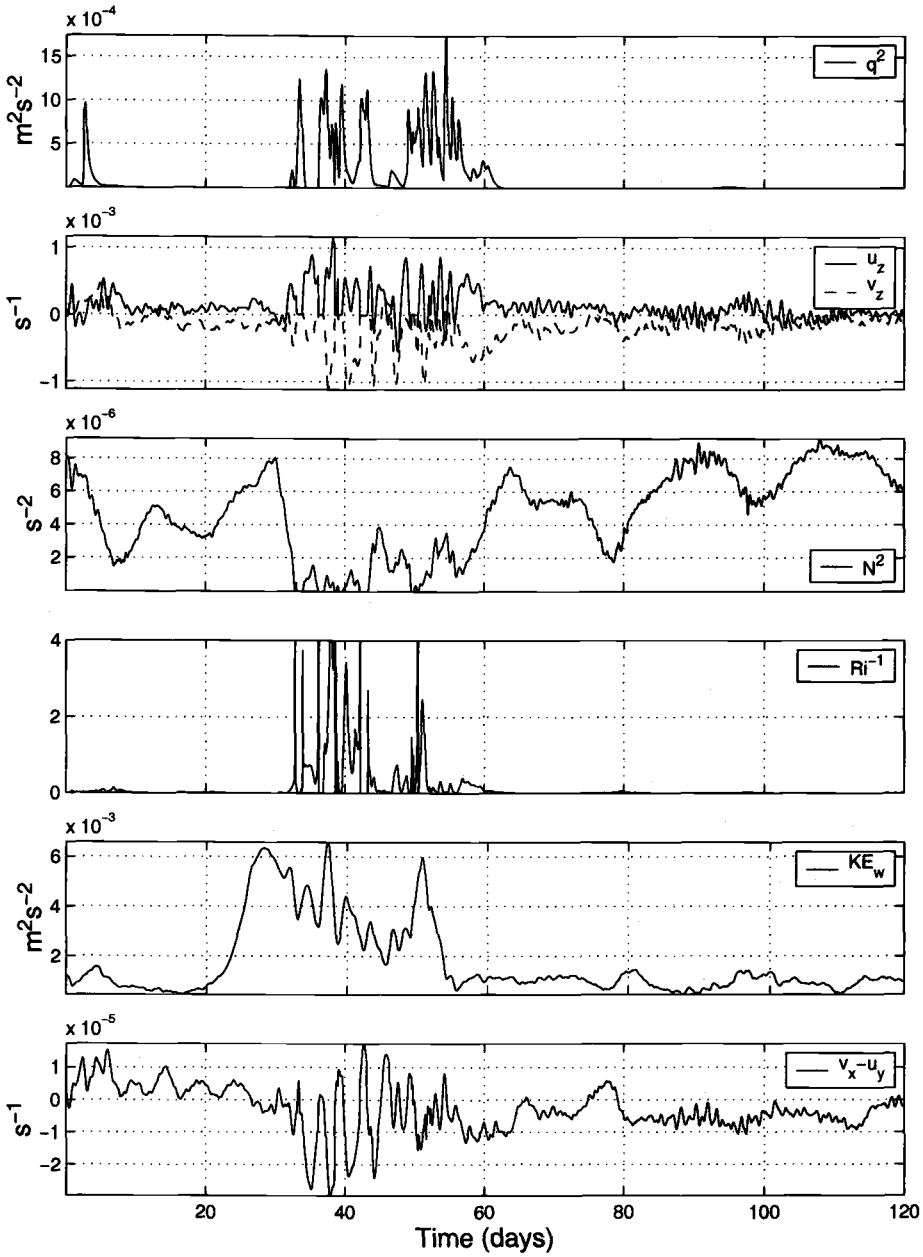

Figure 2.24. Time series at x=270 km, y=384 km, z=-500 m of two times the turbulent kinetic energy q^2, vertical shear u_z and v_z, $N^2=-g\rho_z/\rho_o$, inverse Richardson number Ri^{-1}, wave kinetic energy KE_w (5.1), and relative vorticity v_x-u_y. Day 1 corresponds to 1 Dec. 1996.

the Coriolis parameter inside the gulf of about 40 % (5.4×10^{-5} s^{-1} at the southern entrance to 7.7×10^{-5} s^{-1} at the northern end). The inertial period correspondingly varies from 32 hrs in the south to 22.6 hrs in the north, which naturally raises the question of whether changes in the Coriolis parameter can induce circulation differences. Previous numerical studies have assumed a constant Coriolis parameter (Beier, 1997), but the relevance of this assumption has not been investigated. In our simulations we include two experiments that only differ in the definition of the Coriolis parameter. With wind stress as the sole driving force, we used a variable f (β-plane formulation) in EXP2 and a constant f (f-plane approximation) in EXP3 (Table 2.1). In this section we compare some results from EXP2 and EXP3 that show significant differences in the circulation in this two cases.

The time mean transport stream function and the time mean relative vorticity fields calculated from the depth-averaged velocities and divided by f for experiments 1-3 are shown in Fig. 2.25. North of the sill the differences between the 3 experiments are not significant. South of the sill several differences are present. For the f-plane EXP3, the circulation is more energetic than in the other experiments with the largest differences in the interior. There are no well-developed anticyclonic eddies in the interior for EXP3, with the exception of an anticyclonic eddy at the entrance to the gulf. The magnitude of negative vorticity along the east side in EXP3 is comparable to that in EXP 1 and larger than EXP2. Also, the distribution of negative vorticity along the east side is more uniform in EXP3. A major qualitative difference in the vorticity fields is that positive values

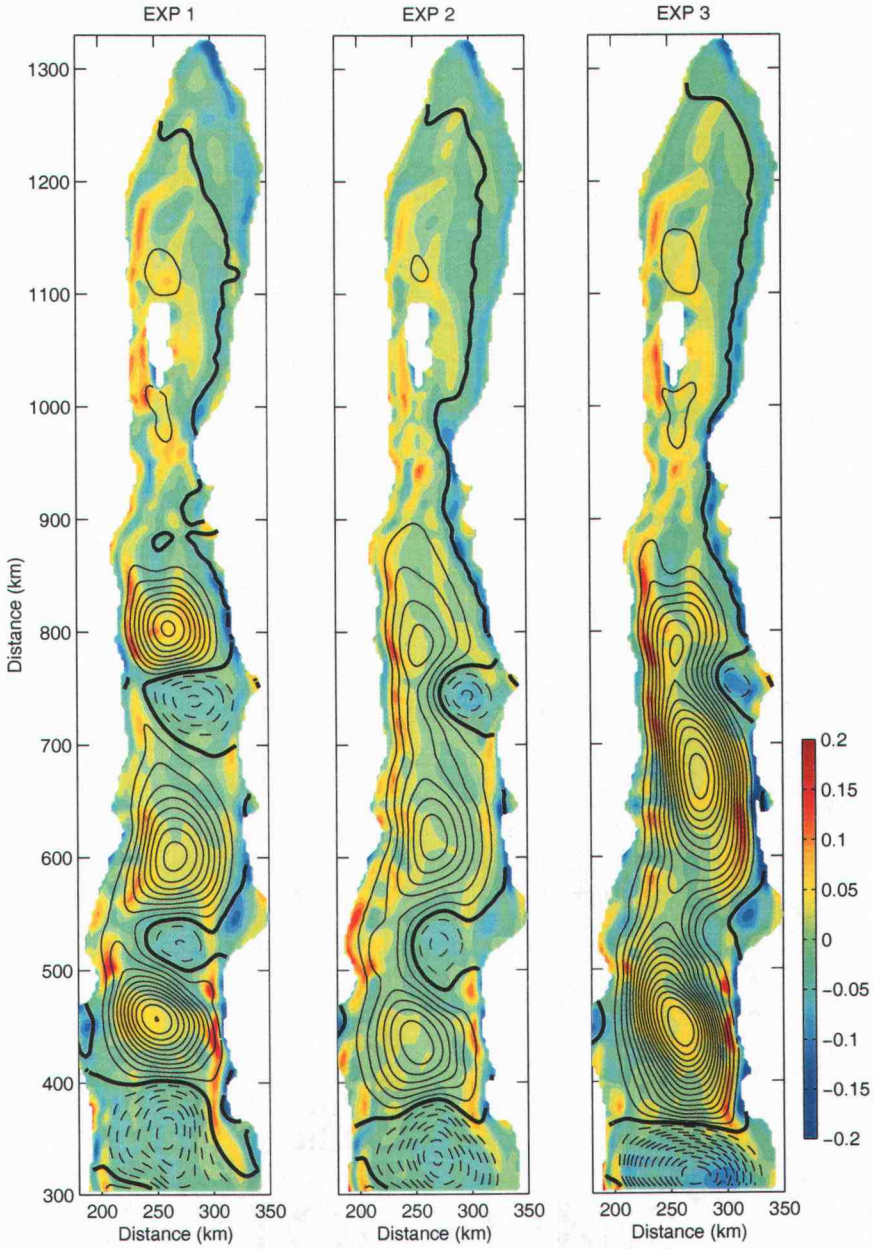

Figure 2.25. Temporal mean transport stream function (contour lines) and relative vorticity calculated from the depth-averaged velocity and divided by f (color) for EXP1, EXP2 and EXP3.

are concentrated along the western side of the gulf with variable f but not with constant f. Correspondingly, with constant f the mean Rossby number of the depth averaged velocities is generally smaller along the west side and bigger along the east side. The absence of anticyclonic eddies between La Paz (y=400 km) and the sill (y=900 km) in EXP3, but their presence in EXP2, illustrates a difference in the eddy generation processes in the two cases. The transport stream function shows that the scale of the cyclonic eddies is larger in EXP3, with a more energetic circulation. The major qualitative differences evident in these three experiments clearly demonstrate that the variation of the Coriolis parameter has an important effect on the atmospherically-forced circulation in the gulf.

2.8. Summary

Numerical experiments are utilized to study the wind-driven mesoscale circulation in the Gulf of California. The model is forced by satellite-derived winds that have significant temporal and spatial variability (Fig. 2.3, 2.4) not included in previous modeling studies of the gulf. The resulting circulation driven by the satellite-derived winds is dominated by the presence of several eddies of alternating sign along the south gulf (Fig. 2.8). Cyclonic eddies are more energetic than anticyclonic eddies. The horizontal scale of the eddies is similar to the width of the gulf, the order of 100 km. In the vertical, the eddies extend to depths of 1000 m.

The position and the horizontal and vertical scales correspond well with the eddies observed by Figueroa et al (2002) in the southern gulf. Near the coast along both sides and in most of the north gulf, the circulation is wind driven and has high variability (Fig. 2.8 and 2.9). Off the coast, in the interior the velocity fluctuations are characterized by lower variability and are poorly correlated with the wind (Fig. 2.8). The temporal mean surface circulation consists of southward down-gulf currents along the coast on both sides with larger magnitude currents along the west side. Under cyclonic eddies there is a northward up-gulf current 800 m deep along the east side and a southward down-gulf current with a similar extent in depth along the west side. In the vicinity of anticyclonic eddies the circulation is more complex, with southward down-gulf currents on both sides, and a northward up-gulf current at the center of the gulf that has baroclinic vertical structure and southward flow at depth. The temporal mean across-gulf averaged, along-gulf circulation can be described as a three layer system similar to the observation-based description given by Bray (1988a). The upper layer has a depth of about 60m and flows southward down-gulf (Fig. 2.17). An intermediate layer with a vertical extent that increases from 100 m in the north to 300 m in the south, flows northward up-gulf. Below the intermediate layer the lower layer extends to 1000 m depth with weak southward down-gulf flow.

The relatively large mean southward surface currents along both sides appear to have strong effects on the mean distribution of relative vorticity. Positive relative vorticity at the surface seems to be produced along the west side (Fig.

2.15), and to extend into the interior in the vicinity of cyclonic eddies. Negative vorticity values are significant near anticyclonic eddies and seem to be connected to the east coast. The local Rossby number indicates that nonlinear advective processes are significant along the coast and in the vicinity of eddies in the south gulf. An inverse relation is found in the along-gulf variations of the time mean across-gulf averaged potential and kinetic energies in the neighborhood of the eddies. A negative correlation between the across gulf averaged potential and kinetic energy suggests that conversion processes are associated with the presence of the eddies (Fig. 2.21).

Regions of relatively high values of turbulent kinetic energy $\frac{1}{2}q^2$ ($\approx 10^{-4}$ cm^2s^{-2}) are found in the interior away from the boundary layers and from the coast near the center of the gulf at depths 350-500 m (Fig. 2.23) and seem to be closely related to low values of the Richardson number *Ri*. High values of q^2 are typically found in locations where the relative vorticity is negative and appear to be related to concentrations of near inertial wave energy.

The atmospherically-forced circulation in the gulf is found to be sensitive to the specification of the Coriolis parameter. In the experiments with constant Coriolis parameter f (EXP3) the circulation is more energetic than that found in the corresponding experiment with variable f (EXP2). There are no well-developed anticyclonic eddies in the central gulf with constant f and the scale of the cyclonic eddies is larger. This demonstrates that even though the gulf is relatively narrow in the east-west direction, the variation of f has an important effect on the circulation.

2.9 Acknowledgments.

This research was supported by the Office of Naval Research (ONR) Coastal Dynamics Program through Grant N00014-93-1-1301. In addition, A.M. was partially supported by the scholarship Fulbright-LASPAU and the Facultad de Ciencias Marinas UABC. The use of computational resources (CM500e's) provided by the College of Oceanic and Atmospheric Sciences and facilitated by ONR grant N00014-99-1-0040 and by NSF grant OCE-952095b (both to A. Bennett) was indispensable for the completion of this research and is gratefully acknowledged. The authors also thank C. Vandetta and T. Leach for assistance with computer use and P. Newberger for initial help with the POM model.

Chapter 3

A Modeling Study of Coastal-Trapped Wave Propagation in the Gulf of California. Part 1, Response to Remote Forcing

Antonio Martinez and John S. Allen

Submitted to *Journal of Physical Oceanography*

3.1 Abstract

The evolution of remotely forced coastal-trapped waves in the Gulf of California is studied using a hydrostatic primitive equation model (POM). The sea level time variability at a remote station south of the gulf is assumed to propagate northward into the gulf as a mode 1 coastal-trapped wave (CTW). To validate this assumption, observations and model results are compared. In general, sea level fluctuations are reasonably well represented by the model with model/data correlations decreasing from 0.76 at Topolobampo, close to the entrance of the gulf, to 0.52 at Santa Rosalia in the central gulf. Model-data correlations of velocity are lower (<0.6). In the gulf, coastal-trapped waves (CTWs) propagate northward along the east side with no significant changes south of the sill, which is 600 km north of the entrance. When incident waves propagating northward in the gulf along the east side arrive at the sill a small fraction of the wave energy enters the northern gulf and is dissipated. Most of the wave energy is steered at the sill to the west side of the gulf where it propagates southward with decreased sea level amplitude. The weakened waves leave the gulf at the southwest boundary approximately 6-7 days after entering. Some of the incident wave energy is lost into down-slope propagating disturbances generated as the CTWs pass resulting in relatively intense bottom currents. Wave disturbances exhibit nonlinear characteristics while propagating. For example, isopycnal displacements in the wave fronts steepen. This occurs primarily for waves of sea level elevation. The

contribution of remotely-forced CTWs in the Gulf of California to the total kinetic energy is comparable to that produced by the wind.

3.2. Introduction

Free coastal trapped waves (CTWs) generated by hurricanes along the Pacific coast of Mexico have been observed propagating northward and entering the Gulf of California (GOC) (Christensen et al, 1983; Enfield and Allen, 1983; Merrifield, 1992). These waves typically have periods of 4 to 20 days and sea level amplitudes at the coast of 20 to 30 cm. Inside the gulf the waves are modified, as they are not observed on the Pacific side of the Baja California peninsula (Spillane et al, 1987). Most of the properties of the CTWs entering the gulf have been derived using sea level observations from tide gauges along the coast (Christensen et al, 1983; Enfield and Allen, 1983).

Observation of sea level, bottom pressure, currents and temperature were collected in the central Gulf of California by the Scripps Institution of Oceanography and the Centro de Investigación Cientifíca y de Educación Superior de Ensenada (CICESE) during 1983-1984. From this data set, Merrifield and Winant (1989) found very low correlations between local winds and currents, sea level and temperature, suggesting the importance of remote forcing. Incident CTWs are clearly observed along the east side of the gulf, but are not as readily identified

on the west side. Dissipation in the shallow north has been the most common explanation for the disappearance of poleward propagating CTWs (Merrifield, 1992; Ramp et al. 1997). Breaking and generation of eddies have also been proposed as possible mechanisms able to dissipate incident CTWs (Christensen et al. 1983).

In this two part study the evolution of remotely forced CTWs in the Gulf of California is investigated using a hydrostatic primitive equation model. In Part 1 we study the propagation of remotely forced CTWs inside the Gulf of California for 80 days during summer 1984 (July 5 to September 23). The model is forced by an incident mode 1 CTW with a time-dependent amplitude derived from sea level observations south of the gulf. The propagation of the incident CTWs and the resulting behavior of mesoscale disturbances in the gulf are examined. The possible contribution of remote forcing to the overall mesoscale circulation in the gulf is also evaluated. In Part 2 (Martinez and Allen, 2002a) we complement the direct simulation in Part 1 by analysis of a set of experiments using idealized incident wave pulses with variable amplitudes and time scales.

3.3. Model

We use the Princeton Ocean Model (Blumberg and Mellor, 1987) for the hydrostatic primitive equations. Potential density is utilized as a single variable in

place of temperature and salinity as in Allen et al (1995). A horizontal rectangular grid with Cartesian coordinates (x,y) is used with 3 km horizontal resolution and 50 sigma levels in the vertical. The y coordinate is aligned in the along-gulf direction and is oriented towards the northwest along the Baja California peninsula (Fig. 3.1). The x coordinate has an across-gulf orientation, directed towards the northeast. The velocity components in the (x,y) directions are (u,v). The numerical domain (Fig. 3.1) has open boundary conditions at the south, west, and at the north. The entrance of the gulf is near y=300 km. The analyses of the numerical experiments are primarily focused on the gulf itself, typically in the region y>400 km. On the northern boundary we use standard Orlanski radiation conditions for both depth-averaged and internal velocity and for sea level and an advection condition for density (Petruncio, 1996). On the western boundary an auxiliary wall with no normal mass flux and with density fixed to the initial value is used. A wave maker is applied at the south boundary following the method used by Wilkin and Chapman (1990). The along-gulf velocity component and the density are specified along the south boundary as a function of the across-gulf coordinate x, the vertical coordinate, and time. The spatial distributions of velocity and density are obtained using the linear CTW model of Brink and Chapman (1987). The time-dependence is specified using sea level observations as described in the next section. A zero gradient boundary condition is applied to the across-gulf velocity and to the external fields. Several tests have been performed to assure that the circulation inside the gulf is not affected by the position of the boundaries at the south and

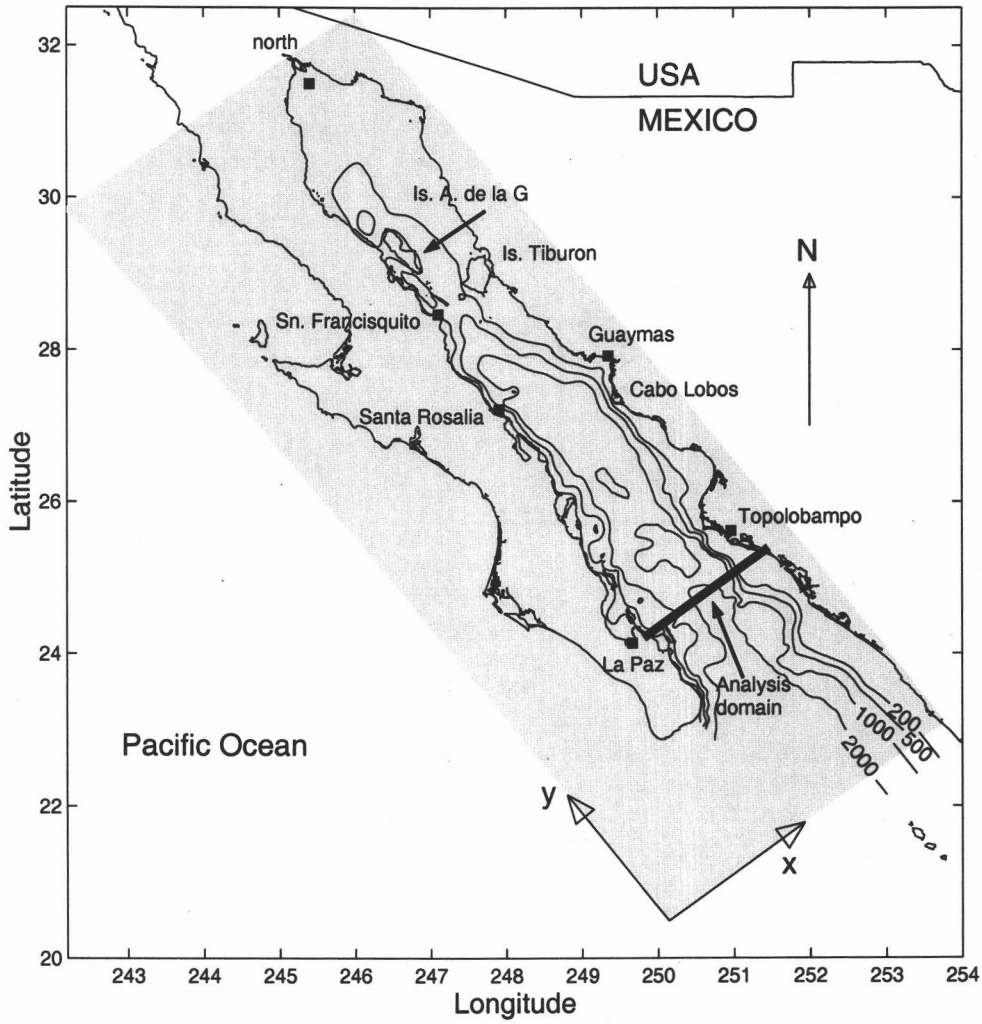

Figure 3.1: The Gulf of California and geometry of the numerical domain shaded in gray. Results presented are obtained primarily from analysis inside the gulf. The thick line across the gulf in the south at y=400 km shows the southern extent of the analysis domain.

west. The external and internal mode time steps are 3 s and 120 s, respectively. We use a constant horizontal viscosity coefficient of 15 m^2s^{-1}, which we consider an intermediate value (Oey, 1996) able to preserve mesoscale features. In every experiment we start from rest, with horizontally homogeneous depth-dependent stratification (Fig. 3.2). The initial density field is determined from hydrographic measurements in the gulf (Bray, 1988). No other forcing (wind or buoyancy flux) is considered in these experiments. The distribution of the 50 vertical sigma levels is also shown in Fig. 3.2. In the southern part of the model domain, the topography has been smoothed so that next to the south boundary the first 25 grid points in the y direction have a uniform topography with no alongshore dependence and on the next 25 grid points, the topography varies linearly to realistic values. On the Pacific side of the model domain, outside of the gulf, the topography was smoothed to make it uniform north of 25 N. The Coriolis parameter varies as in a β-plane approximation, linearly in the north-south direction.

3.4. Incident coastal-trapped waves

Waves generated south of the Gulf of California have been detected propagating poleward along the coast. The observed phase speed is consistent with a CTW mode 1. To simulate the incident wave field, we prescribe the properties of

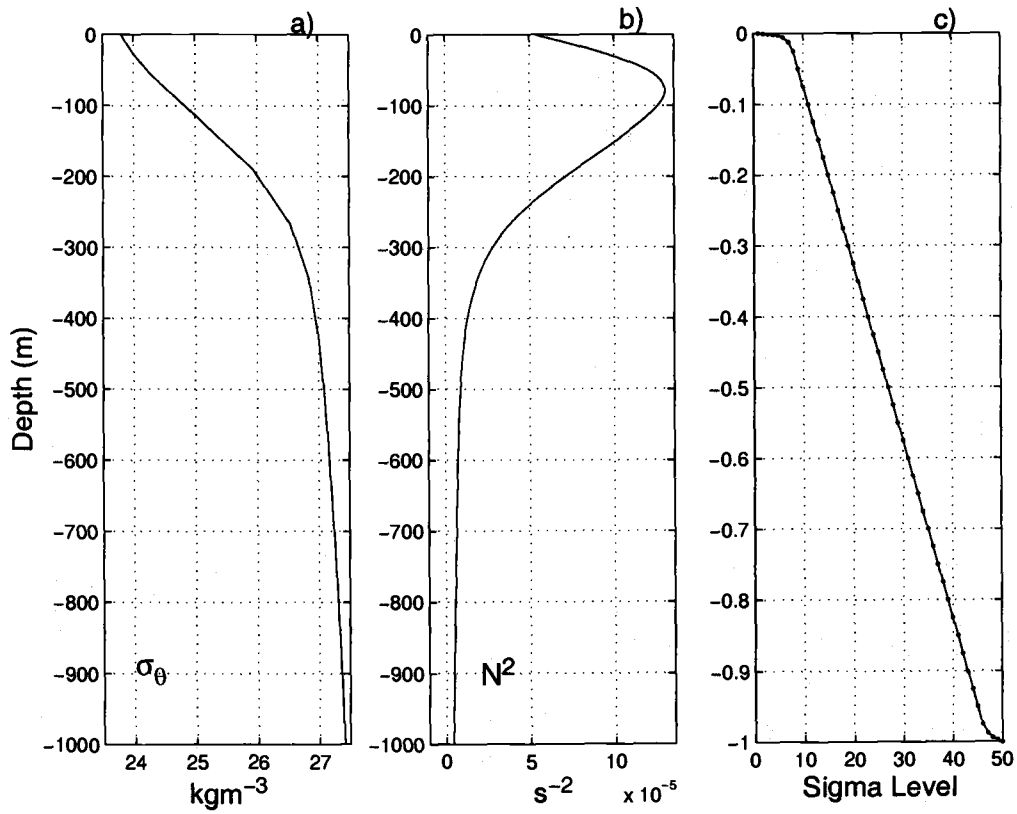

Figure 3.2: Initial density profile (a), corresponding initial N^2 (b) and distribution of vertical coordinate sigma levels (c).

the waves at the south boundary, i.e., we specify the normal along-gulf velocity v and the density ρ,

$$v_{bdry} = R_v(x,z)\phi(t), \tag{3.4.1a}$$

$$\rho_{bdry} = R_\rho(x,z)\phi(t), \tag{3.4.1b}$$

where $\phi(t)$ is the time variability and $R_v(x,z)$, $R_\rho(x,z)$ are the appropriate mode 1 structures. The time variability at the boundary is obtained from sea level measurements at Acapulco, the closest tide gauge to our south boundary (Fig. 3.1). This station is located 1300 km south of the Gulf of California entrance. Sea level time series are low-pass filtered, and the 3, 6, and 12-month harmonics are removed. Our simulation corresponds to the 80 day period from July 5 to September 23 1984. During this time model results can be compared with the observations of Merrifield and Winant (1989). With the use of such a remote station we are assuming that all the variability in sea level observed at Acapulco propagates northward as a free CTW mode 1 and enters the gulf. Our assumption is supported by previous observations of events propagating along the Pacific coast of Mexico. The observed events have wave properties consistent with a CTW mode 1 (Enfield and Allen 1983, Christensen et al 1983, and Merrifield, 1992). The CTW mode 1 structures $R_v(x,z)$ and $R_\rho(x,z)$ are calculated using the linear CTW model of Brink and Chapman (1987) with a 60x50 (x-z) grid. The mode is normalized according to Brink (1989), and then interpolated to the model grid. To calculate the structure of the incident mode we use the bottom topography, the vertical

distribution of N^2 (Fig. 3.2), and the Coriolis parameter at the south boundary. As recommended in Brink and Chapman (1987), several tests have been carried out to ensure stability of the solutions and to test the sensitivity to changes in the horizontal and vertical resolution.

3.5. Linear coastal-trapped waves in the Gulf of California.

Disturbances propagating into the Gulf of California typically have sea level amplitudes of 20 cm, with peak amplitudes of 30 cm (Christensen et al., 1983). Linear theory has been used to successfully explain some of the properties of the observed waves (Enfield and Allen 1983, Christensen et al 1983, Merrifield 1992). In this section we describe the properties of linear CTWs in the gulf.

The CTW mode 1 at the south boundary (y=0) (Fig. 3.3) has a nearly uniform vertical distribution of the along-gulf velocity on the shelf with no change of sign. Maximum velocities are next to the coast. Off the shelf, the velocity decreases with depth and decays with distance offshore. Density fluctuations (Fig. 3.3) are maximum at about 200 m. Repeating the linear CTW mode 1 calculation for several xz-sections along the gulf, we find that the CTW mode 1 does not change substantially south of the sill, retaining a structure similar to that in Fig. 3.3. North of the sill (y>870 km), the topography changes abruptly and so do the properties of the modes. The effect of changing topography on the properties of the

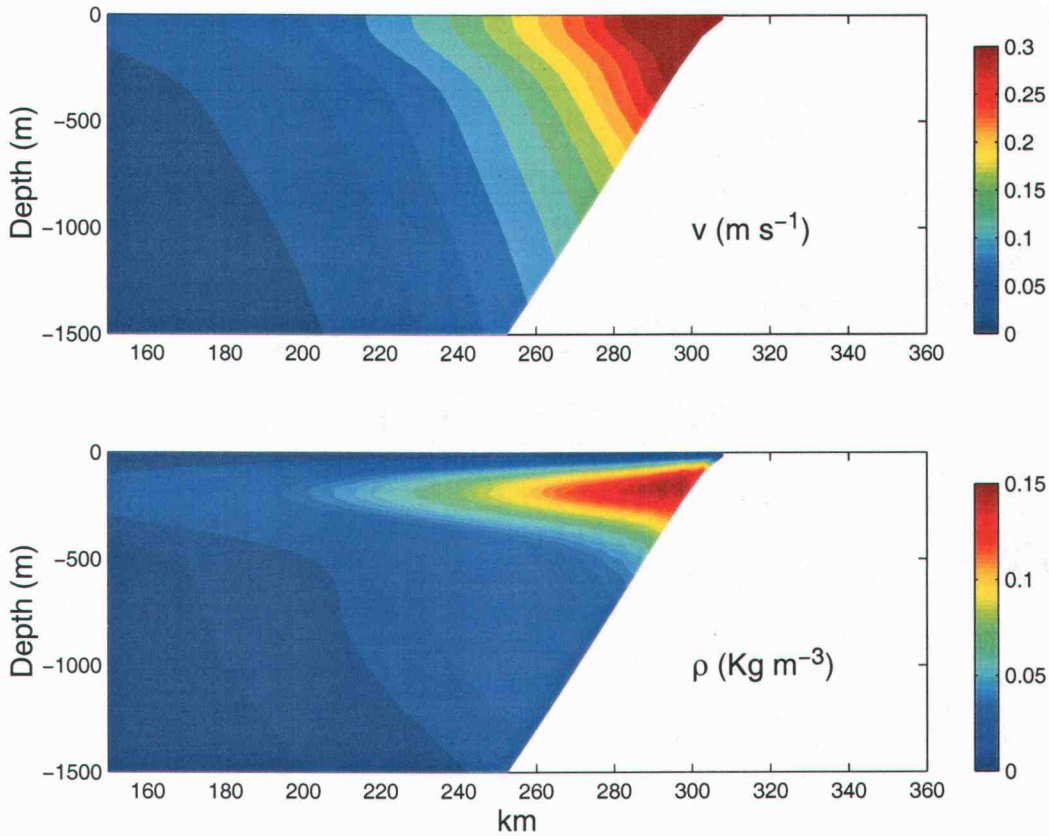

Figure 3.3: Coastal trapped wave mode 1 obtained with the CTW linear model of Brink and Chapman (1987) on the south boundary. Along-gulf velocity (top) and density anomaly (bottom).

mode 1 CTW can be illustrated with space-dependent dispersion diagrams (Fig. 3.4). To construct these, the properties of the waves are calculated on several transects across the gulf. The wave properties are calculated for a mode 1 CTW propagating northward along the east side of the gulf and for a wave propagating southward along the opposite side (Fig. 3.4). In terms of CTW properties, the gulf (y>300 km in Fig. 3.4) can be divided in two parts: The south deep gulf (300<y<870 km) and the shallow north (y>870 km) with a sill separating the two regions at y=870 km. Even though the topography is very irregular along the gulf, the linear properties of the CTW do not change substantially in the south gulf. The division point at y≈870 km is determined by the presence of the sill and is characterized by an abrupt change of the phase speed of waves traveling on both sides. The change in phase speed at the sill is independent of the frequency. The effect of the sill on the phase speed is more dramatic than the one produced by the gulf topography itself near y=300 km. Assuming that incident waves conserve frequency while scattering and that some energy remains in mode 1, the sill would modify the alongshore scale of the incident waves. North of the sill, the wavelength decreases on both sides. Low frequency waves seem to be less sensitive to the topographic changes, as the wavelength changes are smaller both near the sill and near the gulf entrance.

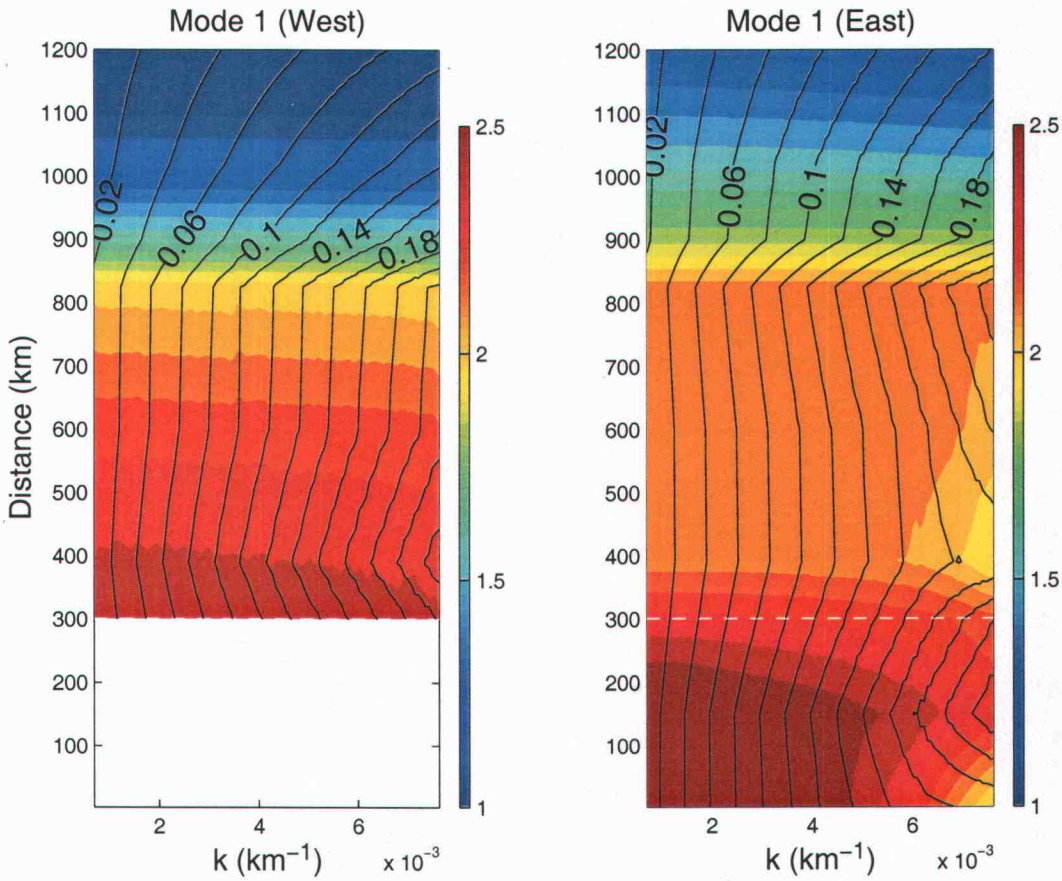

Figure 3.4: Dispersion relation for CTW mode 1 in the Gulf of California for waves traveling along the east side (right) and along the west side (left). The horizontal coordinate is the wave number (in km^{-1}), the vertical coordinate is the distance along the gulf from the south boundary of the numerical domain. The color contours are the phase speed (ms^{-1}) and the black contours lines are constant frequency normalized by the Coriolis parameter. The dashed line at y=300 km shows the entrance to the gulf.

3.6. Model results.

3.6.1. Comparison with observations

Observations of sea level from tide gauges and bottom pressure sensors along the coast show disturbances that propagate northward along the coast and into the gulf (Fig. 3.5). The larger disturbances are present at Topolobampo ($y \approx 420$ km), Guaymas ($y \approx 760$ km) and Isla Tiburon ($y \approx 940$ km) on the east side of the gulf. On the west side the signals are somehow modified. They are sometimes detected at San Francisquito ($y \approx 940$ km), but are generally not evident at Sta. Rosalia ($y=750$ km) on the west side of the central gulf. The absence of disturbances at Santa Rosalia suggests that the waves are dissipated north of Guaymas.

To assess the model performance we compare our model results with the observations described in Merrifield and Winant (1989). The assumption that time variability in Acapulco sea level propagates as a CTW mode 1 is tested by correlations between Acapulco sea level and sea level and bottom pressure measurements inside the gulf (Table 3.1). The correlation is high (0.77) between observations at Acapulco and at Topolobampo (close to the entrance of the gulf at $y=300$ km, see Fig. 3.1). This indicates that most of the variability in Acapulco propagates poleward and enters the Gulf of California in the form of a CTW mode 1. It takes five days for the signal at Acapulco to arrive at Topolobampo, which

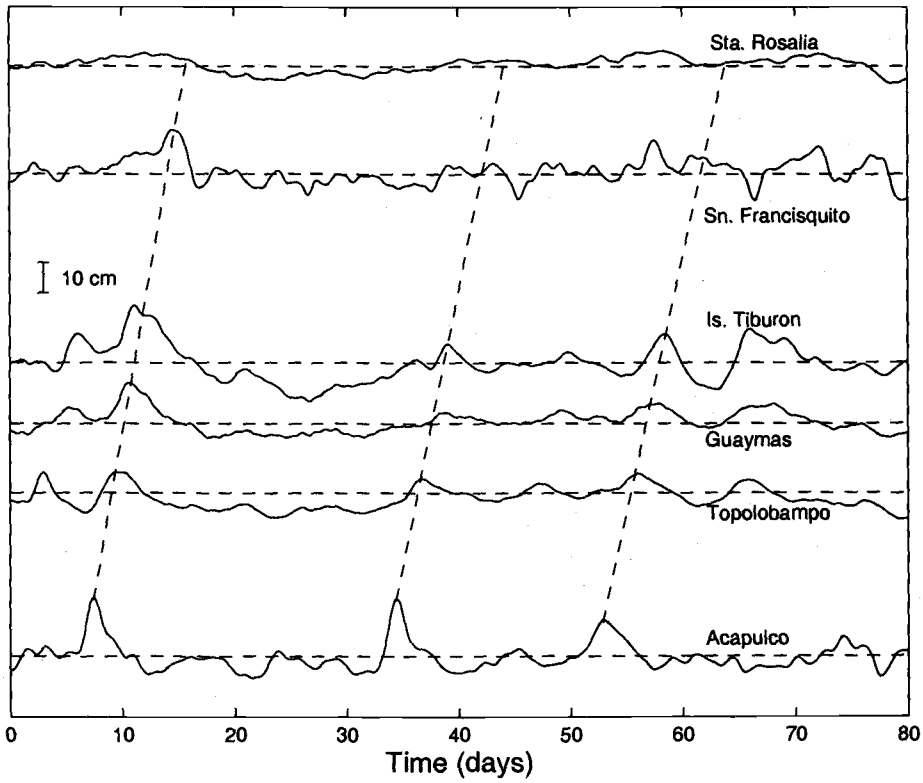

Figure 3.5: Sea level at six stations along the coast (Fig. 1). The separation between the curves is proportional to their along-coast distance. The dashed lines show propagation of some of the larger disturbances at a speed around 3 m s^{-1}. Day 0 corresponds to July 5, 1984.

corresponds to a mean phase speed of 3 ms^{-1} in agreement with previous observations (Enfield and Allen, 1983). The lag in Table 3.1 has been adjusted to zero at Topolobampo for easier comparisons. The correlation between Acapulco observed sea level and modeled sea level is in general high everywhere and does not decrease significantly along the gulf. In contrast, the correlations between observed sea level at Acapulco and observed sea level in the gulf decrease to the north by more than 50 %. The decreased correlation as the wave propagates along the gulf shows that the incident CTW is significantly modified as it propagates along the gulf. The observed lags (column 3) are in general very similar to modeled lags (column 4). The difference varies from 2 to 7 hrs except at Santa Rosalia, where the lag difference is 16 hrs. The correlations between local observed sea level and modeled sea level at the six stations inside the gulf (Table 3.2), show a relatively high correlation at Topolobampo (0.76) decreasing towards the north (0.67 at Isla Tiburon). This is expected, since the correlations between observations decrease in a similar way. The model correlation is lower off the coast, (0.51 at Guaymas 200) than on the shelf (0.69 at Guaymas 100). Along the west side, the model-data correlations are lower and at Santa Rosalia the correlation (0.52) has decreased 33% compared with that at Topolobampo. Time series of observed and modeled sea level are shown in Fig. 3.6. The model sea level fluctuations show reasonably good agreement with the observed. Some fluctuations found in the observations at the northern stations (San Francisquito at days 239 and 258, Isla Tiburon at day 248), seem to be locally generated, since they do not show

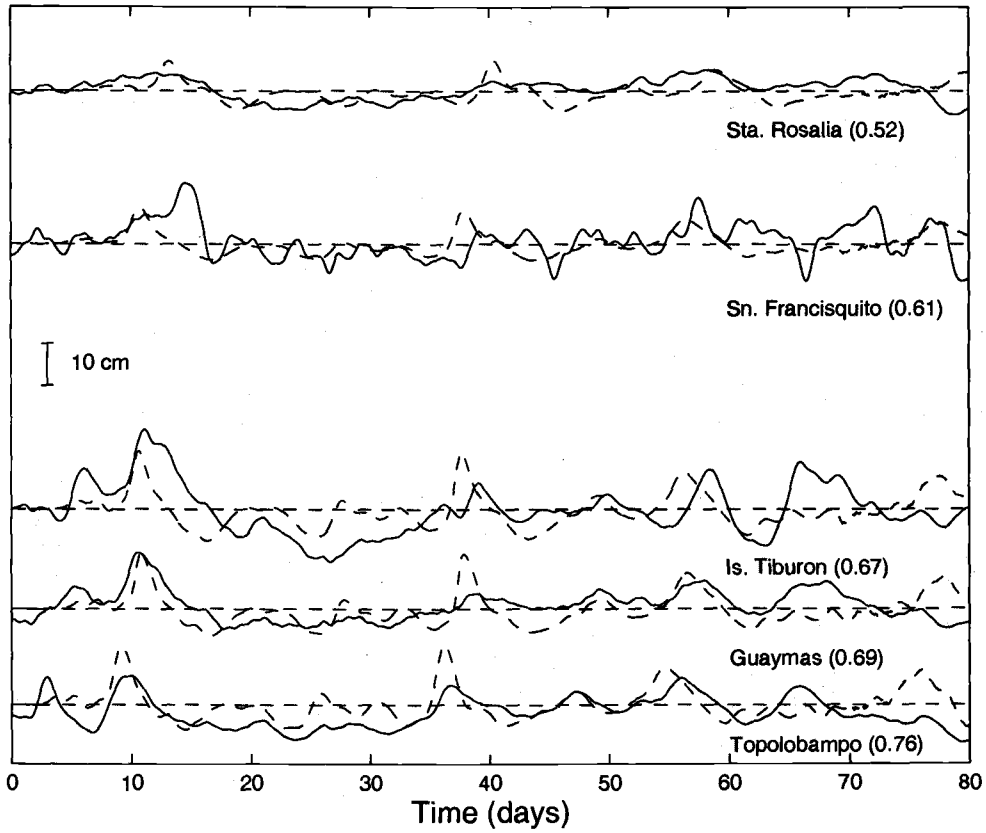

Figure 3.6: Observed sea level at five stations in the gulf (blue lines) and corresponding model sea level at the same stations (red lines). The separation between the curves is proportional to their along-coast distance. The numbers to the right of the station name are the model-data correlations.

Table 3.1. Maximum correlations and lags (days) between observed sea level at Acapulco and observed near-coast bottom pressure at six stations in the gulf, designated O-O, calculated for 80 days (5 July-23 September 1984). Also, corresponding correlations and lags between observed sea level at Acapulco and model sea level at the same six stations, designated O-M. Ac = Acapulco, Top = Topolobampo, Gy1 = Guaymas 100m (bottom pressure at 100 m depth), Gy2 = Guaymas 200m, IT = Isla Tiburón, SF = San Francisquito, SR = Santa Rosalía.

η	O – O	O – M	O - O_{lag} (days)	O - M_{lag} (days)
Ac – Top	0.77	0.97	0	0
Ac – Gy1	0.63	0.95	1.5	1.8
Ac – Gy2	0.45	0.96	2.2	1.9
Ac – IT	0.59	0.94	2.4	2.6
Ac – SF	0.38	0.96	2.8	2.7
Ac – SR	0.33	0.96	2.8	3.5

Table 3.2. Correlations between observed near-coast bottom pressure measurements and model sea level at six stations in the gulf calculated for 80 days (5 July-23 September 1984).

Topolobampo	0.76
Guaymas 100m	0.69
Guaymas 200m	0.51
Isla Tiburón	0.67
San Francisquito	0.61
Santa Rosalía	0.52

propagation. There are no clear indications in the observed sea level of the propagating disturbances arriving at Santa Rosalia.

The correlation between observed local sea level and observed currents resolved into principal axis components is poor (Table 3.3). The maximum correlation occurs at Topolobampo 100_{70}, and the magnitude of the correlation rapidly decreases north of this location. A comparison of observed and modeled currents (Table 3.4) shows lower correlations in general than found with sea level. In this case, to plot the current components and to calculate the correlation coefficients the currents are rotated in the direction of the principal axis and then the magnitude of the complex vector correlation is calculated (Kundu, 1976). The correlation is low even at Topolobampo 100_{70} (0.58) and generally decreases to the north. At Santa Rosalia and off the coast the correlations are lower (<0.5). The variations of the observed and model major axis velocity components (Fig. 3.7) have similar time scales. The magnitudes are similar at Topolobampo, but the observed velocity fluctuations are substantially larger at Guaymas. The sign of the fluctuations during the largest events, e.g. around days 12 and 45 is the same in the model and in the observations, but some small events show fluctuations of opposite sign. Differences in the general behavior of sea level and of velocity fluctuations associated with CTWs are also found in Part 2 where the response to idealized incident waves is examined. As the CTWs propagate along the gulf, the velocity fluctuations are more strongly modified than those in sea level, resulting in greater loss of correlation in the direction of propagation for the velocity compared to sea

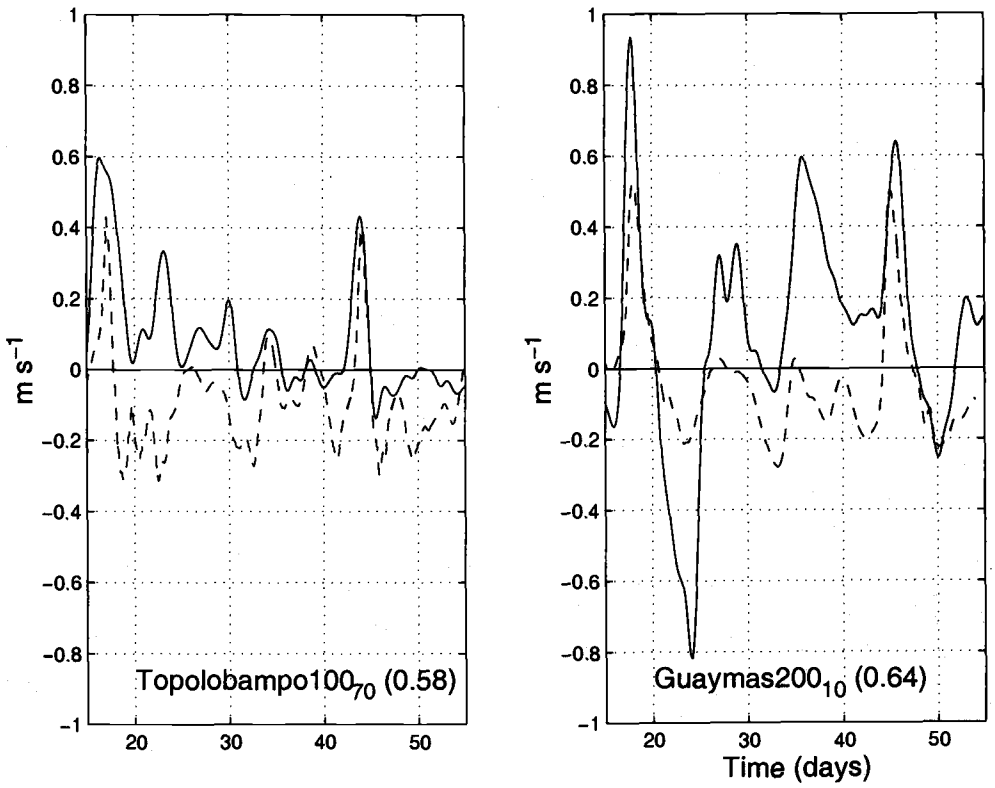

Figure 3.7: Time series of observed (cont) and model (dashed) major axis velocity component at Topolobampo 100_{70}, and at Guaymas 200_{10}. The numbers to the right of the station name are the model-data correlations for the 40 day time period in Table 4. The notation for the current measurement depth m (subscript) and total water depth m (number following station) is the same as in Table 3.

Table 3.3. Correlations between measured velocities, resolved into major (v) and minor (u) axis components, and near-coast bottom pressure measurements from the same locations calculated for 80 days (5 July-23 September 1984). The notation for the current measurements is: measurement depth (m) as subscript, total water depth (m) as number following station. For example, Guaymas 200_{10} corresponds to velocities measured at 10 m depth in water of total depth 200 m.

	η - U	η - V
Topolobampo 100_{70}	-0.49	0.34
Guaymas 15_5	-0.19	0.17
Guaymas 200_{10}	-0.09	0.18
Santa Rosalía 90_{10}	-0.07	-0.04

Table 3.4. Magnitudes of the complex correlations between measured velocities and corresponding model velocities, both resolved into principal axes components, calculated for 40 days (5 July-15 August 1984). The notation for the measurement depth m (subscript) and total water depth m (number following station) is the same as in Table 3.3.

Topolobampo 100_{70}	0.58
Guaymas 15_5	0.53
Guaymas 50_{10}	0.57
Guaymas 50_{20}	0.51
Guaymas 200_{10}	0.64
Guaymas 1000_{50}	0.35
Guaymas 1000_{300}	0.38
Guaymas 1000_{500}	0.43
Guaymas 1000_{850}	0.47
Santa Rosalía 90_{10}	0.41
Santa Rosalía 90_{30}	0.44
Santa Rosalía 90_{90}	0.47
Santa Rosalía 200_{10}	0.49

level. In addition, lags obtained from sea level and velocity differ in arrival times and in the sequence in which the signals are detected.

The model seems to be unable to modify the incident CTWs such that as the waves propagate inside the gulf the correlations decrease as rapidly as found with the observations. This could be due to the absence in the model of currents generated by other forcing mechanisms, such as wind, tides, and surface buoyancy fluxes, which are not included in this experiment. In a modeling study of the wind-driven circulation in the Gulf of California, Martinez and Allen, (2002c) found energetic southward coastal currents on both sides, modified in the south gulf by the presence of several eddies with spatial scales of the order of the gulf width (≈100 km). The interaction of wind-forced currents in the gulf with the observed incident CTWs may result in alterations to the waves, which are weakened and not detected on the Pacific side of the Baja California peninsula. Bottom dissipation in the northern gulf has been suggested as the primary mechanism that drains energy from the incident waves (Merrifield, 1992; Ramp et al., 1997). Results of the numerical experiments in Part 2 show that the incident waves loose about 60% of their total kinetic energy inside the gulf. Most of the dissipation occurs through bottom friction at the sill. A very small fraction of the incident energy enters the north gulf, so the energy dissipation by bottom friction in the north accounts just for a small fraction of the total dissipation. Generation of eddies has been proposed as a mechanism by which CTW may loose part of their energy (Christensen et al., 1983). Eddy generation is observed in our simulations and is described in detail in

Part 2. The generation of eddies is dependent on the amplitude and time scale of the incident waves. CTWs with large amplitudes or long time scales generate eddies along the coast. However, the energy decrease by this mechanism does not strongly alter the propagation characteristics of the incident waves in the gulf.

3.6.2. CTW propagation in the Gulf of California

Waves introduced in the numerical domain in the manner described in section 3 propagate northward along the east side of the gulf with no major evident changes south of the sill. Some characteristics of the wave propagation in the gulf may be seen in fields of the depth-averaged velocity vectors and of sea level one day apart for days 10-13 (Fig. 3.8). On day 10 of that time period an elevation wave, i.e. a wave characterized by elevated sea level, is propagating northward in the gulf. When the wave arrives at the sill its properties are modified. At the sill the wave splits in two waves. Part of the wave continues propagating northward while the other part turns back and propagates southward along the western side of the gulf. The depth-averaged velocity and sea level fluctuations associated with the wave propagating north of the sill are much weaker than those of the incident wave (Fig. 3.8). On day 13, the velocity in the north is weaker than on day 12, suggesting that the small fraction of the wave that propagates to the north is affected by high dissipation. The wave propagating southward along the Baja California shelf has

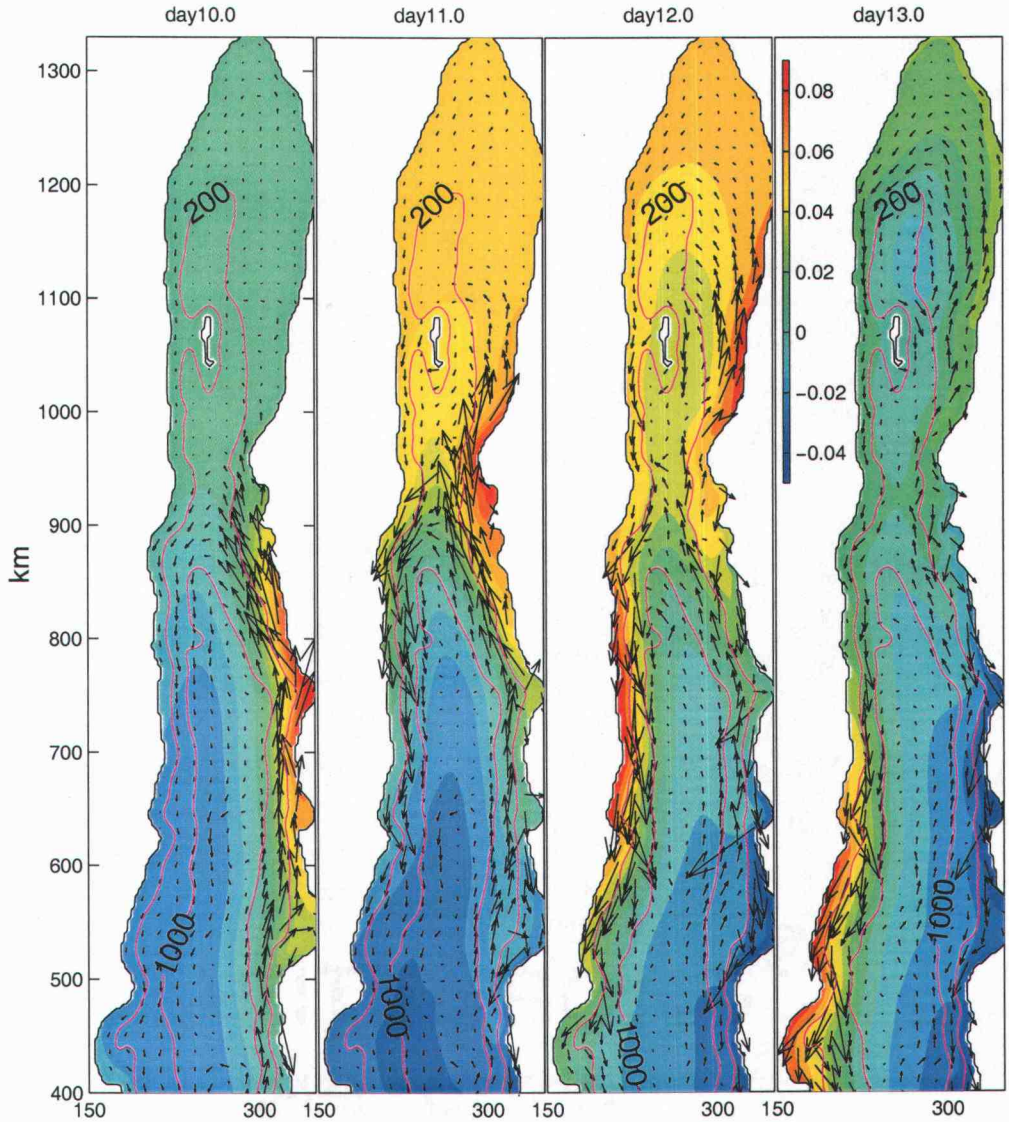

Figure 3.8: Fields of depth-averaged velocity vectors and sea level (color) one day apart for days 10-13.

smaller sea level amplitude than the incident wave, even though the velocity does not exhibit a substantial reduction. The depth-averaged velocity and sea level fluctuations are in general confined to the shelf and slope along both sides south of the sill. In the north gulf, the Rossby radius of deformation determined from the wave phase speed decreases in response to topographic changes (Fig. 3.4). As a result, CTWs might be expected to have a shorter offshore scale north of the sill. The model results seem to show, however, that the waves that propagate north of the sill have a larger offshore scale, e.g. on day 12 at y=1100 (Fig. 3.8).

The maximum correlation coefficients and the corresponding lags between model sea level at Topolobampo and sea level at all other locations in the gulf are plotted in Fig. 3.9. Only correlations higher than 0.8 are colored. In general, the correlation rapidly decreases off the coast except in the north where constant correlations extend across the gulf. A uniformly high correlation along the east side shows that the wave is not significantly modified while propagating northward south of the sill. North of the sill, the correlation is not continuous along the coast. The correlation is high north of the sill except for a small region along the northern coast. This low correlation region extends along the east side from about y=1000 km to the north. Along the west side, the correlation decreases from north to south. The lag shows how the waves propagate around the gulf. In the southern gulf (y<900 km) the waves propagate with no significant change in phase speed. On the sill at y=900 km most of the wave steers so that it continues to propagate southward along the Baja California peninsula. North of the sill, the gulf is flooded with a

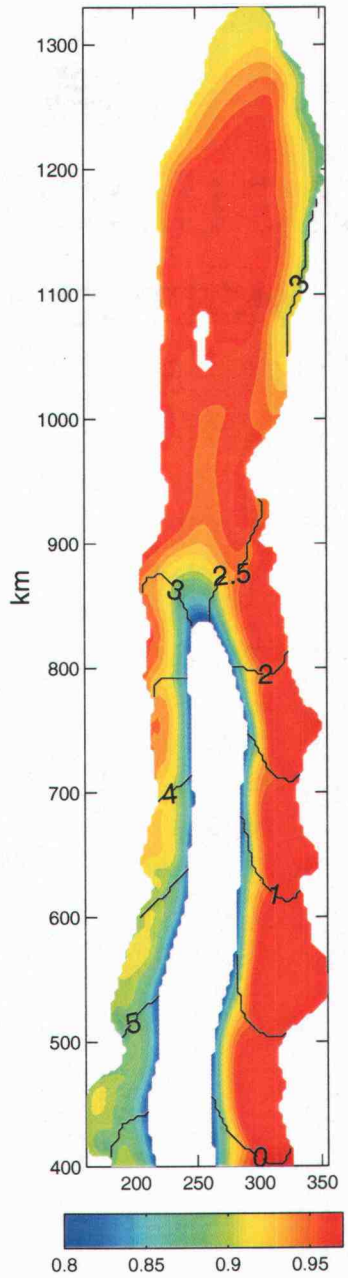

Figure 3.9: Sea level correlations between Topolobampo and other locations in the gulf (color; only correlations > 0.8 are plotted) and the corresponding lags (contour lines) in days. The contour interval is 0.5 days.

rapidly propagating sea level signal, formed at the steering point (y=900 km), that reaches the northern gulf in about 7 hrs. This yields a mean phase speed of 17 m s^{-1} that is much faster than the CTW mode 1 and much slower than a typical long gravity wave phase speed of 44 m s^{-1}. A more detailed description of the behavior of the propagation in the northern gulf is given in Part 2. The time variability of the forcing used in this study includes a range of wave frequencies and amplitudes. The lag in Fig. 3.9 represents the average result for all these incident disturbances. In Part 2 similar experiments are conducted for individual idealized incident wave pulses. These experiments reveal a dependence of lag, and thus of propagation speed, on the amplitude of the incident wave. Large amplitude depression waves propagate slower than large amplitude elevation waves and take 36 hours longer to circuit the gulf.

The effects of the waves in the gulf on the mesoscale circulation are shown in x-z across-gulf sections of mean and rms along-gulf velocity and density anomaly (Fig. 3.10). South of the sill, the distributions of the rms alongshore velocity and density anomaly fields in those sections on both sides of the gulf are similar to the mode structures in Fig. 3.3. Signatures of the CTWs are found on both sides from y=384 km north to y=804 km. The along-gulf velocity exhibits the largest rms values near the coast on the east side. On the west side south of the sill, the waves have been modified and weakened and the larger rms velocity values are deeper and at y=384 km appear to be slightly separated from the coast. South of the sill, the density anomaly has maximum rms values at depths of about 180 m on the

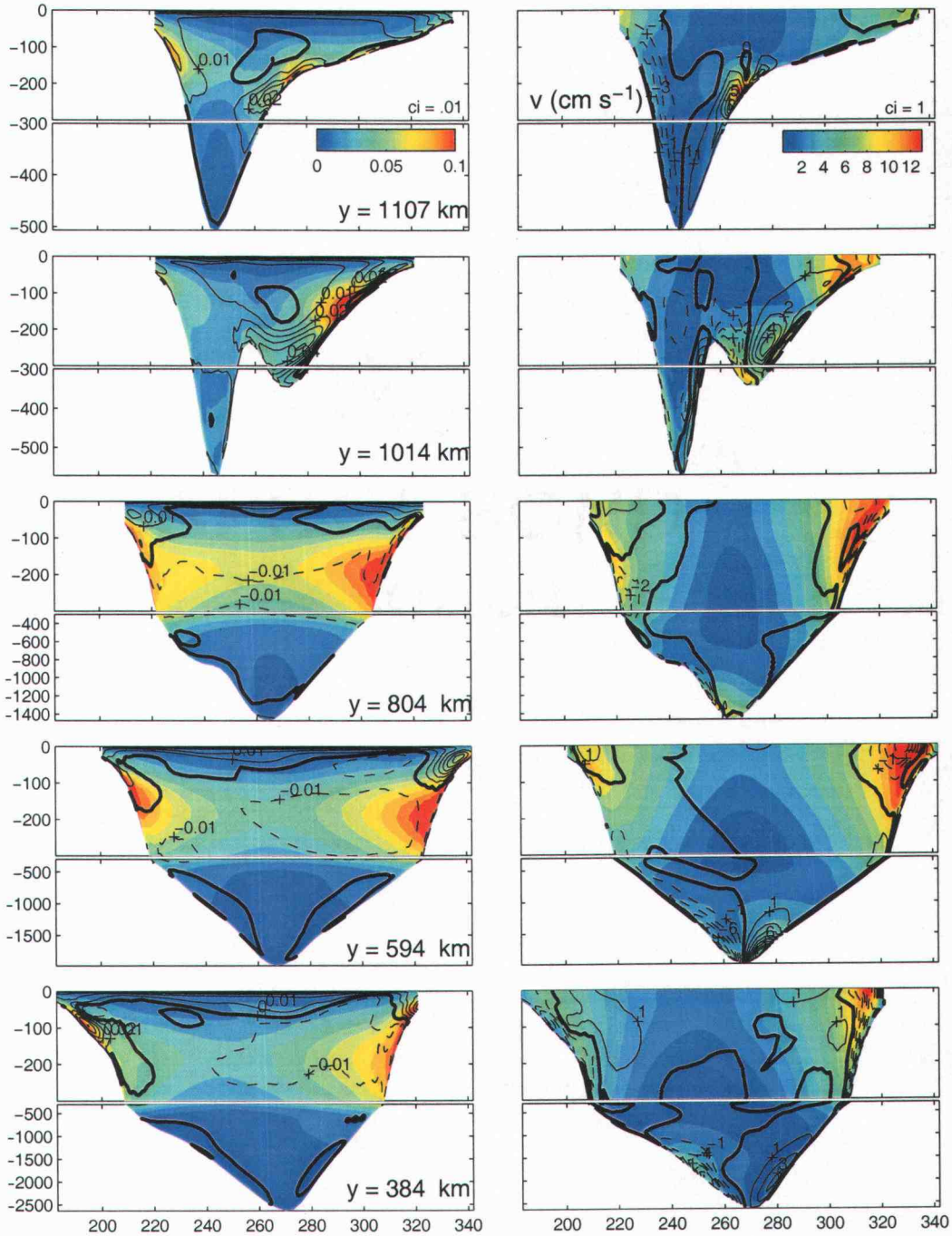

Figure 3.10: Mean (contour) and rms (color) density anomaly (left) and along-gulf velocity (right) in different across-gulf sections at the y-coordinate values indicated. Positive mean velocities are in the northward up-gulf direction.

east side and 100-120 m on the west side. North of the sill at y=1014 km there is a CTW mode 1 structure in the rms field of both velocity and density on the east side. On the west side, the variability is very weak. North of AGI at y=1107 km the rms velocity and density do not exhibit a trapped-wave like structure. Instead, the maximum rms values are found 75 km off the coast on the shelf break, with very small values on both sides. In general the alongshore velocity rms is higher on the east side than on the west side. The rms values of velocity and density on the west side are larger south of the steering point than in the north, consistent with the incident wave turning and propagating southward along the west side.

The larger sea level disturbances in Fig. 3.5 are elevation waves with associated alongshore velocities in the direction of the propagation of the signal. The time mean along-gulf velocity (Fig. 3.10) produced by the incident waves is negative (southward) along the east side next to the coast (y<900 km). On the west side the mean values are weaker and more irregular, but are generally positive (northward) at y=594 and 804 km. Consequently, the mean residual circulation shows a dominant contribution of depression waves. In the idealized experiments described in Part 2 it was found that the phase speed is dependent on the amplitude of the wave and the magnitude of the mean currents produced by the wave vary inversely with the phase speed. Depression waves propagate slower than elevation waves of the same amplitude and their contribution to the mean circulation is correspondingly stronger. For typical amplitudes, it takes depression waves 16-28 hrs longer than elevation waves to travel through the Gulf of California. Relatively

strong mean currents are found near the bottom at some sections (y=384, 594, and 1914 km). The formation of the bottom currents seems to be related to the down-slope propagation of disturbances generated as the incident waves pass. The formation of the bottom currents will be discussed in more detail in section 5*d*. North of the sill, the mean density anomaly is positive almost everywhere and is related to net advection of deep water to the north, as discussed in section 5f.

3.6.3. Energy distribution

The along-gulf distribution of kinetic energy integrated over depth and across the gulf $(\Delta y \int \frac{1}{2} \rho_o (u^2 + v^2) dxdz)$ and of integrated potential energy anomaly $(\Delta y \int (\rho - \rho(t = 0)) gzdxdz)$ as a function of time (Fig. 3.11) shows clearly that even though part of the incident CTW propagates north of the sill, no significant wave energy reaches the north gulf. The larger sea level events in Fig. 3.5, propagate along the east side of the gulf with little dissipation of total kinetic energy (Fig. 3.11). Most of the kinetic energy does not continue to propagate northward north of $y \approx 950$ km. Instead, the CTWs turn and continue propagating along the west side with decreased energy. The waves exiting the gulf have substantially less integrated kinetic energy than those entering. The potential energy anomaly shows a distribution similar to the kinetic energy, except that there

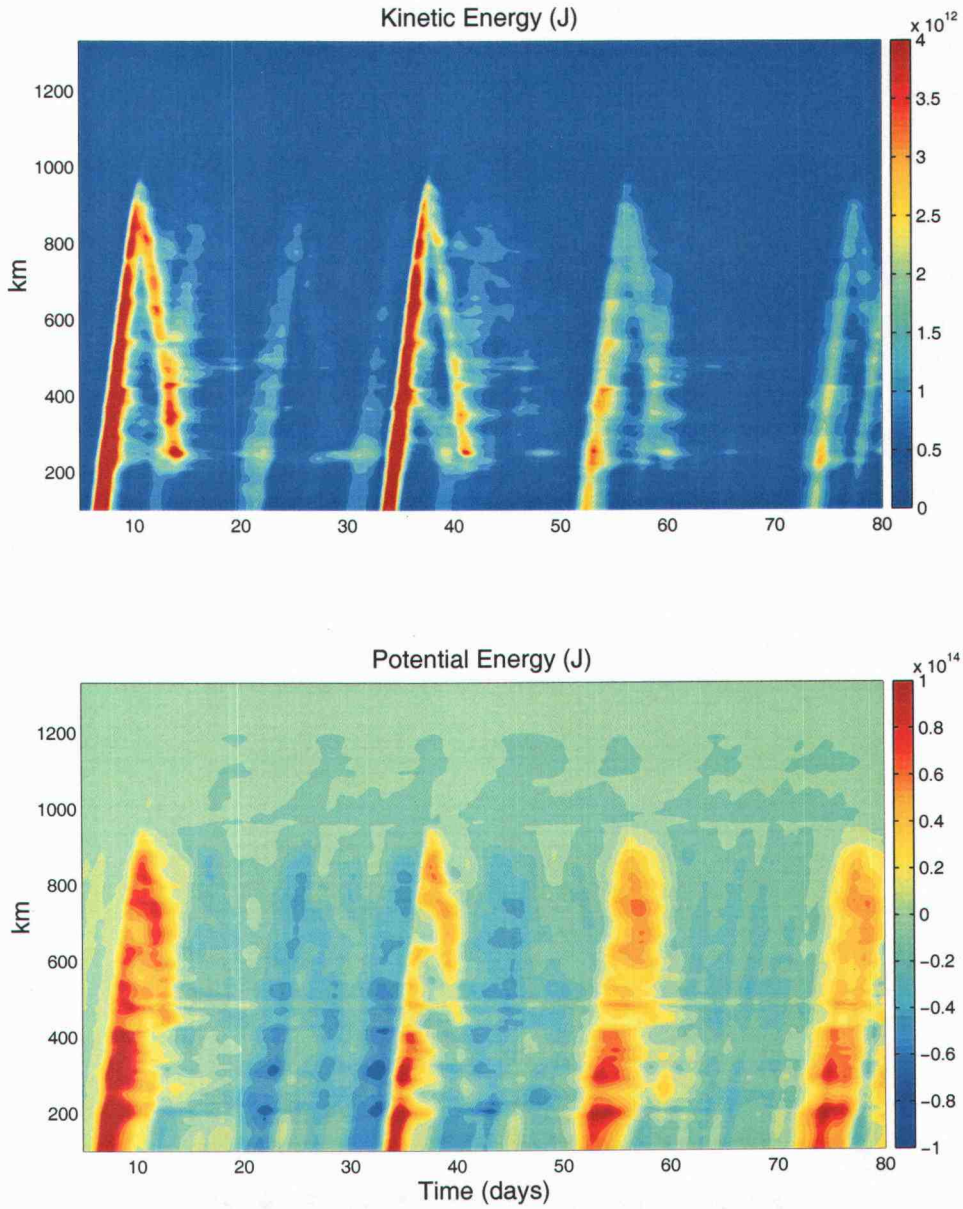

Figure 3.11: Along gulf distribution of depth and across-gulf integrated total kinetic energy $(\Delta y \int \frac{1}{2} \rho_o (u^2 + v^2) dxdz)$ and potential energy anomaly $(\Delta y \int (\rho - \rho(t = 0)) gzdxdz)$ as a function of time.

appears to be relatively less potential energy propagating southward. In addition, the time scale seems to be larger in the potential energy fluctuations compared with the time scales of the kinetic energy variations.

The spatial distribution of the temporal mean external potential energy ($EPE = \frac{1}{2}\overline{\rho_o g \eta^2}$) where η is the surface elevation and the overbar represents a time average, in Fig. 3.12 illustrates the behavior of the sea level fluctuations. Large values of mean external potential energy (EPE) are found trapped near the coast along the east side. North of y= 1050 km the mean EPE is not trapped near the east coast and it extends across the north gulf. Along the western Baja California side, EPE is much weaker than along the east side. The CTWs traveling southward along the Baja California peninsula have decreased their amplitudes by 50%. The distribution of EPE across the gulf for y> 1100 km indicates that there are disturbances in the north that are no longer confined to the coast. The temporal mean external kinetic energy ($\frac{1}{2}\overline{\rho_o D(U^2+V^2)}$) where D is the total depth of the water column, $(U,V) = D^{-1}\int_{z=-h}^{z=\eta}(u,v)dz$ and ρ_o=1000 kg m^{-3}, shows a different pattern (Fig. 3.12). The mean values of external kinetic energy (EKE) are large near the coast along the east side from the entrance to the sill at y=900 km. Smaller but still appreciable values of EKE are also found near the coast along the west side south of y=950 km with noticeably reduced magnitude present south of y=600 km. Little mean EKE is present north of y=950 km. The differences in behavior of the mean EPE and mean EKE north of y=950 km is presumably related to scattering of

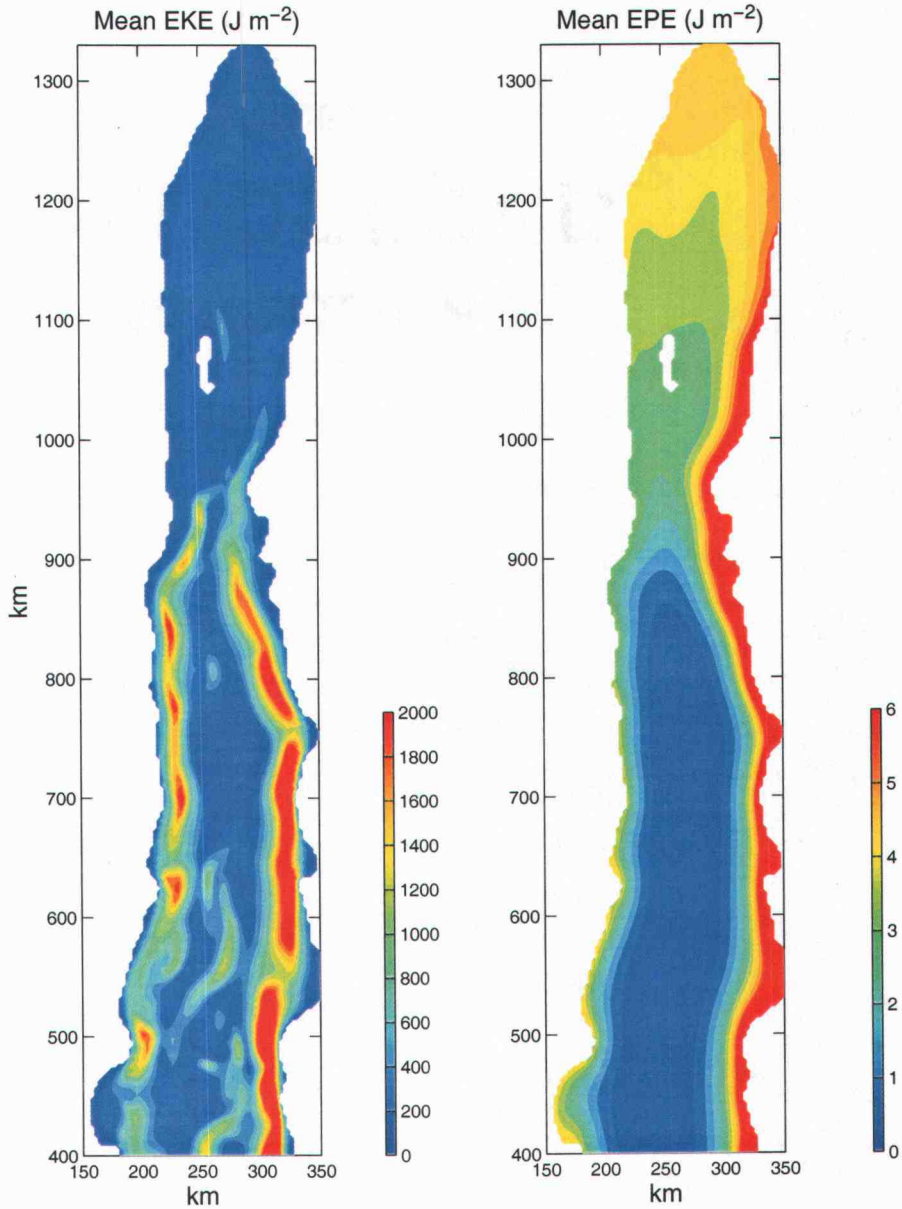

Figure 3.12: Temporal mean external potential energy $EPE = \frac{1}{2}\overline{\rho_o g \eta^2}$ (right) and mean external kinetic energy $\frac{1}{2}\overline{\rho_o D(U^2 + V^2)}$ obtained from the depth-averaged velocities (left).

incident CTW energy at the sill into wave motions with different physical characteristics.

The along-gulf distribution of the temporal mean kinetic energy KE integrated over depth and across the gulf (and in y over one grid cell Δy) is shown in Fig. 3.13. Also shown is the corresponding kinetic energy density, which is KE divided by the local across-gulf area times Δy. South of the gulf, the values of KE are fairly uniform along the gulf. In the vicinity of the sill, between y=800 and 1000 km, KE decreases by 80% compared to the values in the south. The nearly uniform distribution of KE south of the sill indicates that substantial energy loses do not occur in the south gulf. North of the sill, the mean KE represents a small fraction of the energy content in the south. The kinetic energy density also is very uniform in the south gulf increasing to the largest value near the sill. In the north gulf, the values of the KE density are about 50% of the values south of the sill. For comparison, results from a similar calculation of KE and KE density obtained from a numerical experiment of wind-driven circulation in the gulf (Martinez and Allen, 2002c) are also plotted in Fig. 3.13. The values of KE produced by wind-forcing and by incident CTW's are comparable, with similar values north of the sill, but with generally larger KE due to wind forcing in the south. In the vicinity of the sill the contributions of CTWs to mean KE are larger than for the wind as shown clearly in the KE density plot.

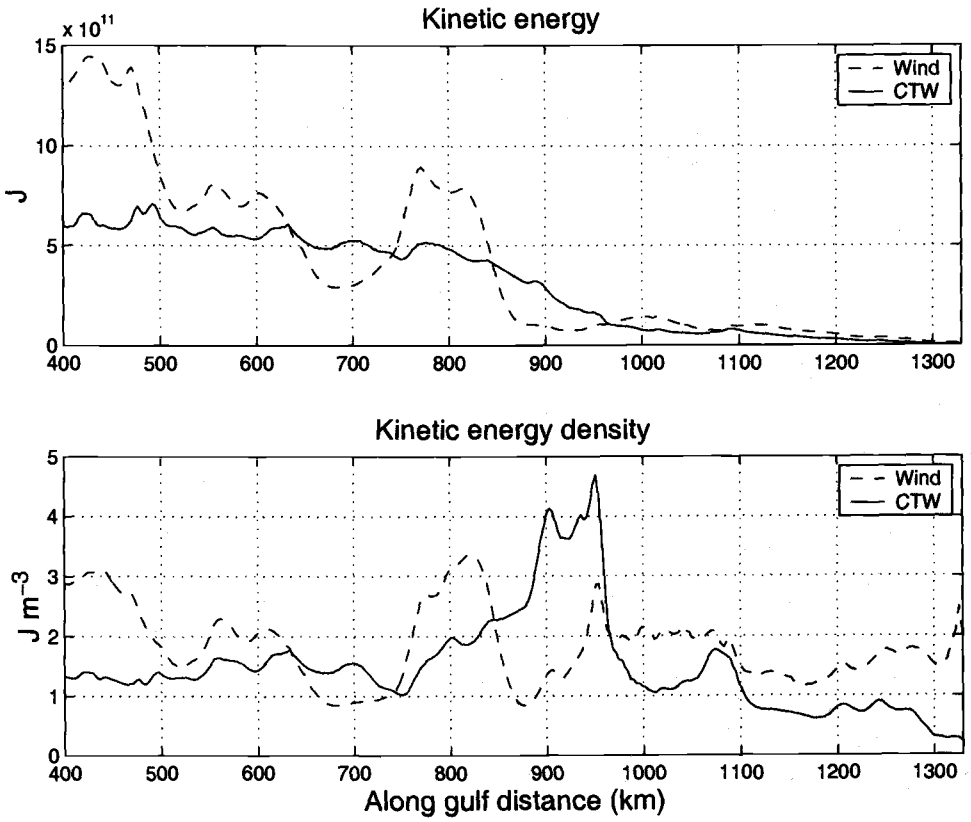

Figure 3.13: The along-gulf distribution of the temporal mean kinetic energy KE integrated in depth and across the gulf (and in y over one grid cell Δy) for the CTW forcing (solid line) and for the wind-driven experiment in Martinez and Allen (2002b) (dashed line). Also shown is the corresponding kinetic energy density which is KE divided by the local across-gulf area times Δy.

3.6.4. Bottom currents

There is a significant mean circulation developed near the bottom of some sections, mainly in the south gulf (Fig. 3.10). The formation of bottom currents in the south gulf seems to be related to the generation by the passing CTWs of energetic disturbances near the coast that propagate down-slope. Two sequences in time of across-gulf sections of along-gulf velocity at y=564 km are shown in Fig. 3.14. On day 9, an elevation CTW passes the section with northward velocities of about 30 cm s^{-1} near the coast. One day later the "tail" of the wave crosses the section, but on day 11 a separation from the coast of the northward velocity begins to occur with southward currents developing next to the coast. The core region of northward velocities begins to propagate down-slope, and by day 12 it reaches the bottom. After day 13, the northward bottom currents intensify for the next 3 days reaching magnitudes of over 25 cm s^{-1}. The northward bottom currents begin to decrease on day 17 such that by day 20 the magnitudes have decreased to about 9 cm s^{-1}. When elevation CTWs arrive on the west side with southward velocities a similar separation process following the wave passage seems to occur, but no down-slope propagation is observed. The formation of bottom currents by down-slope propagating events is dependent on the amplitude and sign of the passing CTW. Depression waves are also able to excite down-slope propagation. When a depression wave passes through the same transect (days 25-29 in Fig. 3.14) a

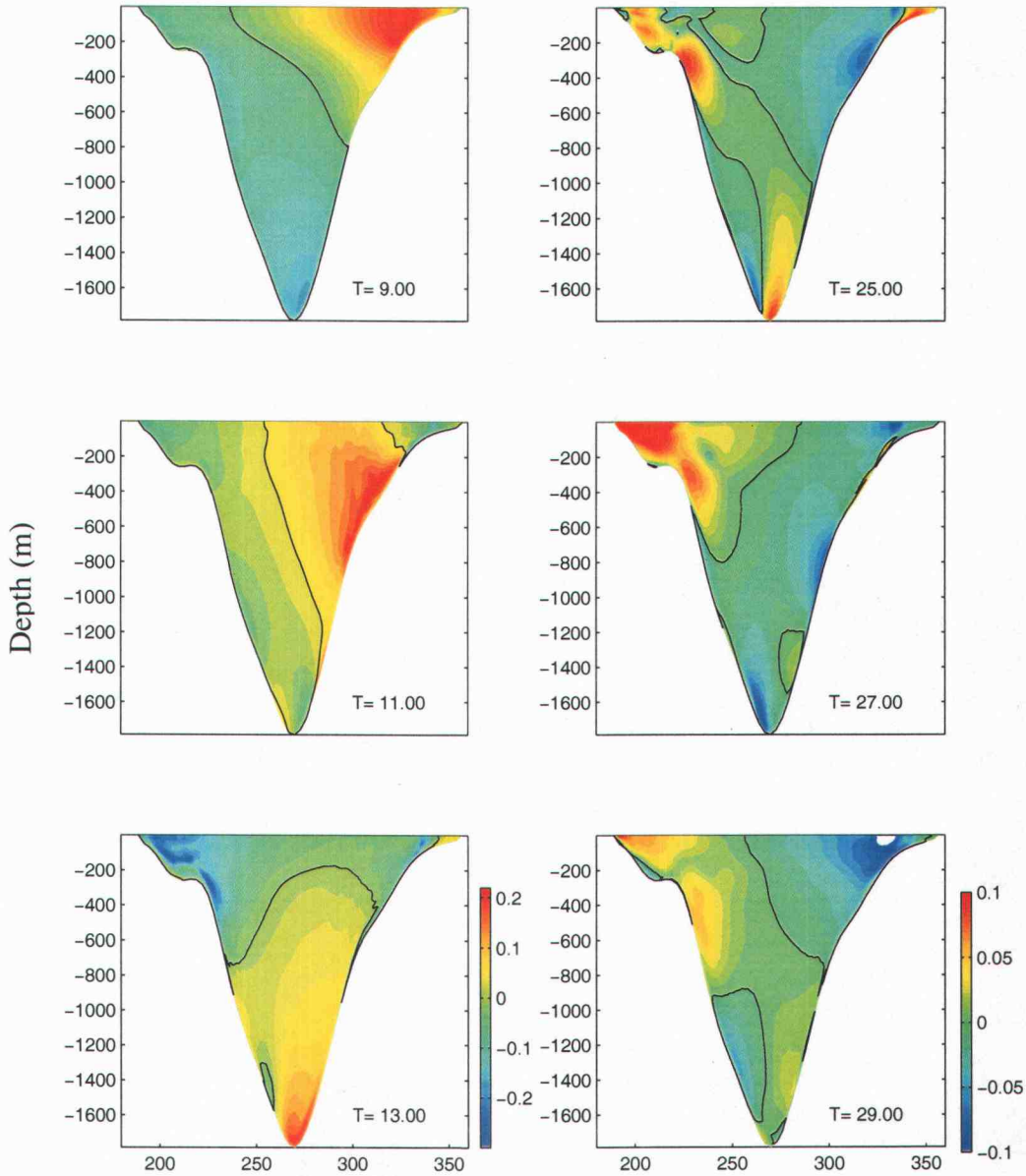

Figure 3.14: Across-gulf sections of the along-gulf velocity at y=564 km on days 9, 11 and 13 when an elevation wave is passing on the east side and on days 25, 27 and 29 when a depression wave is passing on the east side. The contour-line represents zero velocity. Positive values are in the northward up-gulf direction.

similar separation occurs. On day 25, the "tail" of a depression CTW begins to separate in a manner analogous to the elevation CTW on day 11. A core region of negative southward along-gulf velocity begins to propagate down-slope and a narrow northward current develops next to the coast. The core region of southward velocities has propagated to depth around 800 m by day 27 but subsequently loses energy and is not found near the bottom on day 29. In these examples, stronger currents result near the bottom following the passing of the elevation CTW. This relative behavior is typical and leads to the northward mean near bottom currents shown in Fig. 3.10.

Similar separation and down-slope propagation occurs in other sections, but the separated current core does not always reach the bottom even for elevation CTWs. In a set of experiments involving idealized propagating CTWs in Part 2, the same behavior is observed. The formation of down-slope propagating disturbances occurs for both elevation and depression CTWs, but when the passing wave is a depression CTW the down-slope propagating disturbances typically dissipates before reaching the bottom. Longer CTWs generate larger down-slope propagating disturbances. The dynamics of the down-slope propagating disturbances require further investigation but they may have properties similar to the low frequency vertically propagating coastal Kelvin waves studied theoretically by Romea and Allen (1983).

3.6.5. Nonlinear effects

Different mechanisms for the dissipation of CTWs in the Gulf of California have been proposed. Wave breaking was proposed by Christensen et al. (1983), but Gjevick and Merrifield (1993) concluded that for realistic wave amplitudes nonlinear effects should be negligible. In the study of idealized incident CTW propagation in the gulf described in Part 2, evidence is found for nonlinear effects in CTWs with realistic amplitudes and time scales. Specifically, for incident single wave pulses it is found that the propagation velocity increases with wave amplitude, that elevation waves with realistic positive amplitudes in sea level steepen at the front of the wave whereas negative amplitude depression waves steepen at the rear, and that large amplitude long period waves produce separation in the currents as they pass.

The displacement of isopycnals is much larger and opposite in sign to the change in sea level for a CTW mode 1. The time evolution of isopycnals on the 200 m isobath shows some interesting features (Fig. 3.15). Sea level elevations are accompanied by depressions of the isopycnals. There are several events that show steepening as the signal moves northward along the east side. One is the large sea level event around day 8 (Fig. 3.5) that appears as a very steep front in density at y=384 km followed in time by small-scale disturbances. Evidently some energy is dissipated as the wave propagates to y= 564 km since the isopycnal depths are smoother at that location. As the signal continues north, it steepens again and at

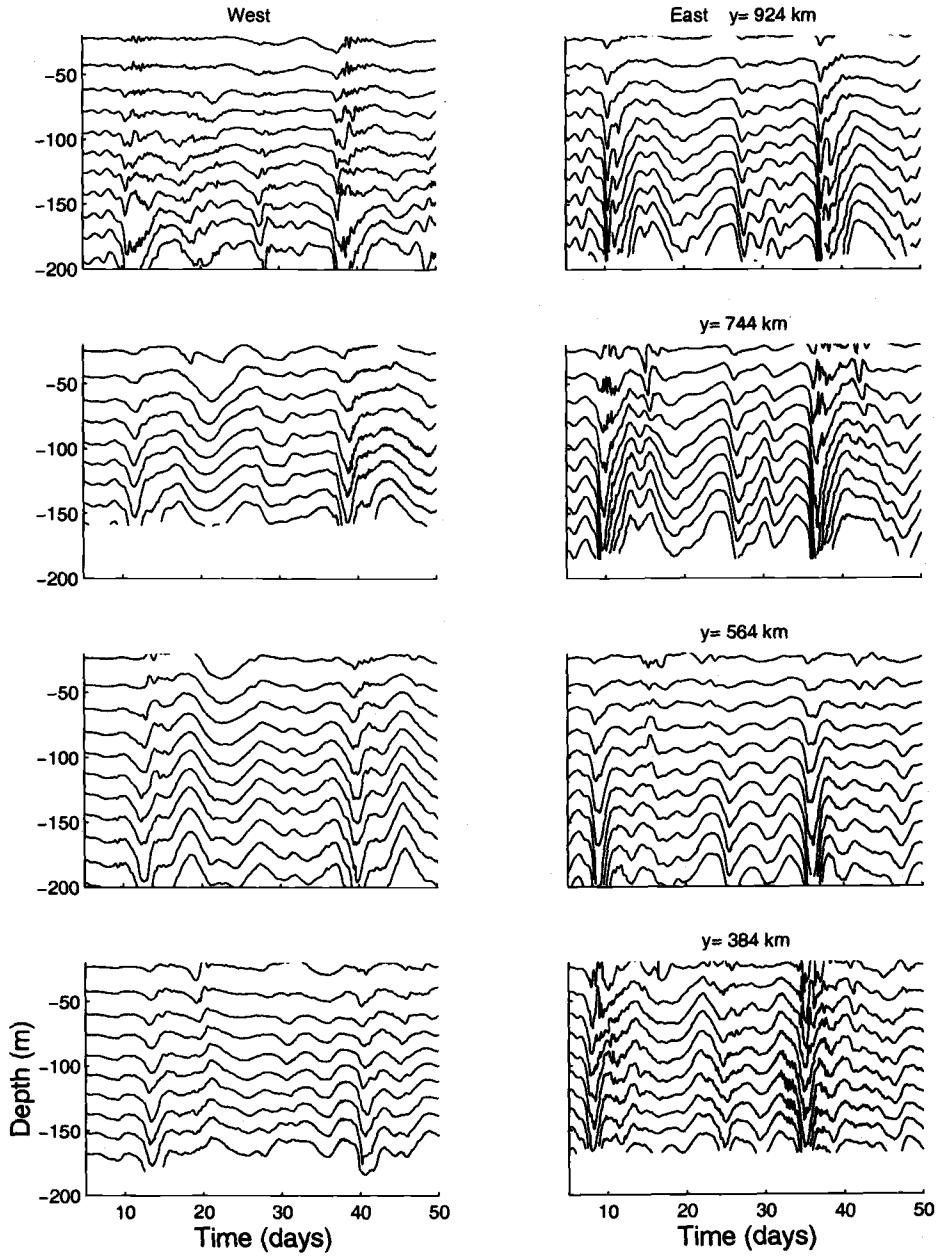

Figure 3.15: Time series of the depth of isopycnals along the 200 m isobath at the indicated values of y. The panels on the left are for the west side and the panels on the right are for the east side of the gulf. The chosen isopycnals have a uniform distribution of initial depth as shown most clearly for small time at y=384 km on the west side.

y=744 km some small-scale disturbances are evident. When the wave arrives at the sill y=924 km, the signal has a large slope at the front, but the magnitude of the small-scale disturbances are smaller. Similar evolution occurs for the signals on days 25, 30 and 52, which steepen as they propagate northward. On the west side, the time variation of isopycnal depths is noisier in general near the sill at y=924. Vertical isopycnal displacements are smaller and smoother towards the south and the steepening is weaker than found on the east side.

The time-dependent behavior for days 30-50 of the terms in the depth-averaged along-gulf momentum equation at six locations on the 100 m isobath along the east side of the gulf is shown in Fig. 3.16. During this time period a large amplitude elevation wave present at y=252 km on days 33-35 propagates in the gulf. The nonlinear advective term makes a significant contribution to the total balance in the gulf between y=444 km and y=826 km. Before the large amplitude elevation wave reaches the gulf (y=252 km) the nonlinear term is relatively small. The primary balance is between the acceleration, pressure gradient and the Coriolis terms. The diffusion term is also appreciable. After the wave enters the gulf (y=444 km) the nonlinear term increases and is the same size as the Coriolis term. The nonlinear term appears to vary on a shorter time scale than the other large terms. As the wave continues to propagate to y=636 km, the overall time scale of the disturbance increases while the relative magnitude of the nonlinear term decreases. Apparently, when the nonlinear terms increase some sort of short waves are produced, dispersing the original disturbances and decreasing the nonlinearities. In

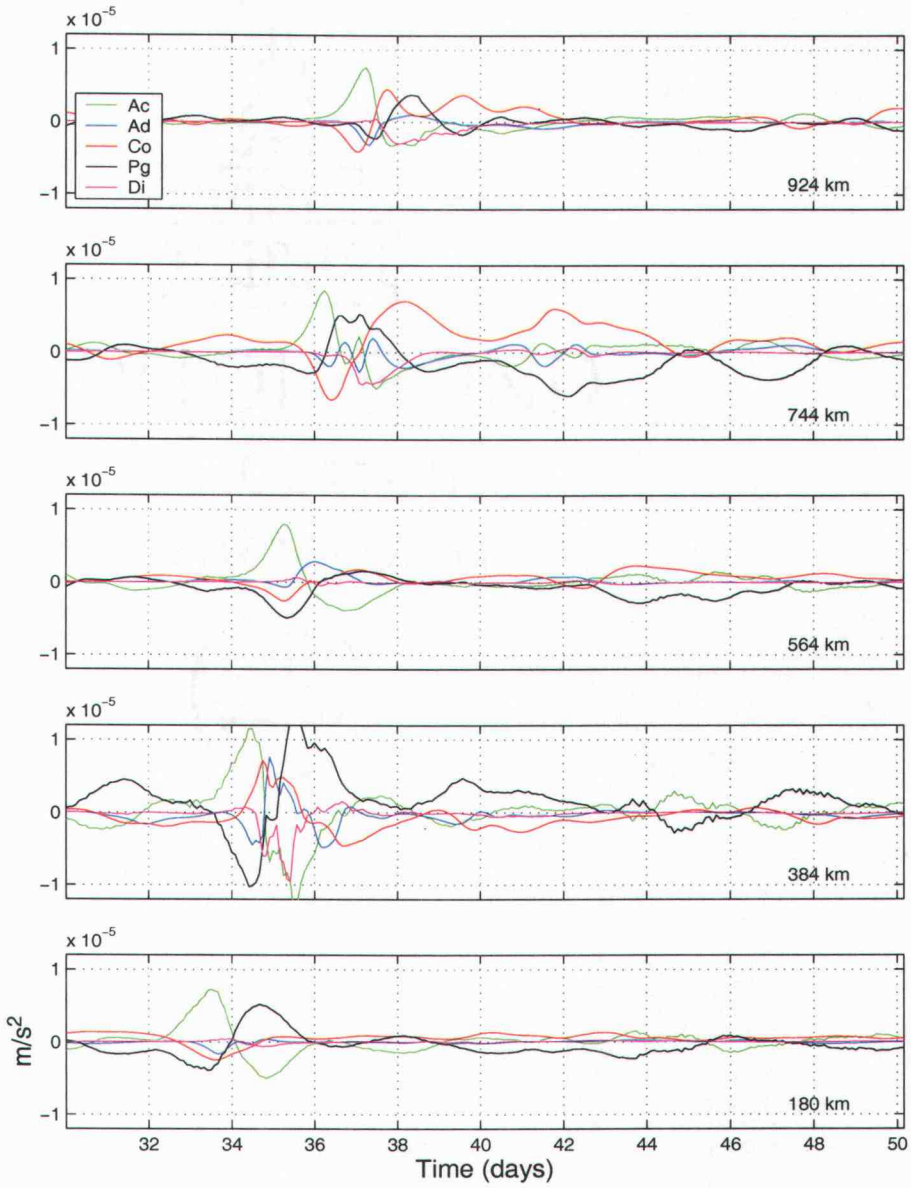

Figure 3.16: Time series of terms in the depth-averaged along-gulf momentum equation at six locations on the 200 m isobath along the east side of the gulf. The lower panel is from a location (y=252 km) south of the entrance to the gulf which is at y=300 km. The sill begins at y=828 km. The upper panel at y=1212 km is located north of the sill. Ac-Acceleration, Ad-Advection, Co-Coriolis, Pg-Pressure gradient, and Di-Diffusion terms.

the north gulf away from the sill $y \geq 1020$ km, the relative contribution of the nonlinear terms is small and the balance is between acceleration, pressure gradient, and Coriolis force terms.

3.6.6. Density balance

CTWs are able to redistribute water masses. The effects of idealizad incident CTWs in the gulf have been investigated in Part 2. An elevation CTW produces a flux of dense water out of the gulf, resulting in a small warming. Density decreases along the gulf except in the north (y>1200 km). A depression CTW has the opposite effect, pumping warm water out of the gulf. The density increases along the gulf except in the north (y>1200 km). The equation for the evolution of the density may be written as

$$\frac{\partial \rho}{\partial t} + \nabla \bullet \rho \underline{v} = \nabla_H \left(A_H \bullet \nabla_H \rho \right) + \frac{\partial}{\partial z} \left[K_H \frac{\partial \rho}{\partial z} \right], \qquad (3.6.1)$$

where A_H and K_H are the horizontal and vertical diffusion coefficients, $\underline{v}=u\underline{i}+v\underline{j}+w\underline{k}$ and $\nabla_H = (i\partial_x + j\partial_y)$. Fig. 3.17 shows the time mean of the terms in (3.6.1) integrated in the across-gulf direction and in depth (e.g., $T^{-1}\Delta y \int(\rho_t)dtdxdz$) as a function of y. The change in integrated density anomaly is negative south of the sill and positive north of the sill. The distribution of density anomaly indicates that elevation CTWs

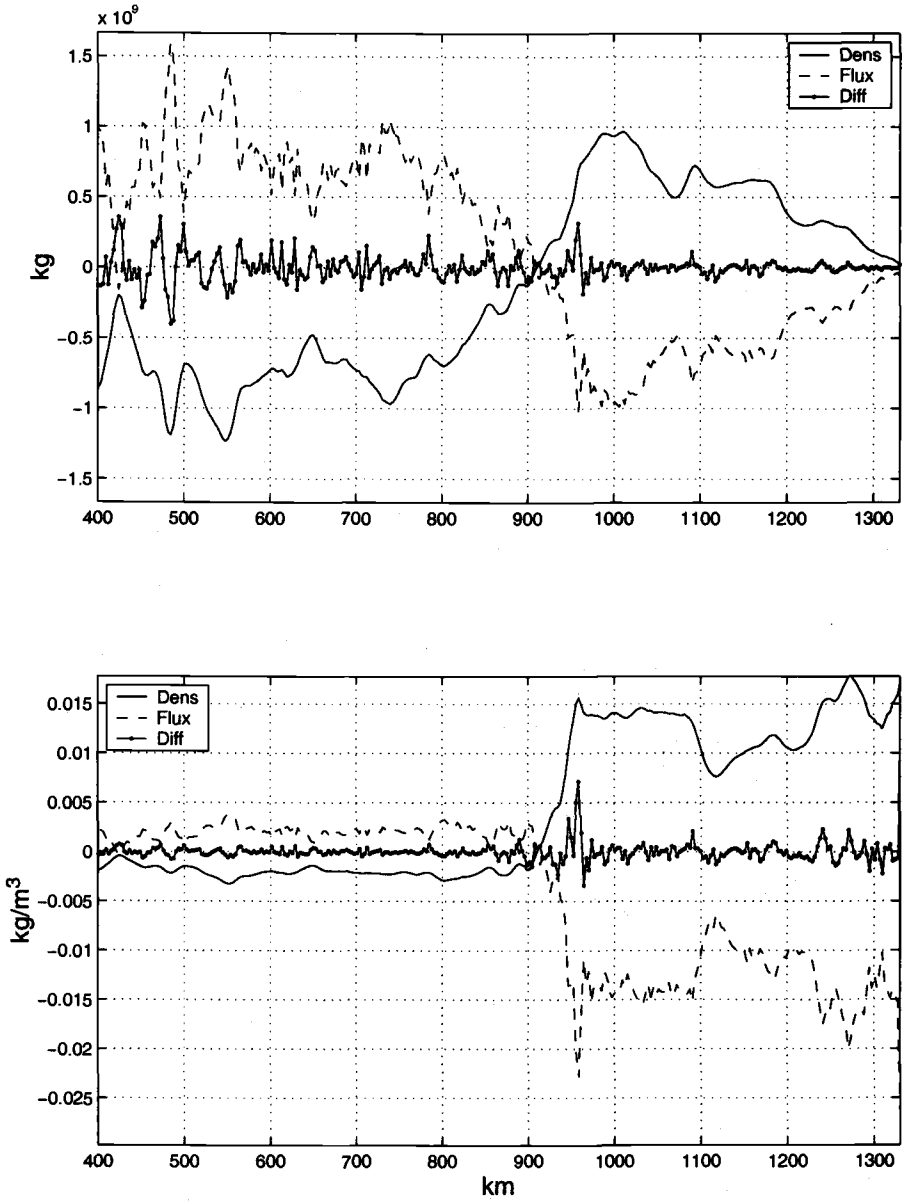

Figure 3.17: The along-gulf distribution of the balance of density integrated in the x-z direction along a section of width Δy. The solid line represents the change in density relative to the initial value; positive values indicate sections where density has been increased. The dashed line is the flux of density and the dotted line is the diffusion of density.

dominate the flux of density in the south gulf while depression CTWs dominate north of the sill. The diffusion of density plays a minor role in the balance, but is larger in the south gulf. The same balance divided by the across-gulf volume (Fig. 3.17), shows that the changes in average density north of the sill are larger than those south of the sill.

3.7. Summary

The propagation of remotely forced CTWs in the Gulf of California is investigated using a three-dimensional primitive equation model. The evolution in the gulf of an incident CTW mode 1 with realistic time-dependent amplitude is studied for 80 days during summer 1984. The correlation between model variables and observations is reasonably good for sea level, but lower for currents. The favorable agreement between model and observations supports the importance of remote forcing in the Gulf of California. With the absence of flows produced by other forcing mechanisms, the model does not adequately represent the observed decrease in correlation of sea level fluctuations from a station at the entrance of the gulf with sea level at other stations in the central gulf, particularly at Santa Rosalia. Incident waves propagate northward along the east side in the south gulf. At the sill, the CTWs are steered and split into two waves (Fig. 3.8). The wave that enters the north gulf contains just a small fraction of the total incident energy (<20%) and

is dissipated (Fig. 3.11). The other wave turns and propagates southward along the west side with its energy appreciably reduced (Fig. 3.11 and 3.12). Some energy is scattered into down-slope propagating disturbances (Fig. 3.14). For elevation waves these disturbances produce relatively intense bottom currents. For depression waves, the down-slope propagating signal is weaker and more rapidly dissipated.

Nonlinear effects are found to be important for CTWs with large, but realistic amplitudes. Nonlinear advection is important in the term balance for the alongshore depth-integrated momentum equation in the large amplitude waves. Large amplitude CTWs steepen as they propagate northward along the east side of the gulf (Fig. 3.15). Some energy is lost through the generation of high frequency disturbances which appears to decrease the steepening. CTWs are also able to redistribute properties. In particular the density field is modified by the incident CTWs. The density of the water in the north is increased while that in the south is decreased (Fig. 3.17). North of the sill the mean integrated kinetic energy produced by the CTWs is small compared to that in the south, as most of the incident wave energy turns at the sill and propagates southward along the west side. The mean integrated external kinetic energy along the west side in the south gulf is significantly reduced compared to that found in the incident waves along the east side. The CTWs that leave the gulf at the southwest corner have only a small fraction of the incident wave energy.

3.8. Acknowledgments.

This research was supported by the Office of Naval Research (ONR) Coastal Dynamics Program through Grant N00014-93-1-1301. In addition, A.M. was partially supported by a Fulbright-LASPAU scholarship and by the Facultad de Ciencias Marinas UABC. The use of computational resources (CM500e's) provided by the College of Oceanic and Atmospheric Sciences and facilitated by ONR grant N00014-99-1-0040 and by NSF grant OCE-952095b (both to A. Bennett) was indispensable for the completion of this research and is gratefully acknowledged. We thank M. Merrifield and C. Winant for providing the velocity and bottom pressure measurements described in Merrifield and Winant (1989). The authors also thank C. Vandetta and T. Leach for assistance with computer use and P. Newberger for initial help with the POM model.

Chapter 4

A Modeling Study of Coastal-Trapped Wave Propagation in the Gulf of California. Part 2, Response to Idealized Forcing

Antonio Martinez and John S. Allen

Submitted to *Journal of Physical Oceanography*

4.1. Abstract

The propagation of idealized incident coastal trapped waves in the Gulf of California is investigated using a hydrostatic primitive equation model (POM). The incident waves are idealized as a single disturbance characterized by an amplitude and a time scale, which are varied in a set of different experiments. Our results show that incident waves propagate northward up-gulf along the east side with no significant change. At the sill, which is 600 km north of the entrance, the waves splits and most of the energy is steered to the west side where it propagates southward down-gulf with decreased amplitude (50%). A small fraction (10-20 %) of the incident energy enters the north where is dissipated. Sea level at the entrance of the gulf is well correlated with sea level everywhere inside the gulf. In contrast, correlations of depth-averaged velocity between Topolobampo (close to the entrance of the gulf) and locations around the gulf decrease along the propagation path of the wave. Most of the dissipation of wave energy in the gulf takes place through bottom friction in the vicinity of the sill. Incident waves with large, but realistic, amplitudes exhibit some nonlinear properties. Phase speeds increase as the amplitudes of the incident waves increase. Elevation waves steepen. On the east side, large amplitude elevation waves produce a down-gulf current adjacent to the coast such that the up-gulf currents associated with the wave separate from the coast. The separation process seems to be connected with subsequent down-slope propagation of energy. Eddies with a spatial scale of 50-80 km are generated by

long time scale or large amplitude waves. Elevation waves can generate energetic anticyclonic eddies.

4.2. Introduction

Free coastal trapped Waves (CTWs) generated by hurricanes along the Pacific coast of Mexico have been observed propagating northward and entering the Gulf of California (GOC) (Christensen et al, 1983; Enfield and Allen, 1983; Merrifield, 1992). These waves typically have periods of 4 to 20 days and sea level amplitudes at the coast of 20 to 30 cm. Inside the gulf the waves are modified, as they are not observed on the Pacific side of the Baja California peninsula. In this two part study the evolution of remotely forced CTWs in the Gulf of California is investigated using a hydrostatic primitive equation model (POM). In Part 1 (Martinez and Allen, 2002a) the model is forced by an incident mode 1 coastal-trapped wave (CTW) with time dependent amplitude derived from sea level observations south of the gulf during the 80 day period July 5 to September 23 1984. It is found that the propagation and scattering of CTWs in the gulf are strongly affected by topography and coastline variations. In the southern gulf, incident CTWs (hereafter designated ICTWs) propagate with no appreciable change in properties, although some of the incident wave energy is lost. The possible mechanisms that can drain energy from the wave include bottom friction,

breaking, scattering into higher modes, interactions with the local circulation, and generation of other features such as eddies or residual currents. At present there are no detailed studies about the possible role of these mechanisms in association with CTW propagation in the gulf. In Part 2 we complement the simulation in Part 1 by analysis of a set of experiments in which we vary the amplitude and the time scale of idealized incident wave pulses with single-signed displacements in coastal sea level. We study the behavior of the wave propagation in the gulf as a function of incident wave amplitude and time scale and attempt to identify the mechanisms by which energy is lost. An outline of the paper is as follows: the model formulation and the numerical experiments are described in section 2. Basic characteristics of the propagation and nonlinear effects are discussed in sections 3 and 4, respectively. A summary is given in section 5.

4.3. Model

We use the Princeton Ocean Model (POM) for the hydrostatic primitive equations (Blumberg and Mellor, 1987). The model domain and the model parameters are the same as in Part 1. The y coordinate is aligned in the along-gulf direction and is oriented towards the northwest, generally along the Baja California peninsula (Fig. 4.1). The orthogonal x coordinate has an across-gulf orientation, directed towards the northeast. The velocity components in the (x,y) direction are

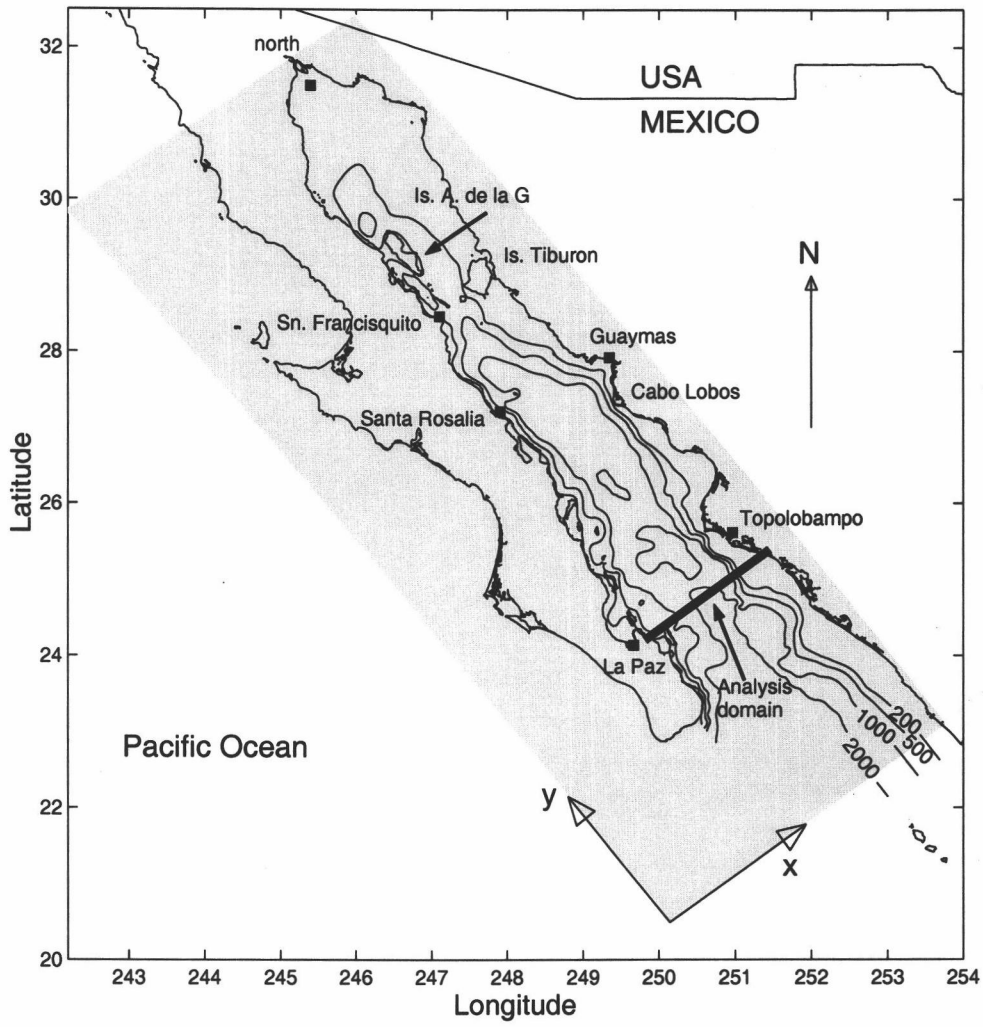

Figure 4.1: The Gulf of California and geometry of the numerical domain shaded in gray. Results presented are obtained primarily from analysis inside the gulf. The thick line across the gulf in the south at y=400 km shows the southern extent of the analysis domain.

(u,v). The open boundary conditions are applied as discussed in Part 1. A wave-maker is prescribed at the southern boundary following the method used by Wilkin and Chapman (1990). The along-gulf velocity and the density are specified along the south boundary as a function of the across-gulf coordinate x, the vertical coordinate z, and time. The spatial distribution of velocity and density are obtained using the linear CTW model of Brink and Chapman, (1987). No other forcing (wind or buoyancy flux) is utilized in these experiments.

Waves generated south of the Gulf of California have been observed propagating poleward along the coast (Christensen, et al. 1983; Enfield and Allen, 1983). The observed phase speed is consistent with a CTW mode 1. To simulate incident waves at the south boundary, we specify the normal along-gulf velocity v and the density ρ,

$$v_{bdry} = R_v(x,z)\phi(t), \tag{4.3.1a}$$

$$\rho_{bdry} = R_\rho(x,z)\phi(t), \tag{4.3.1b}$$

where $\phi(t)$ is the time variability and $R_v(x,z)$, $R_\rho(x,z)$ are the appropriate mode 1 structures calculated using the linear CTW model of Brink and Chapman (1987). In Part 1 (Martinez and Allen 2002a), the time variability $\phi(t)$ is obtained from observed sea level data at Acapulco south of the gulf. In this study we want to

investigate the propagation of idealized incident waves. To do this, we choose the time variability to represent a single isolated pulse given by

$$\phi(t)=A\,sech^2(\alpha-\omega t), \tag{4.3.2}$$

where A is the amplitude, ω^{1} the time scale, and α a constant chosen so that the wave amplitude at the boundary increases smoothly in time.

To study the propagation characteristics of CTWs in the Gulf of California we conduct several experiments. The experiments can be divided in two sets: 1) single pulses with realistic topography and coastline and 2) single pulses with idealized topography and coastline. The amplitudes of the simulated incident CTWs, in terms of the displacement of sea level at the coast at Topolobampo (y=470 km), are ±2, ±16, ±22, and ±30 cm and include values that represent very small waves and larger values that are typical of the observed events. Note that we use the terminology wave amplitude for the *signed* sea level displacements in the incident waves. We consider both elevation waves, with positive sea level displacements and positive amplitudes, and depression waves, with negative sea level displacements and negative amplitudes. Specified time scales range from 2-16 days and are consistent with the time scales of observed events.

4.4. Propagation characteristics

4.4.1. Amplitude dependence

For a large amplitude incident wave pulse of elevation (+30 cm) with a time scale of 4 days we plot the maximum lagged correlation of sea level at Topolobampo (y=470 km) with other locations in the gulf in Fig. 4.2. The lag time in days for maximum correlation is also shown. The lags show that the wave propagates northward along the east side, turns in front of Santa Rosalia near y=850 km, and continues propagating southward along the west side. After a lag of 4.5 days, the wave is at y= 500 km on the western side of the gulf. A corresponding depression wave of the same amplitude and time scale takes an extra 44 hrs to propagate to the same location. That is, the depression wave propagates more slowly and spends almost two more days in the gulf.

The maximum sea level correlations between Topolobampo (y= 470 km) and coastal stations inside the gulf at Guaymas (y= 780 km), north gulf (y= 1330 km), Santa Rosalia (y= 800 km), and La Paz (y= 470 km) (see Fig. 4.1) as a function of the amplitude of an ICTW with a time scale of 4 days are summarized in Fig. 4.3. The sea level signal is not strongly modified between Topolobampo and Guaymas, as indicated by the fact that the correlation is high and uniform for any ICTW amplitude. North of Guaymas, the wave divides into two parts: 1) a small fraction of the energy continues to propagate northward along the eastern side, and

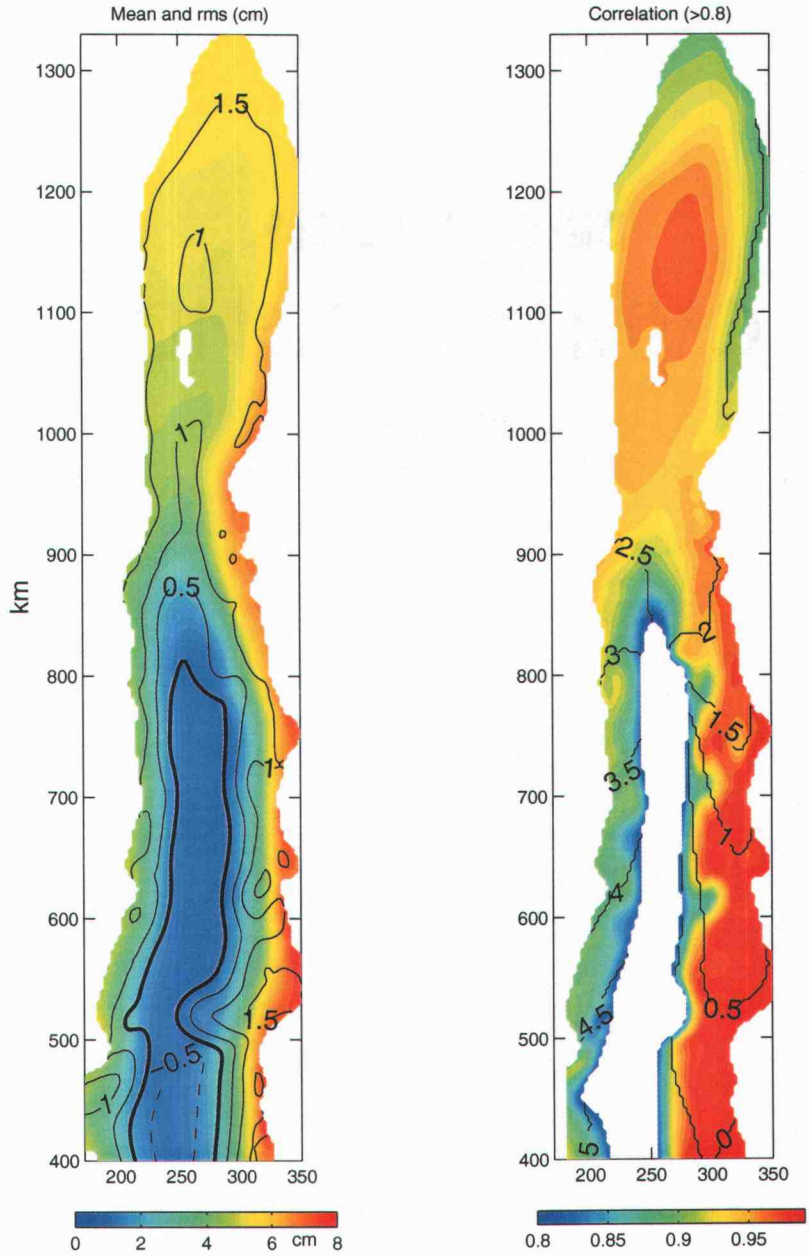

Figure 4.2: Maximum correlations between sea level at Topolobampo (y=470 km) and sea level at other locations in the gulf (color) and the corresponding lags (contour lines) in days for an incident elevation wave with amplitude 30 cm and time scale of 4 days. Only correlations >0.8 are plotted. The contour intervals for the lags are 0.5 days.

2) the rest of the energy propagates southward along the western side (Fig. 4.2). The sea level correlations between Topolobampo and the north gulf station are the lowest of all stations for ICTW amplitudes smaller than 10 cm (Fig. 4.3). The correlations between Topolobampo and Santa Rosalia decrease relative to those between Topolobampo and Guaymas, with larger correlations for smaller amplitude waves. A similar decrease is evident for correlations with La Paz. The corresponding sea level lags (Fig. 4.3) show an increasing propagation speed around the gulf as the wave amplitude increases. Arrival at the north station leads that at Santa Rosalia by 18 hrs, and the lag difference between stations is independent of the amplitude. The lag decreases linearly as the amplitude increases, showing that the phase speed increases approximately linearly with amplitude. After the ICTW passes Guaymas the properties of the wave change. The dispersion diagram for the linear CTW mode 1 in the gulf in Part 1 shows much slower phases speeds in the northern gulf. The distance from Guaymas to the north gulf is about 480 km, so the expected lag for a mode 1 CTW traveling from Guaymas to the north gulf should be much larger than the lag between Topolobampo and Guaymas (35-46 hrs in 312 km), given that the distance is bigger and the phase speed slower. The model phase speeds obtained from sea level, however, are the order of 5.6-6.7 m s^{-1}, that is, twice the phase speed between Topolobampo and Guaymas (1.9-2.6 m s^{-1}).

The magnitude of the complex correlation (Kundu, 1976) of the depth-averaged velocity from water of depth 100 m at Topolobampo with depth-averaged

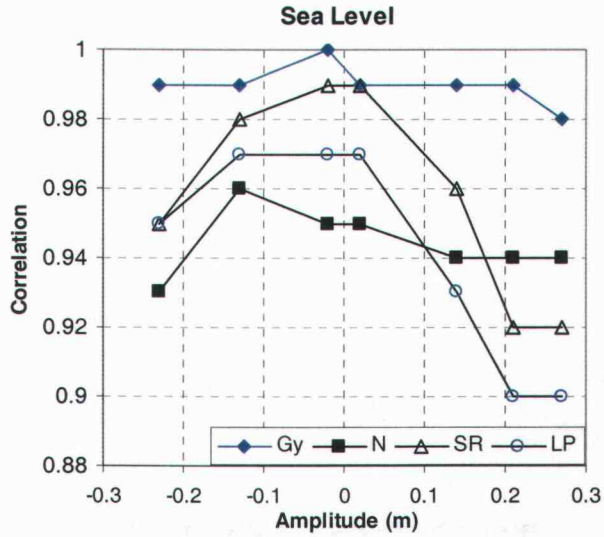

a)

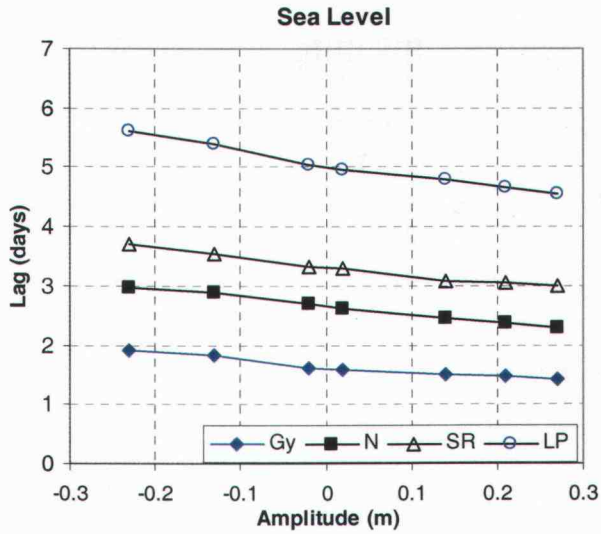

b)

Figure 4.3: Maximum sea level correlations (a) and corresponding lags (in days) (b) between sea level at Topolobampo and sea level at Guaymas (Gy), north gulf (N), Santa Rosalia (SR), and La Paz (LP) as a function of the amplitude of the incident wave at Topolobampo. The incident wave has a time scale of 4 days. Sea level values were taken along the 100 m isobath.

velocities from similar water depths at other locations in the gulf as a function of the amplitude of the ICTW show some differences compared to corresponding correlations of sea level (Fig. 4.4). The velocity signal is strongly modified inside the gulf, resulting in lower correlations than found in the sea level signals. The magnitudes of the velocity complex correlations are typically larger for small amplitudes than for large amplitudes. The correlations at Santa Rosalia on the west coast are higher than those at Guaymas, except for large amplitude waves. At Santa Rosalia, the magnitude of the complex correlation decreases rapidly for large amplitudes suggesting that large amplitude waves are strongly modified at the sill. Differences in behavior of the velocity fluctuations compared to sea level can be seen from the lags (Fig. 4.4). In sea level, the lags show an anticlockwise propagation of the ICTW. For the velocity, the lags show that after the signal passes Guaymas it is subsequently detected at Santa Rosalia, and then La Paz. It arrives in the north gulf last. This indicates that the part of the ICTW that continues to the north gulf and that carries velocity fluctuations has a phase speed reduced by 50%, to about 1.2 m s^{-1}, in agreement with the dispersion relation found in Part 1. The lags at Guaymas, north gulf, and Santa Rosalia, are smaller for small amplitude waves. There is no consistent increase in phase speed with amplitude as seen in the sea level lags (Fig. 4.3). In fact, in the north gulf the lag increases significantly (roughly by 20 hrs) for waves with large amplitude, independent of sign. The relation between velocity lag and amplitude at La Paz is similar to the one obtained for sea level (Fig. 4.3) except that for amplitudes bigger than 12 cm the lag in

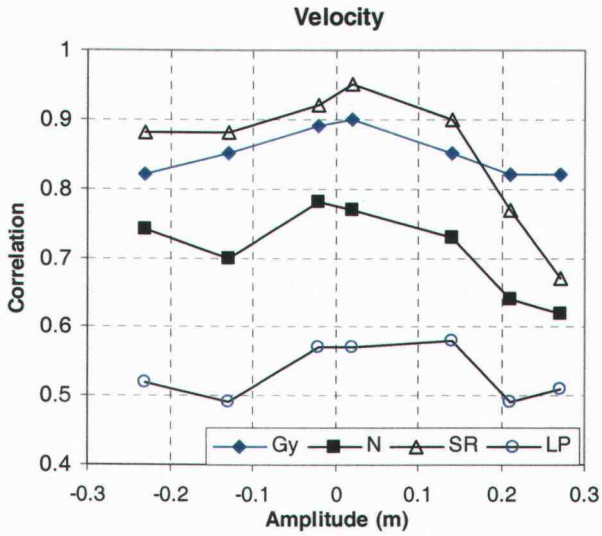

a)

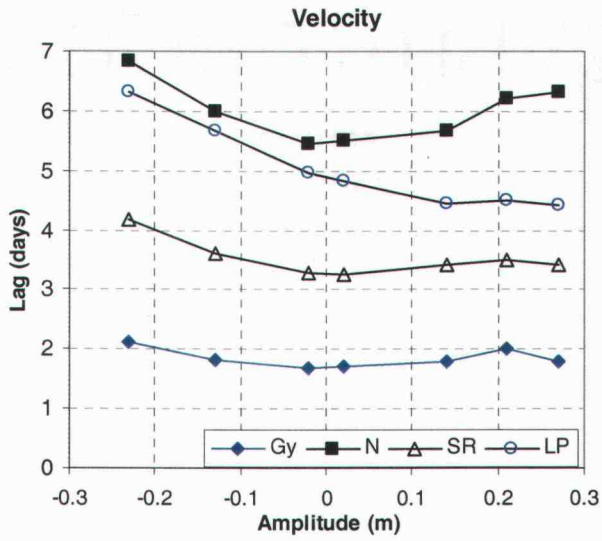

b)

Figure 4.4: Maximum correlations and lags as in Fig. 3 but for the depth-averaged velocities along the 100 m isobath. The maximum magnitudes of a complex correlation coefficient are shown in (a). The correlation sign is reversed at stations N, SR, and LP. The corresponding lags (in days) are shown in b).

velocity remains constant. In general, as for the sea level lag, velocity lag is larger for depression waves. Increasing amplitudes for elevation waves result in increasing lags in the north, and nearly constant lags at the other locations.

The maximum magnitude of the sea level fluctuations decreases as the waves propagate along the gulf (Fig. 4.5). At Guaymas, the magnitude of the wave decreases by 10-20 % depending on the amplitude of the incident wave. At La Paz, the magnitude has decreased by 40-63%. Santa Rosalia sea level amplitude is about 3-7% smaller than at La Paz. The relation between the maximum magnitude of the sea level fluctuations and the magnitude at Topolobampo is more strongly modified for depression waves (Fig. 4.5). Depression wave magnitudes decrease 5-30 % more than those of corresponding elevation waves. Small amplitude waves generally have the smallest decrease in magnitude except in the north gulf.

The change of maximum velocity magnitude (Fig. 4.5) shows that the magnitude of the velocity increases at Guaymas for almost any amplitude. After the ICTW passed Guaymas, part of the wave continues north, but the velocity associated with this wave is relatively small, representing 10-20% of the ICTW velocity at the gulf entrance. Santa Rosalia has a similar variation of velocity magnitude with ICTW amplitude as that found at Guaymas, but with a decrease in the values by 20-40% in relation to Guaymas. The CTW leaving the gulf (close to La Paz) has a velocity magnitude that represents 60-80% of the velocity magnitude of the ICTW at the entrance to the gulf, with higher values found for elevation waves.

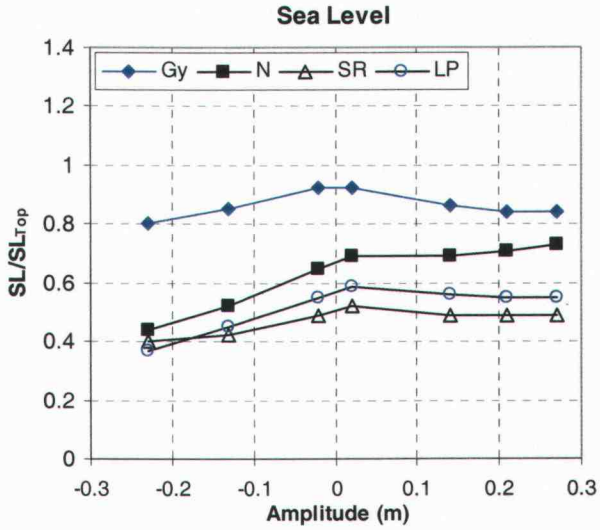

a)

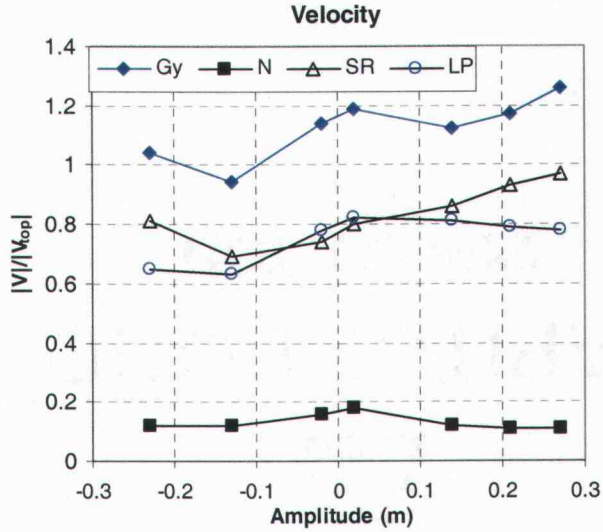

b)

Figure 4.5: Ratios of the maximum magnitudes at the same locations as in Fig. 3 to the maximum magnitudes at Topolobampo of a) sea level ($\eta_i^{\max} / \eta_{Top}^{\max}$), and b) depth-averaged along-gulf velocity ($\left|V_i^{\max}\right| / \left|V_{Top}^{\max}\right|$).

The wave exiting the gulf at La Paz shows a sea level signal almost half the amplitude of the incident wave at Topolobampo (Fig. 4.5), but the correlation does not decay significantly (Fig. 4.3). The decrease in maximum velocity (20%) is not as strong as the one in sea level (50%), but the signal has been strongly modified and is poorly correlated with the ICTW at Topolobampo (Fig. 4.4).

4.4.2. Time scale dependence

To study the evolution of ICTWs inside the gulf as a function of the time scale of the incident wave we consider ICTWs of moderate amplitude (±16 cm at Topolobampo) and we vary the time scale. We consider time scales of 2, 4, 8, and 16 days. For each time scale, elevation and depression waves are studied. The evolution of the ICTW inside the gulf as a function of these time scales shows less sensitivity than found for the amplitude variations in section 3a. Sea level correlations with Topolobampo for these waves (not shown) are generally high. The lowest correlation (0.89) is between La Paz and Topolobampo for a depression ICTW with time scale of 2 days. Correlations for longer waves tend to increase. The corresponding lag does not show any dependence on the time scale of the ICTW and the sea level signal propagates anticlockwise with the north leading Santa Rosalia by 17 hrs.

The velocity is more sensitive than sea level to the time scale of the ICTW. For elevation waves, the correlation decreases as the time scale increases (Fig. 4.6). Guaymas and Santa Rosalia have a similar behavior and are well correlated with the ICTW at Topolobampo. At La Paz, the correlation drops abruptly by 30 to 50 % compared to the correlation at Santa Rosalia. The decreasing correlation for longer waves seems to be related to the generation of eddies and the separation of coastal currents (Section 4). The correlation for depression waves does not change substantially as a function of the time scale (not shown). The lag for elevation waves, with time scales 4 days and less (Fig. 4.6), has a variation similar to that shown in Fig. 4.4, with the signal arriving first at Guaymas, second at Santa Rosalia, next at La Paz, and last in the north (Fig. 4.6). For a time scale of 8 days, the maximum correlation lag is the same for Santa Rosalia and La Paz. Waves with a time scale of 16 days are detected first at La Paz, then at Santa Rosalia. For depression waves, the lag increases as the time scale of the ICTW increases (not shown). In general, for elevation waves the maximum relative sea level and velocity fluctuations increase at almost all stations as the time scale increases.

4.4.3. Behavior in the northern gulf

Interesting behavior is found when the CTW arrives at the sill (y=900 km). The Guaymas basin, located south of the sill, is 2000 m deep. In contrast, north of

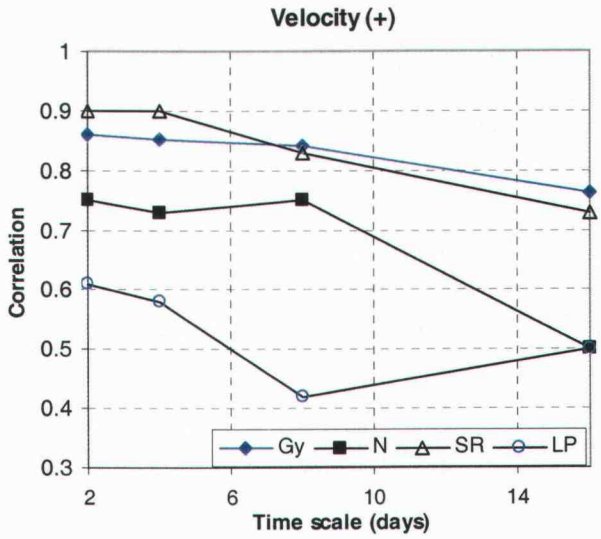

a)

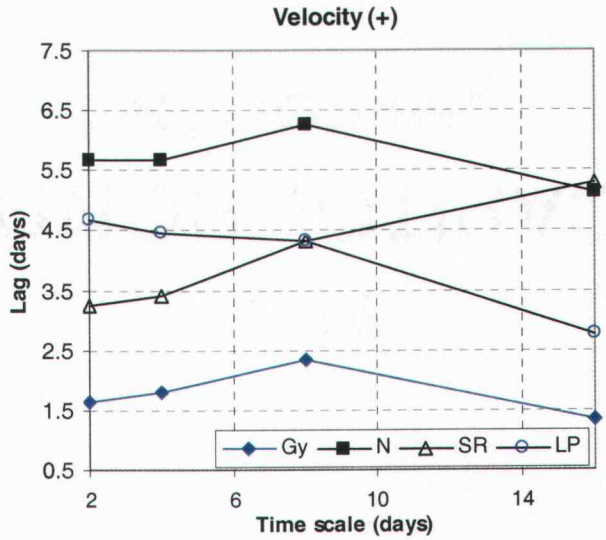

b)

Figure 4.6: Maximum correlations and lags for depth-averaged velocities as in Fig. 4 for incident elevation waves with constant amplitude (+16 cm) as a function of the incident wave time scale.

the sill the gulf is significantly shallower (≈200 m). Shallow depth contours along the east shelf extend to the north gulf. For depths greater than 500 m, however, the contours separate from the east coast and turn south along the Baja California side. We illustrate the behavior in the north gulf by examining the evolution of a large amplitude (≈30 cm) elevation ICTW of time scale 4 days in Figs. 7, 8, and 9. The incident CTW in this case splits into two waves. A small fraction of the energy enters the north gulf and the rest of the wave turns back and propagates southward along the west coast of the gulf. Analysis of sea level and velocity fluctuations in the north gulf suggest the excitation of two wave-like motions with different properties: a fast propagating sea level signal with an average phase speed of about 6 m s^{-1} that arrives at the north gulf station about 24 hrs after the wave passes Guaymas (Fig. 4.3) and a slow velocity signal consistent with a CTW with average phase speed of 1.2 m s^{-1} that arrives at the north station about 4.5 days after the wave passes Guaymas.

The maximum correlation and corresponding lag between sea level at a location on the coast along the east side at y=750 km and sea level at other locations in the north gulf is shown in Fig. 4.7. On the east side south of y=850 km, lines of constant lag extend perpendicular to the coast, with increasing lag toward the north. Off the coast at y=850 km, the phase of the wave shows westward propagation while the phase on the shelf continues to follow the coast. The result is a CTW that is steered, from northward propagation along the east coast to southward propagation along the west coast, about a pivotal point in the center of

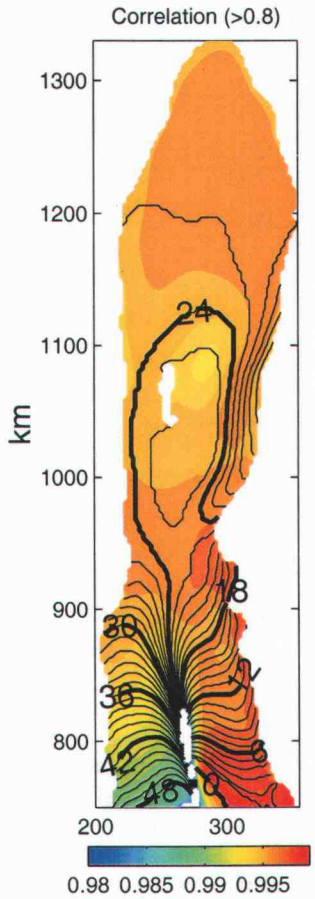

Figure 4.7: Maximum correlations between sea level at a location on the coast along the east side at y=750 km and sea level at other locations in the north gulf (color) and the corresponding lag (contour lines) in hours for an elevation ICTW with amplitude 30 cm and time scale of 4 days.

the gulf. North of Tiburon Island (y=960 km) the correlations are high. The phases show some continued CTW-like propagation along the coast on the east side south of y= 1100 km. The slow-propagating signal on the east side vanishes in the north.

A comparison of the propagation of sea level and velocity signals in the north (Fig. 4.8) reveals features consistent with those discussed in connection with the analysis of correlation coefficients in Figs. 3 and 4. The time-dependent behavior of the velocity field in the north seems to be uncoupled from the evolution of sea level (Fig. 4.8). At day 9, high sea level extends to the north gulf, while the velocity signal is just passing Tiburon island (y=960 km on the east side). By day 10, sea level is already decreasing in the north, while a CTW continues to propagate north along the coast on the east side close to y=1060 km. Finally on day 11, sea level returns to equilibrium and the velocity signal is weak. Evolution of the along-gulf velocity component during the same days (Fig. 4.9) shows a velocity signal north of the sill propagating northward at a slow speed that is not observed for sea level (Fig. 4.8). The velocity signal resembles a CTW strongly modified by topography, with an offshore scale bigger than that of the incident wave south of y=700 km (Fig. 4.9). The velocity signal eventually decays and a signal propagating southward along the west side of the north gulf is not evident.

Bottom friction in the shallow northern gulf has been the most popular mechanism used to explain the observed weakening of ICTWs (Merrifield 1992, Ramp et al. 1997). In Part 1, it was found that just a small fraction of the ICTW enters the north gulf and that dissipation in the north is not enough to explain the

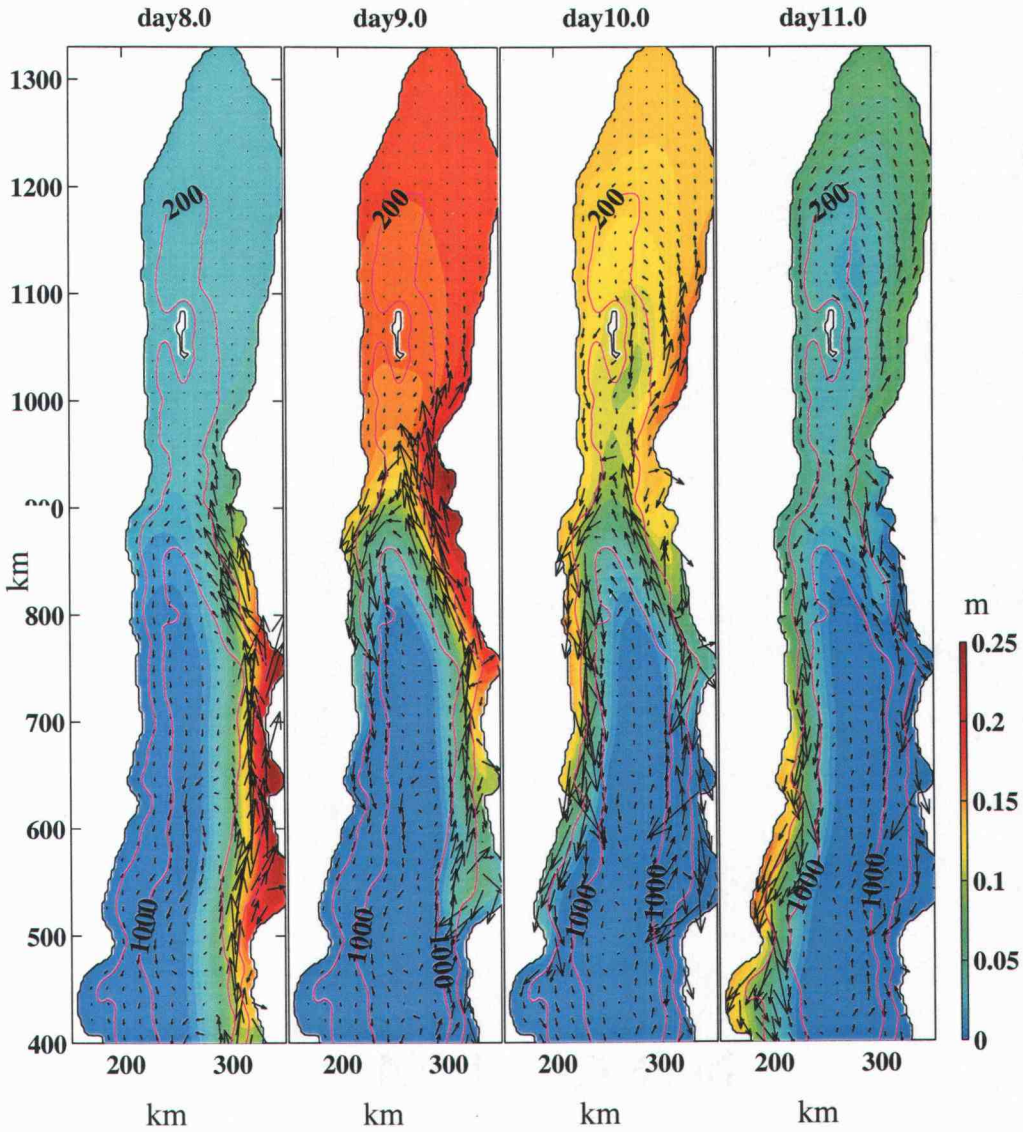

Figure 4.8: Depth-averaged velocity vectors and sea level (color) on days 8-11 for an elevation ICTW with amplitude 30 cm and time scale of 4 days.

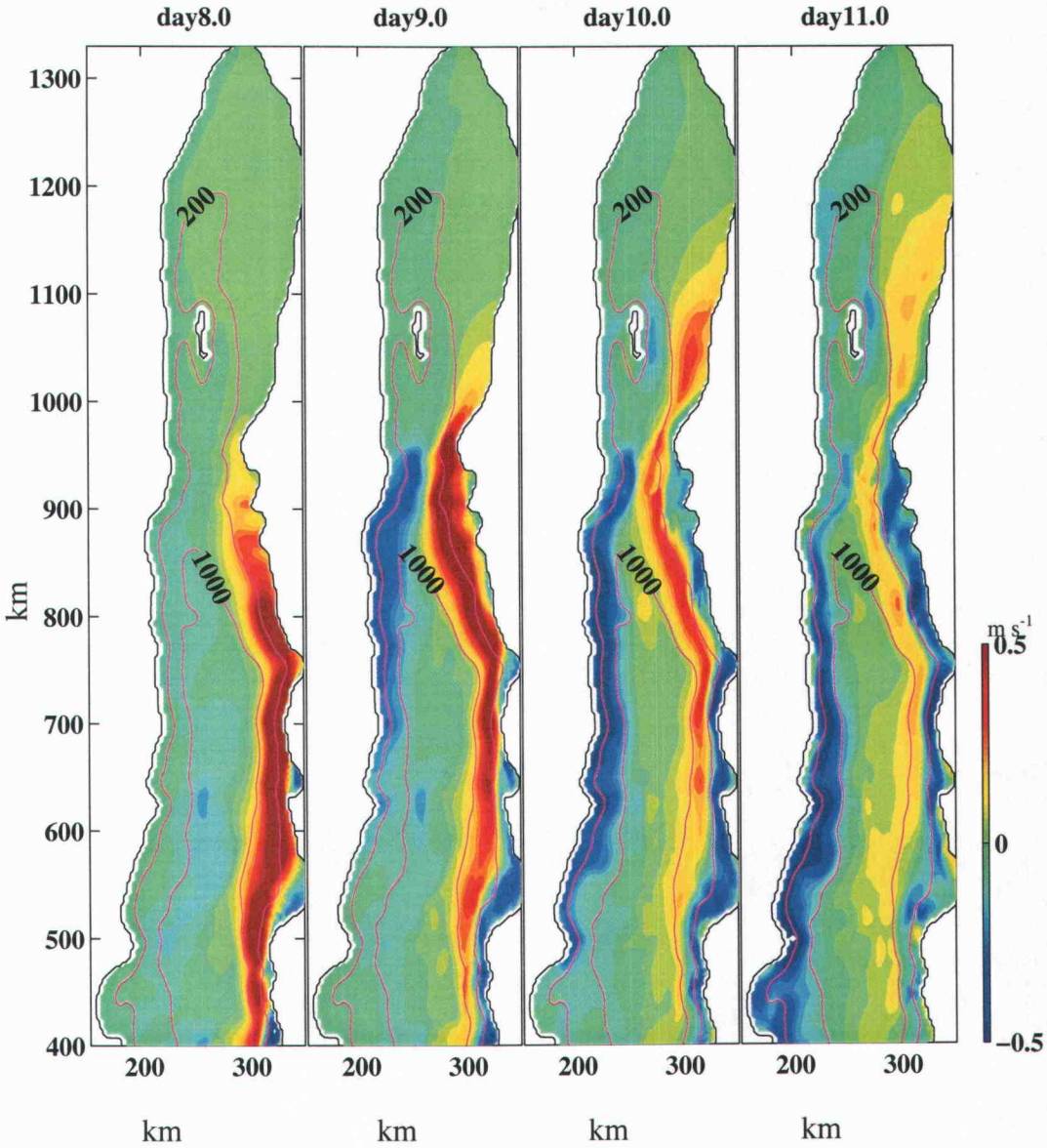

Figure 4.9: Fields of the along-gulf depth-averaged velocity for the same experiment and days as in Figure 4.8.

weakened signals along the west side of the gulf. The time-averaged kinetic energy balance of the depth-averaged velocities, integrated over depth and in the across gulf direction, (Fig. 4.10) shows that the flux of energy into the gulf is balanced mainly by dissipation due to bottom friction. Total dissipation due to bottom friction is very uniform from the south gulf to the sill. Both energy flux and bottom dissipation are small north of the sill, showing that a very small fraction of the ICTW enters the north gulf. At the sill, kinetic energy flux and bottom dissipation are relatively large, and bottom dissipation values are the highest along the gulf. The kinetic energy density balance (i.e. the integrated kinetic energy balance divided by the volume of the across-gulf section) (Fig. 4.10) shows that at the sill, as the gulf narrows and the depth decreases from 2000 m to 400 m the energy flux density increases. This intensified flux of energy is balanced by bottom dissipation. No significant increase in either the total dissipation or the dissipation per unit volume is observed in the north gulf for ICTWs with different amplitudes and time scales.

4.5. Nonlinear effects

Storm generated disturbances along the coast of Mexico have been observed propagating northward over long distances (Enfield and Allen, 1983). The signals appear as isolated waves of elevation with amplitudes of 20 cm or more. In

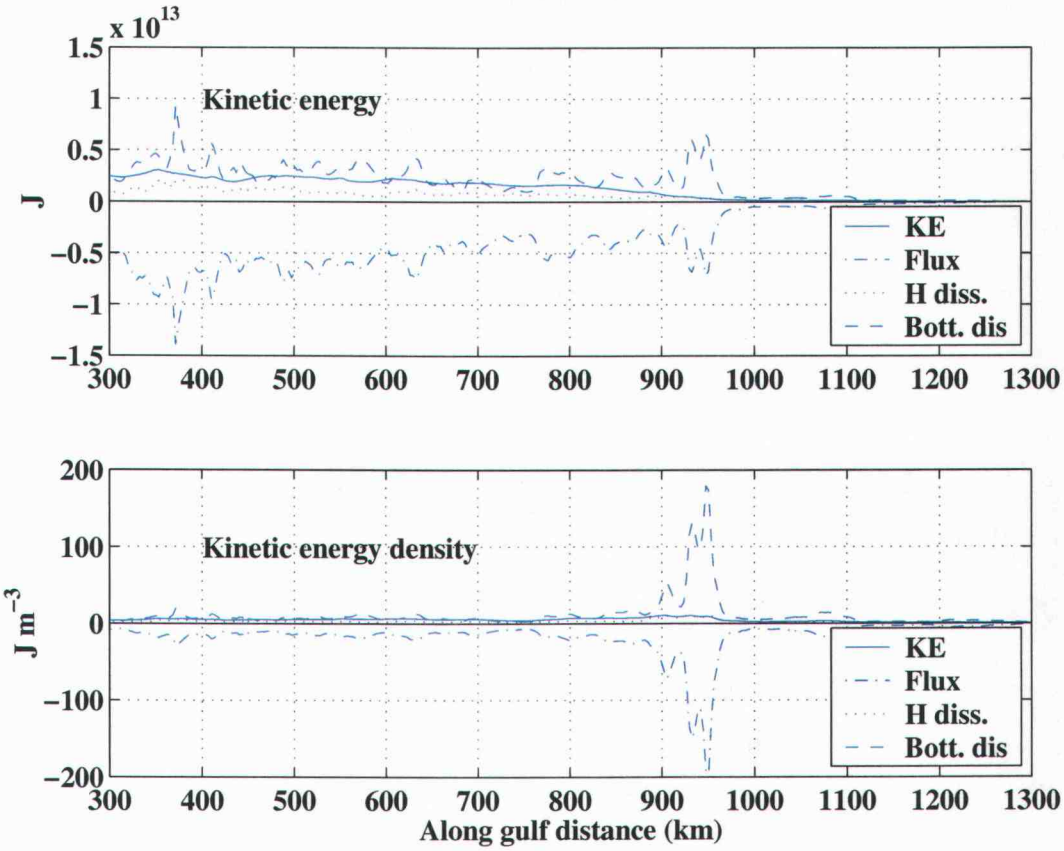

Figure 4.10: Time-averaged kinetic energy balance of the depth-averaged velocities, integrated over depth and in the across-gulf direction, $T^{-1}\Delta y\int(\varphi)dxdzdt$, where φ represents the terms (time derivative, flux, dissipation due to horizontal friction, dissipation due to bottom friction) in the equation for the kinetic energy of the depth-averaged velocity. In the bottom panel, the terms are divided by the volume to give the volume average kinetic energy balance, $(\Delta y\, T\int dxdz)^{-1}\Delta y\int(\varphi)dxdzdt$. Note the flux term includes all terms not associated with the time derivative, horizontal diffusion or bottom friction.

contrast, depression waves generated during winter in the neighborhood of the Gulf of Tehuantepec on the south Pacific coast (16° N) of Mexico do not seem to propagate northward as non-dispersive signals. The relative longevity of elevation waves suggest a wave evolution governed by Korteweg-de Vries (KdV) type dynamics with weak nonlinear effects balanced by dispersion. Theoretical models for weakly nonlinear barotropic shelf waves have been formulated by Smith (1972) and Grimshaw (1977). These models show that nonlinear solitary waves may exist for across-shelf mode 1 as waves of sea level elevation, but not as waves of depression. A formulation for nonlinear stratified CTWs is included in Mitsudera and Grimshaw (1990), although the emphasis there is on resonant forcing of mode 2 by topographic features. Nonlinear effects could be in part responsible for some inconsistencies between observed seasonal changes in propagation speed for free waves and the phase speed predicted by linear theory (Enfield and Allen, 1983).

4.5.1. Wave steepening

In these numerical experiments we find a dependence of the phase speed on the amplitude of the incident wave as discussed in Section 3.a. The phase speed of the sea level signal increases linearly with the amplitude of the wave (Fig. 4.3). The phase speed of the velocity signal also increases with amplitude for depression waves, but for elevation waves the phase speed does not appear to vary

significantly (Fig. 4.4). The dependence of CTW phase speed on incident wave amplitude is clearly seen in comparative time series of sea level (Fig. 4.11). As the signals propagate the crests of the waves of different initial amplitudes separate in time, such that at y=675 the crest of the largest elevation wave leads the crest of the largest depression wave by 2 days. Large elevation waves steepen at the front while the depression waves steepen of the tail.

As found in section 3a, the alongshore velocity shows some behavior not seen in the sea level signals. The dependence of the phase speed on the amplitude found from sea level is also evident in the alongshore component of the velocity (Fig. 4.12). As in the sea level signals, elevation waves, with positive alongshore velocity (V>0) on the east side and negative (V<0) on the west side, preserve the initial shape of the incident wave better than depression waves. Dispersive effects behind the main wave are evident in the velocity signal. Waves with a given sign generate a secondary wave behind with an opposite sign. The sea level amplitude of the secondary wave is small compared to the amplitude of the main wave (Fig. 4.11), but the magnitude of alongshore velocity (V) of the secondary wave is comparable to the velocity associated with the main wave (Fig. 4.12) at y=744 and 924 km. As the wave propagates northward some steepening in velocity occurs at the front (tail) of elevation (depression) waves. The sea level amplitudes of depression waves decrease 50% or more while they propagate along the east side (Fig. 4.11), while elevation waves do not change amplitude significantly there. On the west side, elevation waves decrease in amplitude by 30%, while there is no

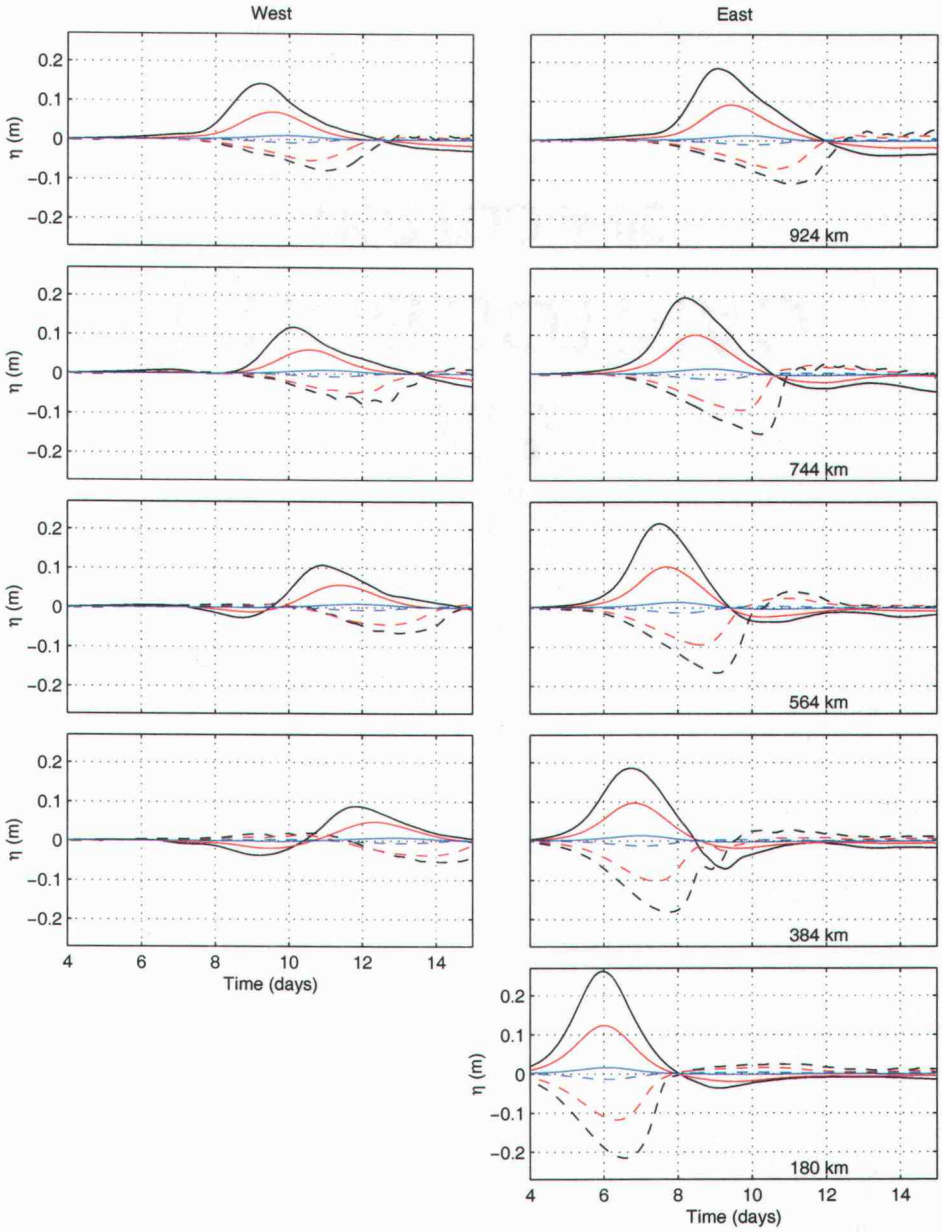

Figure 4.11: Time series of sea level along the 100 m isobath at different locations along the gulf from the east (right) and from the west side (left). Each curve represents a different experiment (total 6) where the amplitude of the incident wave is varied. The time scale for all experiments is 4 days. The initial amplitudes are ±30 cm, ±16 cm, and ±2 cm.

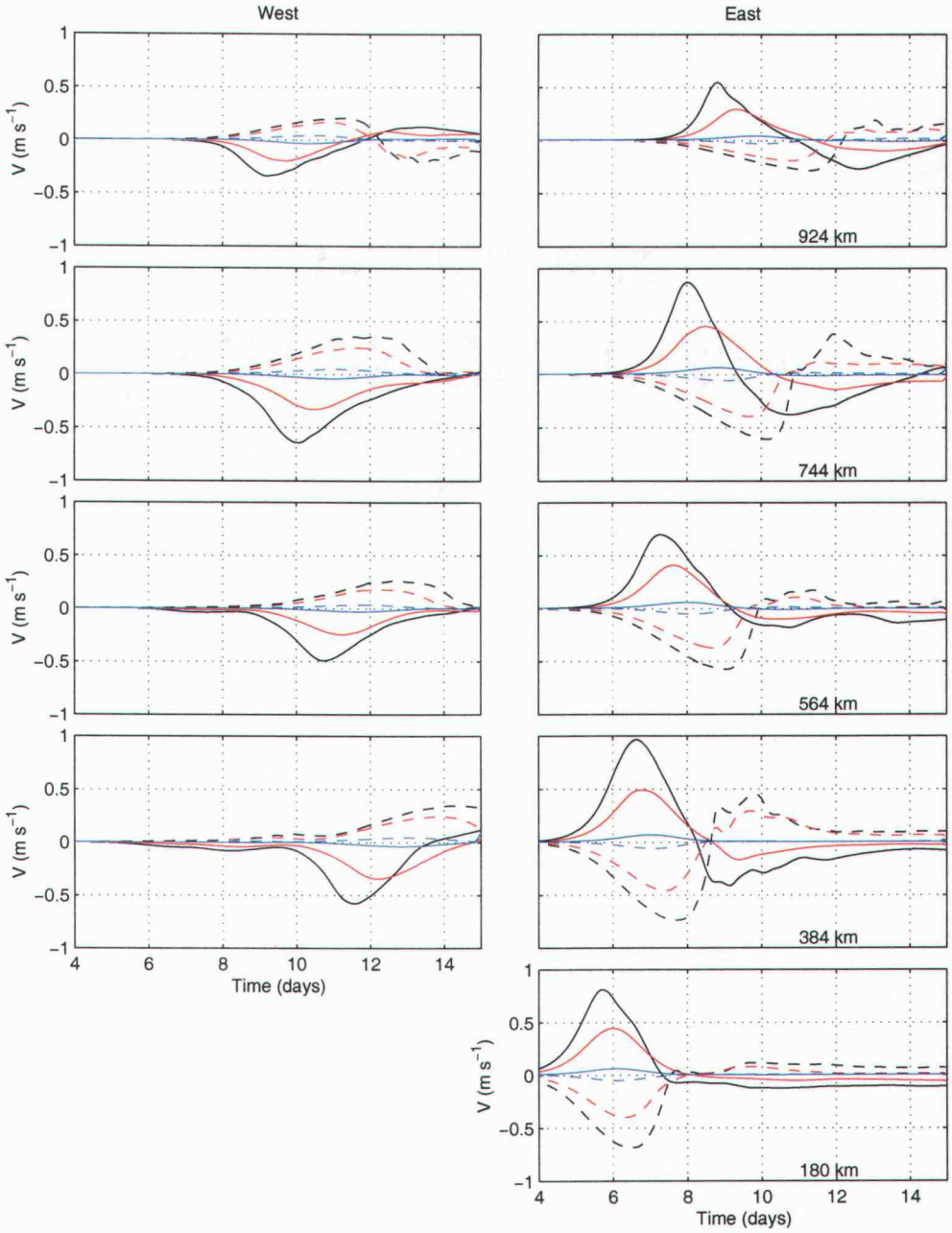

Figure 4.12: Same as Fig. 11 for the depth-averaged velocity.

noticeable amplitude change in depression waves. As found in sea level, the initial shape and velocity amplitude is better conserved for elevation waves.

It is interesting to compare the time series of sea level and along-gulf velocity of the CTWs in Fig. 4.11 and 4.12 with time series for the depths of isopycnals shown in Fig. 4.13. Elevation waves produce a sinking of isopycnals while depression waves produce isopycnal rising. The vertical displacements are larger below 50 m for both elevation and depression ICTWs. Note that the gradients that develop in the isopycnal depths are considerably stronger than those in sea level. Depression waves steepen at the tail. Behind the tail higher frequency disturbances seem to be generated, but the leading part of the wave shape is not highly distorted. The elevation wave also generates high frequency disturbances as the crest passes y=384 km. It appears that as the elevation wave propagates to y=564 km the high frequency disturbances weaken and the isopycnal displacements vary more smoothly. Subsequently at y=744 km the wave appears to be steepening again and generating additional high frequency fluctuations.

The relative importance of the nonlinear terms in the alongshore momentum balance is highly dependent on the amplitude of the incident wave. We find for large amplitude waves that the nonlinear advection terms can be appreciable and, for elevation waves, can be one of the dominant terms. Time series of terms in the depth-averaged along-gulf momentum balance at five locations on the 200 m isobath along the east side of the gulf for elevation and depression ICTWs of amplitude ±30 cm are shown in Fig. 4.14. Before the ICTW enters the gulf (y=180

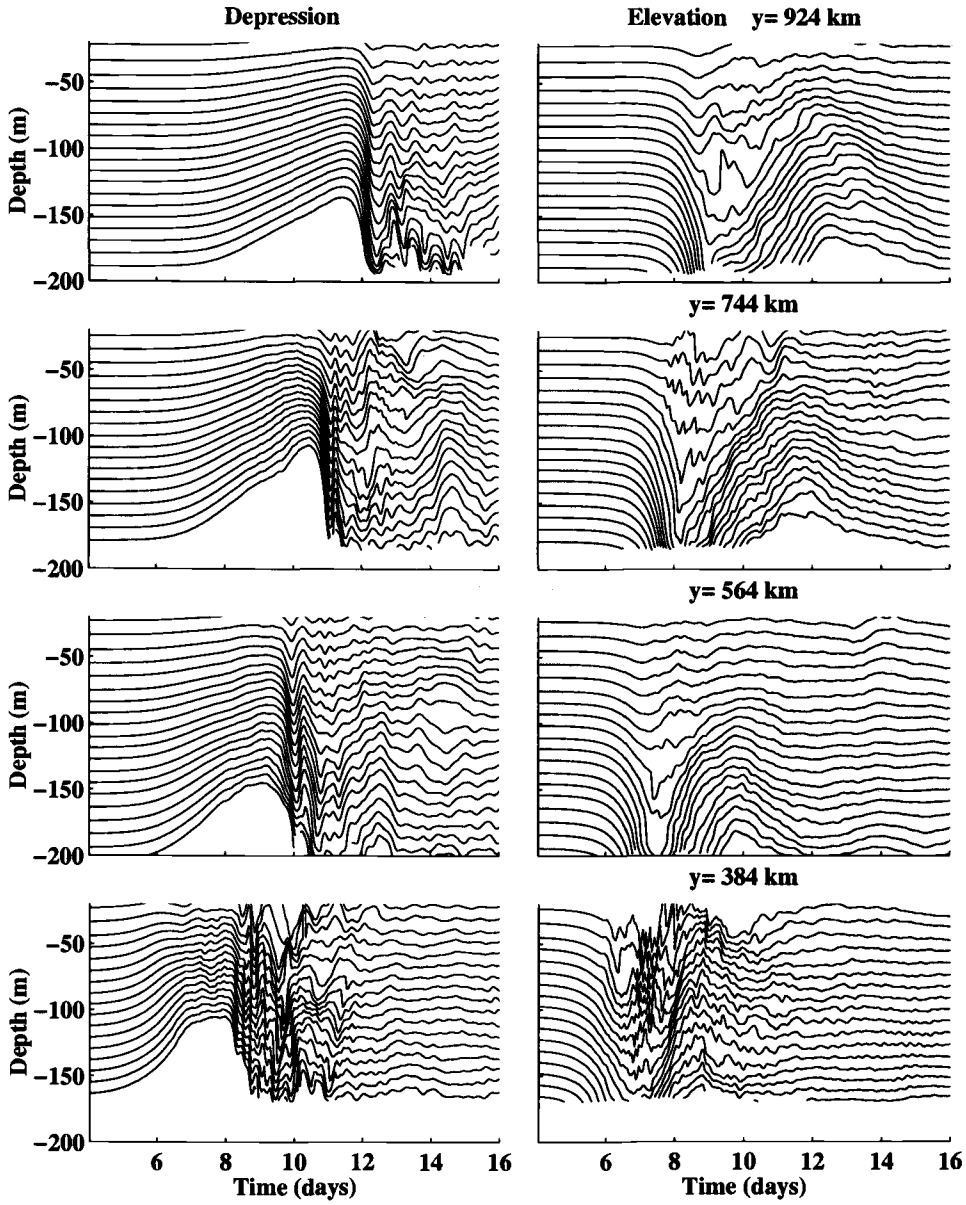

Figure 4.13: Time series of isopycnals depths along the 200 m isobath on the east side. The panels on the right are for a 30 cm elevation wave and the panels on the left are for a -30 cm depression wave at the same values of y. The time scale of the wave is 4 days. The isopycnals have a uniform distribution of initial depth as shown for small time at y=924 km.

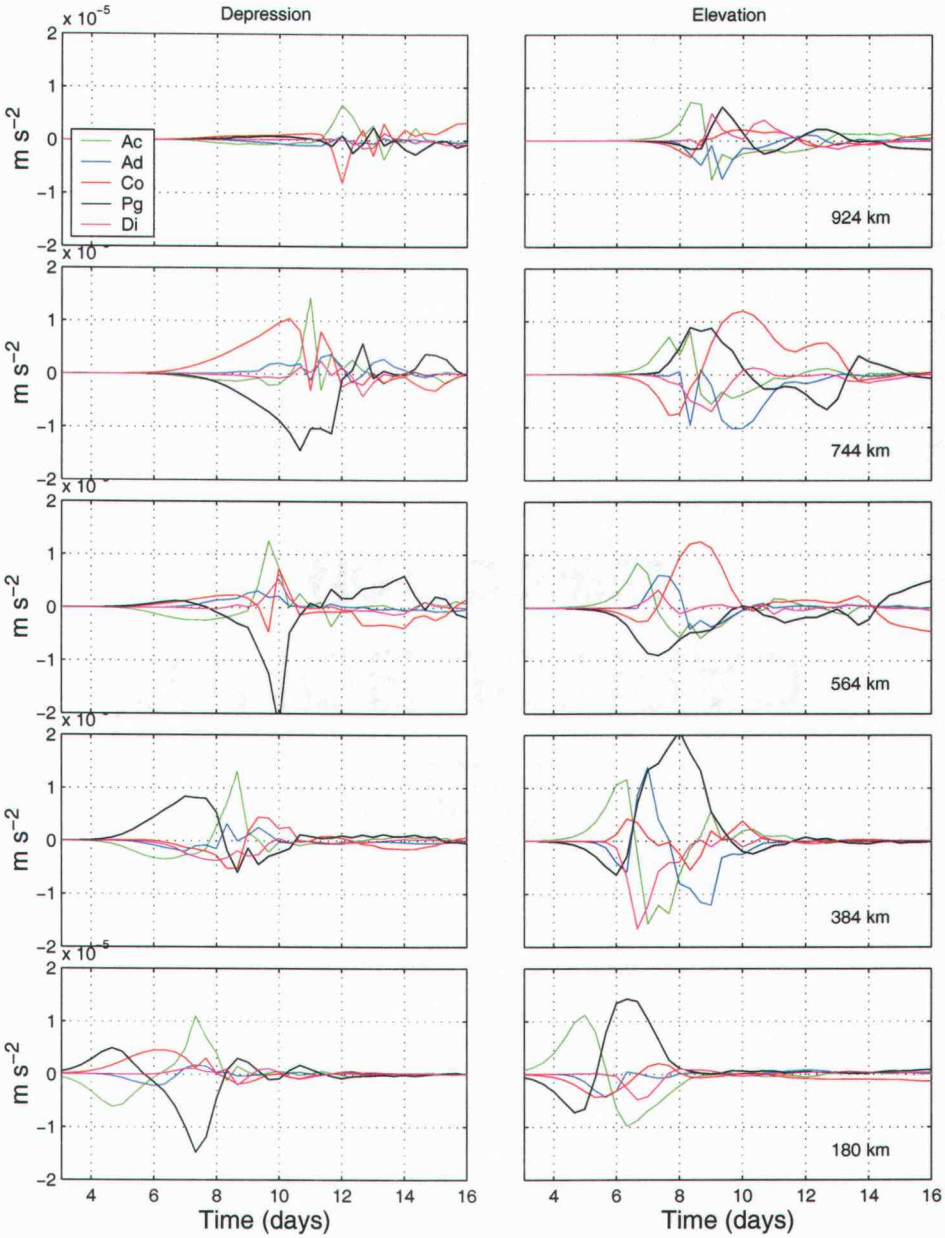

Figure 4.14: Time series of terms in the depth-averaged along-gulf momentum equation at six locations on the 100 m isobath along the east side of the gulf. The panels on the right are for a 30 cm elevation wave and the panels on the left are for a -30 cm depression wave at the same values of y. The lower panels are from a location (y=180 km) south of the entrance to the gulf which is at y=300 km. The sill begins at y=828 km. Ac-acceleration, Ad-advection, Co-Coriolis, Pg-pressure gradient, and Di-diffusion terms.

km), nonlinear terms are non-negligible but are relatively small compared to the acceleration, the Coriolis force and the pressure gradient terms for both elevation and depression waves. Interestingly, at y=180 km the nonlinear terms have the same sign in both the elevation and the depression wave, while the signs of the other terms are reversed. After the elevation ICTW enters the gulf (y=384 km) nonlinear advection becomes one of the dominant terms and it remains large for all y locations to y=924 km. In contrast, for the depression ICTW the nonlinear terms remain at about the same small relative magnitude in the gulf as at y=180 km. Significant nonlinear effects are found for waves with sea level amplitudes of 20 cm or larger. For medium amplitude ICTWs (≈15 cm), nonlinear advective effects occasionally make a significant contribution to the balance, but are not as large as the other terms.

4.5.2. Current separation

The contribution of nonlinear terms to the total momentum balance is dependent on the amplitude of the ICTW and on the position. Topography and coastline modify the incident wave propagation, leading to complex circulation patterns if the amplitude of the wave is large enough to develop nonlinear behavior. The evolution of the alongshore velocity component for an elevation ICTW of 30 cm

amplitude and four day period (Fig. 4.9) shows the development of nonlinear circulation patterns. An elevation ICTW is accompanied by up-gulf northward velocity fluctuations and these are clearly visible along the east side of the gulf (Figs. 8 and 9). After approximately the first half of the wave has passed y=750 km on day 9, however, a southward counter current develops next to the coast. The down-gulf southward current then propagates with the ICTW in such a way that, on day 10 at the tail of the wave, the up-gulf current associated with the ICTW is separated from the coast by a down-gulf current that resembles the offshore structure of a mode 2 depression wave. On days 10 and 11 the width of the down-gulf current increases near the sill in the region between y=800 km and 950 km. By day 11, the secondary wave on the east side has separated from the primary wave that is now propagating southward along the west side. The secondary wave on the east side seems to continue propagating northward into the north gulf with reduced phase speed and decreased up-gulf velocity.

The time mean along-gulf surface velocities for elevation waves with amplitudes 2 cm and 30 cm and time scales of 4 days are shown in Fig. 4.15. The small amplitude (2 cm) elevation wave produces a mean surface circulation with positive up-gulf currents along the east side and negative down-gulf currents along the west side. The currents along both sides are fairly uniform and contiguous to the coast. For the larger amplitude (30 cm) elevation wave, the mean surface velocity along the east side shows an up-gulf current that has separated from the coast with a down-gulf countercurrent next to the coast. Along the west side, the

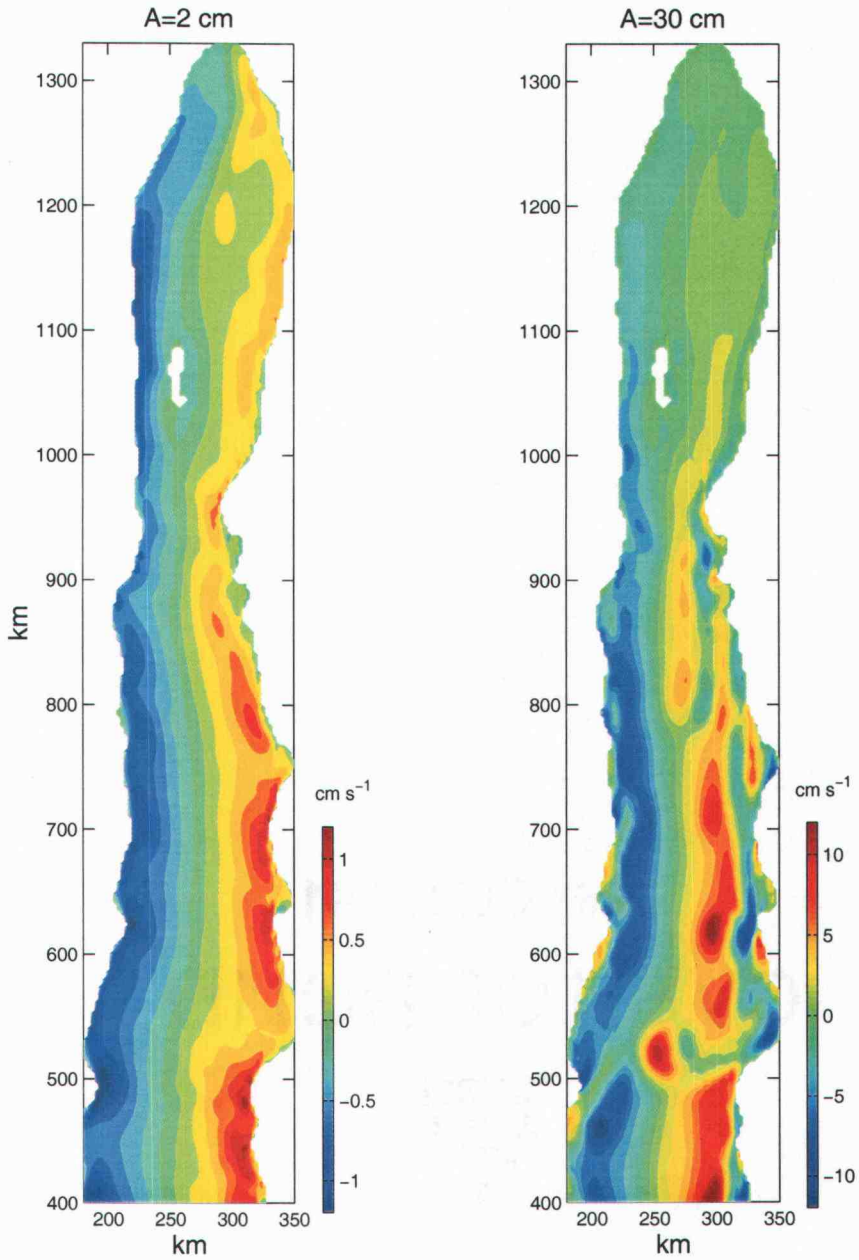

Figure 4.15: Time-mean along-gulf surface velocity for a small amplitude elevation wave of 2 cm (left) and for a large amplitude elevation wave of 30 cm (right). The incident waves have a time scale of 4 days.

separation of the down-gulf current is weaker although still present to some extent. The separation of the basic current associated with the ICTW and the development of a countercurrent adjacent to the coast was found only for elevation waves with sea level amplitudes 16 cm or larger. For small elevation waves, the mean alongshore velocity of the ICTW does not separate, even though after the wave passes there is a secondary wave with down-gulf currents next to the coast. These results suggest that many of the observed ICTWs that propagate into the gulf have the potential to develop circulation patterns similar to those shown in Fig. 4.9. This is consistent with the fact that the formation of a countercurrent and the separation of the wave tail are also observed in Part 1 with realistic forcing. On the west side, where the alongshore velocity associated with an elevation ICTW is down-gulf, weak up-gulf currents adjacent to the coast are generated (Fig. 4.9), but separation similar to that found on the east side is not observed even for large amplitude waves.

In the south on the east side, the up-gulf current associated with the incident wave seems to propagate slowly offshore at (e.g. in Fig. 4.9 at y=570 km). The offshore propagation in the south gulf of the currents associated with the ICTW wave seems to be related to the down-slope propagation observed in Part 1. It was found there that after an elevation wave passes and separation begins to take place, the separated up-gulf velocity signal propagates down-slope and settles in the deepest part of the section. The changes in the vertical and across-gulf structure of the alongshore velocity as an elevation wave passes (Fig. 4.16) shows that process

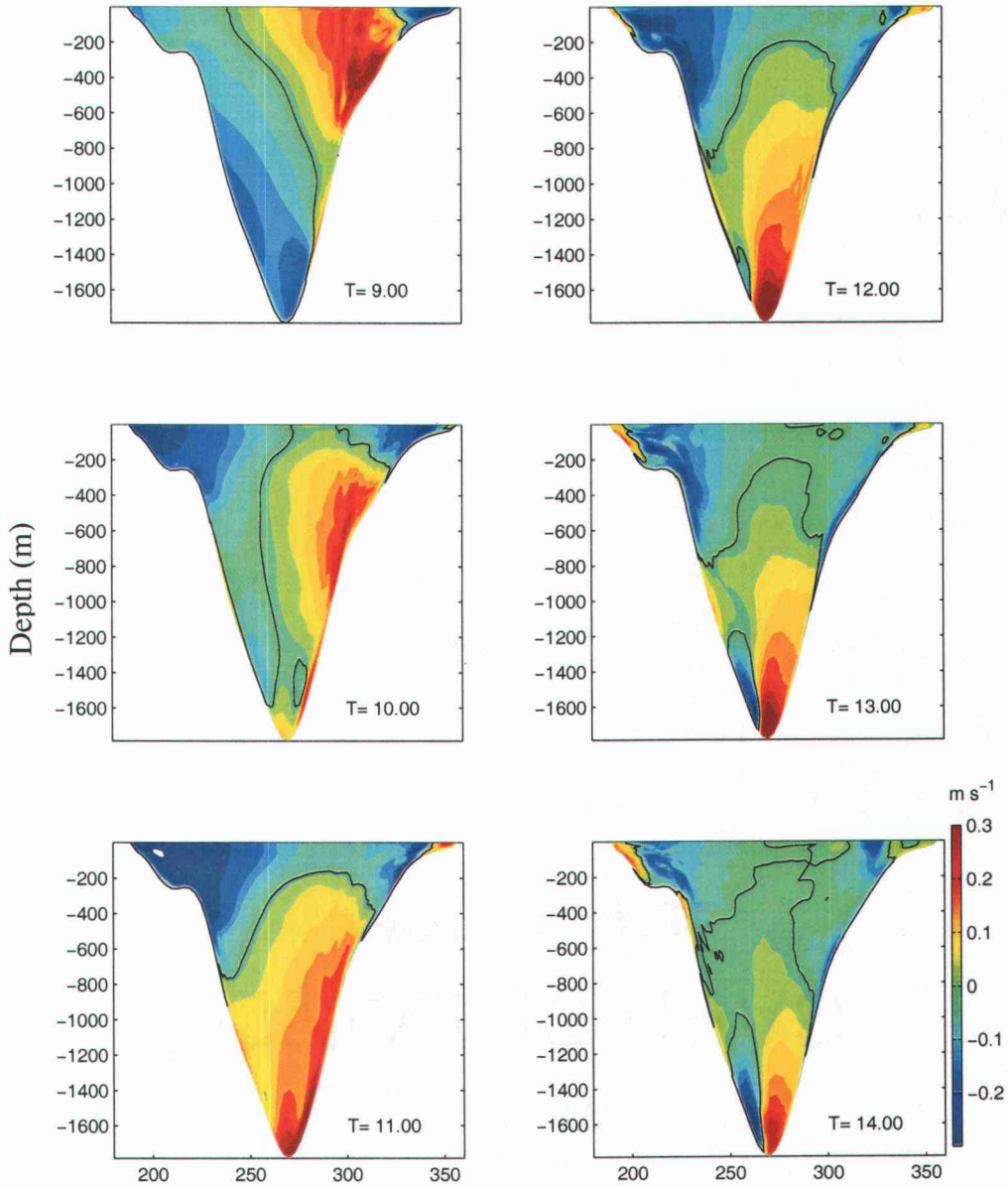

Figure 4.16: Across-gulf sections of the along-gulf velocity at y=564 km for days 9-14. The incident elevation wave has an amplitude of 30 cm and a time scale of 4 days, the same as in Fig. 8, 9 and 15. The black line is the zero contour.

here. After the up-gulf current begins to separate on day 9, it begins to propagate downward along the bottom. By day 13, the vertical average of the along-gulf velocity is very weak (Fig. 4.9), but the up-gulf current is in fact at the bottom of the section (Fig. 4.16) where it remains and gradually weakens. In Part 1, down-slope propagation that reaches the bottom is just observed along the east side of the gulf and for incident elevation waves. In this study, we confirm those observations, as down-slope propagation that reaches the bottom is not found for incident depression waves of any amplitude or time scale. Elevation waves with amplitudes bigger than 5 cm in sea level and any time scale resulted in down-slope propagation.

In an attempt to better understand the causes of the separation and of the development of the countercurrent we ran some additional numerical experiments. First, we utilized a rectangular channel with dimensions similar to the gulf and a constant depth of 1000 m forced by an incident first mode baroclinic Kelvin wave. No countercurrent or separation was observed for incident elevation waves of any amplitude. A second experiment had a constant depth of 1000 m similar to the first one, but included the actual coastline of the gulf. In this case, a narrow countercurrent was developed similar to the one shown in Fig. 4.9. As the wave passed, small anticyclonic eddies were generated in the inlets and bays and these propagated slowly westward. In two more experiments, the average across-gulf depth of the gulf was used, so that the depth was a function of the along-gulf coordinate only, in both a rectangular channel and in a channel with realistic

coastline. In both cases, the wave was strongly modified by the topography. No countercurrent or separation was observed in the experiment in the rectangular channel. The inclusion of a realistic coastline produced a narrow countercurrent and some weak eddies. Overall, the experiments indicate that separation and the formation of countercurrents is a nonlinear effect influenced by both the coastal shelf and slope topography and by irregularities in the coastline.

4.5.3. Eddy generation

One of the possible mechanisms for energy dissipation of ICTWs in the Gulf of California is the generation of mesoscale eddies (Christensen et al., 1983). Mesoscale eddies have been frequently observed in the gulf (Badan et al., 1985; Emilson and Alatorre, 1997; Pegau et al., 2002; Figueroa et al., 2002), but to our knowledge, the only other modeling study that produces eddies in the south gulf is that by Martinez and Allen (2002c) where the formation of eddies in the south gulf was found in wind-driven numerical experiments. In this study, we present some results that show eddy generation by ICTWs and we describe some of their main characteristics.

The formation of a countercurrent by an elevation ICTW was discussed in section 4b. The countercurrent flows southward down-gulf adjacent to the coast in such a way that for large amplitude waves the up-gulf currents associated with the

elevation ICTW separate from the coast. The development of the countercurrent and the separation of the tail wave are illustrated in Fig. 4.8 and 4.9. When the wave passes by inlets along the east side, the up-gulf current of the ICTW induces anticyclonic circulation inside the bay, e.g. on day 9 at y=540 m in Fig. 4.8. If the ICTW has a long time scale or large amplitude, anticyclonic eddies with length scales of 50-80 km are generated (Fig. 4.17). In addition, the circulation pattern produced by elevation waves along the east side, with an up-gulf current separated from the coast and a countercurrent adjacent to the coast (Fig. 4.9), provides strong horizontal shear conducive to the formation of anticyclonic eddies. The positions where the eddies are generated (Fig. 4.17) seem to be related to the locations of the largest variations in the coastline. The horizontal scale of the eddies is similar to that of the width of the shear zone adjacent to the coast and to the size of the coastline irregularities. Most of the eddies propagate westward at a very low speed (~3 cm s^{-1}) and are observed to last for at least 25 days after the wave passes, with maximum velocities of 20 cm s^{-1} or more. In the vertical, the signature of the eddies typically extends to 200 m and for some cases reaches 500 m depth. Depression waves do not produce separation or a countercurrent, even though a few cyclonic eddies are generated mainly in the south gulf on the west side close to La Paz. Eddies generated north of La Paz are very weak. Long waves (time scale 8 days or greater) of moderate sea level amplitude (≈16 cm) produce bigger and stronger eddies than short waves (4 days time scale) with large amplitudes (≈30 cm). The generation of eddies is also observed in the additional experiments described in

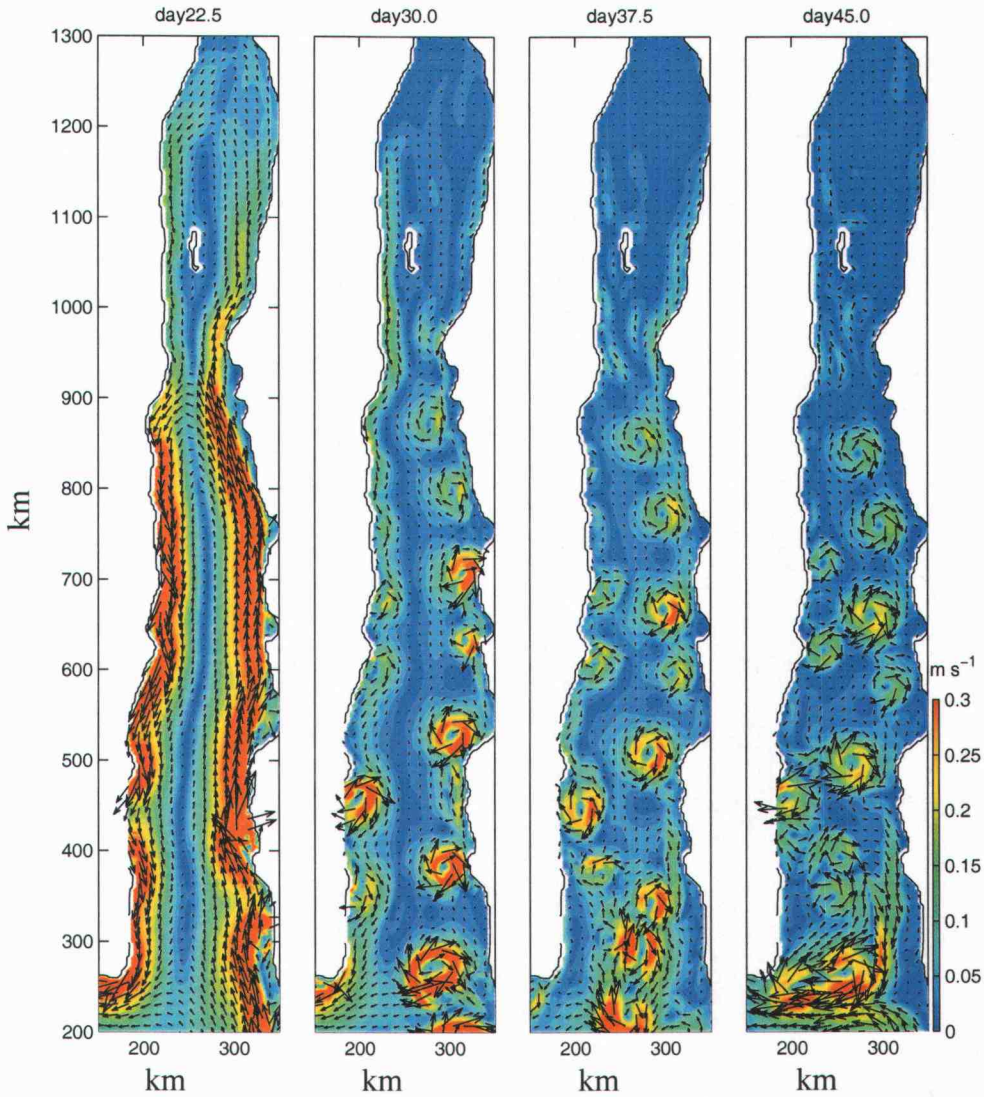

Figure 4.17: Surface velocity vectors every 7.5 days from day 22.5 to day 45. The color contours represent the magnitude of the velocity vectors (m s^{-1}). The incident wave has a sea level amplitude of 16 cm and a time scale of 16 days.

section 4b, where we utilize a flat bottom in a rectangular channel or with a realistic coastline. In the rectangular channel, the formation of eddies is observed only on the west side near the tip of the Baja California peninsula. When the real coastline is included, the formation of anticyclonic eddies along the east side is also observed.

4.5.4. Density balance

In Part 1 it was found that incident CTWs are energetic enough to generate a time mean distribution of kinetic energy along the gulf that is similar in magnitude to that forced by the wind (Martinez and Allen, 2002c). Some of the energy of the incident waves is used to redistribute water masses. Similar to Part 1, we examine the resulting density balance by calculating the across-gulf and vertical integrals of every term in the density equation as in Martinez and Allen (2002a). The results for an experiment with an elevation ICTW of amplitude 16 cm and period four days are plotted in Fig. 4.18. Elevation ICTWs have mean up-gulf northward surface velocities on the east side and weaker down-gulf southward velocities on the west side (Fig. 4.15), effectively pumping lower density surface water into the gulf. After the wave exits, the mean density anomaly integrated in (x,z) is negative everywhere except in the northern gulf, producing a net warming along the gulf (Fig. 4.18). The density flux is positive (down-gulf) everywhere,

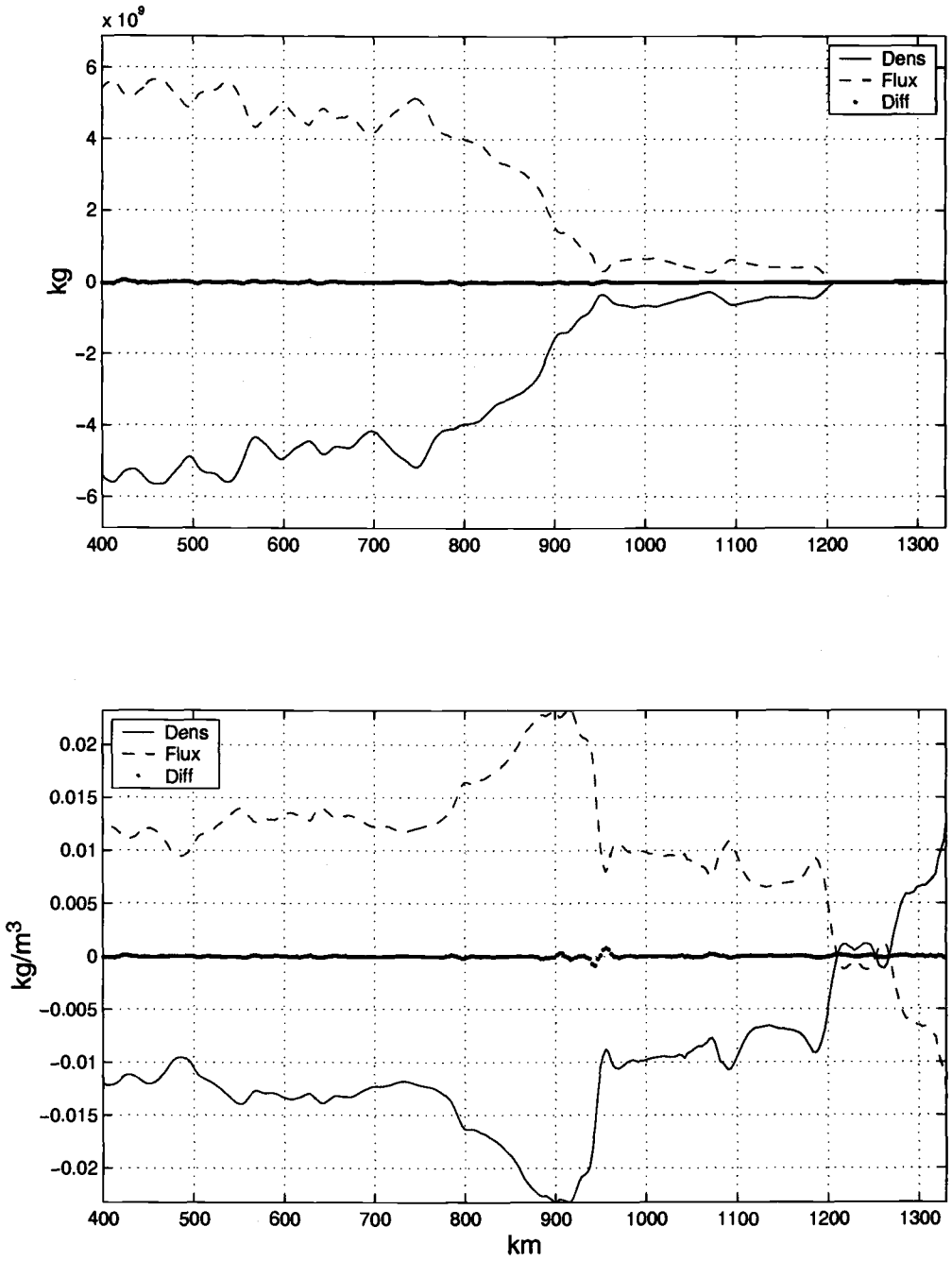

Figure 4.18: The along-gulf distribution of the balance of density integrated in the x-z direction along a section of width Δy. The solid line represents the change in density relative to the initial value; negative values indicate sections where density has been decreased. The dashed line is the flux of density and the dotted line is the diffusion of density.

decreasing to the north. The mean density anomaly per volume shows a very uniform distribution north and south of the sill. On the sill the density anomaly per volume has the largest magnitude, indicative of stronger fluxes developed by the changing topography. A depression wave has a similar distribution with the signs reversed and is not shown. The realistic forcing in Part 1 produces a combination of the results obtained with single elevation or depression ICTWs. The density anomaly is negative south of the sill and positive to the north changing sign on the sill (y=920 km). This indicates a dominance of the density flux by elevation waves in the south.

4.6. Summary

A three-dimensional primitive equation circulation model with realistic topography and stratification is used to investigate the propagation of baroclinic coastal-trapped waves (CTWs) in the Gulf of California. The behavior of idealized single incident wave disturbances with different amplitudes and time scales is examined. The numerical results are consistent with the results in Part 1 and provide new information about the evolution of CTWs in the gulf. As found in Part 1, an incident CTW enters the gulf and propagates northward along the east side of the south gulf with no significant changes in propagation characeristics. At the sill, the wave splits and most of the wave energy is steered so that it propagates

southward down-gulf along the west side. Only a small fraction of the wave energy enters the shallow north gulf where two types of behavior are found: 1) a relatively slow disturbance, with a clear but weak velocity signal that is consistent with a trapped wave, propagates northward along the east coast and eventually dissipates in the far north, 2) a very fast sea level signal propagates and spreads over the entire northern region.

Sea level near the entrance of the gulf (Topolobampo) is well correlated (>0.9) with sea level everywhere inside the gulf (Fig. 4.2 and Fig. 4.3). Velocity correlations between Topolobampo and locations around the gulf decrease as the wave propagates. The ratio of maximum sea level amplitudes and velocity magnitudes for the waves exiting the gulf compared to those for the incident waves is larger for elevation than for depression waves (Fig. 4.5). Most of the bottom dissipation takes place at the sill (Fig. 4.10). No significant bottom dissipation was found in the north gulf region for any amplitude or time scale of the ICTW.

Incident waves with realistic amplitudes exhibit several nonlinear properties. The propagation velocity is amplitude dependent and waves with large, but realistic, amplitudes steepen. Larger amplitude waves have faster propagation velocities. A large negative amplitude depression wave takes almost two more days to propagate from Topolobampo to La Paz than a large positive amplitude elevation wave (Fig. 4.4). Steepening of the wave is observed in sea level and in velocity. In general, time series of sea level signals are relatively smooth (Fig. 4.11) and are not strong indicators of the nonlinear processes that take place. Along-gulf velocity

time series are a somewhat better indicator of nonlinear processes, for example, steepening is a little more evident in the alongshore velocity signal (Fig. 4.12). The strongest indicators of wave steepening are given by time series of the vertical displacement of isopycnals (Fig. 4.13). For example, as a large amplitude elevation wave propagates, the isopycnal slopes increase, some higher frequency fluctuations are generated, and the slopes decrease before increasing again (Fig. 4.13). This behavior suggests that as the wave steepens and nonlinear terms become significant, partial breaking takes place and energy is dissipated smoothing the wave.

Large amplitude elevation waves generate a down-gulf countercurrent adjacent to the coast. The countercurrent is strong enough to separate the up-gulf current in the tail of the wave from the coast (Fig. 4.15). After the wave passes, the circulation consists of a down-gulf current next to the coast and an up-gulf current offshore adjacent to the down-gulf current (Fig. 4.9). The up-gulf current slowly separates from the coast and propagates offshore and vertically downward along the bottom (Fig. 4.16). Variable coastline, shelf-slope topography, and nonlinear effects are required for the separation to take place.

Coastal-trapped waves with long time scales, or large amplitude waves of any time scale, generate eddies along the coast. The eddies have scales of 50-80 km and typically extend vertically to depths of 150 to 500 m. Elevation waves generate anticyclonic eddies, while depression waves produce cyclonic eddies. Elevation waves produce a larger number of eddies than similar amplitude depression waves.

After the wave passes, the eddies are observed to last at least 25 days. No eddy formation was observed north of the sill (Fig. 4.17).

Coastal sea level observations show large amplitude elevation waves entering the gulf. Depression waves are in general smaller. Single elevation waves in these experiments produce a density decrease along the gulf while depression waves increase the density (Fig. 4.18). The results in Part 1 suggest that in the north gulf density is increased because depression waves dominate over elevation waves even though elevation waves have larger amplitude. South of the sill, however, elevation waves dominate the density flux and density is decreased.

4.7. Acknowledgments.

This research was supported by the Office of Naval Research (ONR) Coastal Dynamics Program through Grant N00014-93-1-1301. In addition, A.M. was partially supported by a Fulbright-LASPAU scholarship and by the Facultad de Ciencias Marinas UABC. The use of computational resources (CM500e's) provided by the College of Oceanic and Atmospheric Sciences and facilitated by ONR grant N00014-99-1-0040 and by NSF grant OCE-952095b (both to A. Bennett) was indispensable for the completion of this research and is gratefully acknowledged. We thank M. Merrifield and C. Winant for providing the velocity and bottom pressure measurements described in Merrifield and Winant (1989). The

authors also thank C. Vandetta and T. Leach for assistance with computer use and P. Newberger for initial help with the POM model.

Chapter 5

Summary

Numerical experiments are utilized to study the wind-driven mesoscale circulation in the Gulf of California in chapter 1. The model is forced by satellite-derived winds that have important spatial and temporal variability (Fig. 2.3, 2.4) not included in previous modeling studies of the gulf. The resulting circulation driven by the satellite-derived winds is dominated by the presence of several eddies of alternating sign along the south gulf (Fig. 2.8). Cyclonic eddies are more energetic than anticyclonic eddies. The horizontal scale of the eddies is similar to the width of the gulf, the order of 100 km. In the vertical, the eddies extend to depths of 1000 m. The position and the horizontal and vertical scales correspond well with the eddies observed by Figueroa et al (2002) in the southern gulf. Near the coast along both sides and in most of the north gulf, the circulation is wind driven and has high variability (Fig. 2.8 and 2.9). Off the coast, in the interior, the velocity fluctuations are characterized by lower variability and are poorly correlated with the wind (Fig. 2.8). The temporal mean surface circulation consists of southward down-gulf currents along the coast on both sides with larger magnitude currents along the west side. Under cyclonic eddies there is a northward up-gulf current 800 m deep along the east side and a southward down-gulf current with a similar extent in depth along the west side. In the vicinity of anticyclonic

eddies the circulation is more complex, with southward down-gulf currents on both sides, and a nortward up-gulf current at the center of the gulf that has baroclinic vertical structure and southward flow at depth. The temporal mean across-gulf averaged, along-gulf circulation can be described as a three layer system similar to the observation-based description given by Bray (1988a). The upper layer has a depth of about 60m and flows southward down-gulf (Fig. 2.17). An intermediate layer with a vertical extent that increases from 100 m in the north to 300 m in the south, flows northward up-gulf. Below the intermediate layer the lower layer extends to 1000 m depth with weak southward down-gulf flow.

The relatively large mean southward surface currents along both sides appear to have strong effects on the mean distribution of relative vorticity. Positive relative vorticity at the surface seems to be produced along the west side (Fig. 2.15), and to extend into the interior in the vicinity of cyclonic eddies. Negative vorticity values are significant near anticyclonic eddies and seem to be connected to the east coast. The local Rossby number indicates that nonlinear advective processes are significant along the coast and in the vicinity of eddies in the south gulf. An inverse relation is found in the along-gulf variations of the time mean, across-gulf averaged, potential and kinetic energies in the neighborhood of the eddies which suggests that conversion processes are associated with the presence of the eddies (Fig. 2.21).

Regions of relatively high values of turbulent kinetic energy q^2 ($\approx 10^{-4} cm^2 s^{-2}$) are found in the interior away from the boundary layers and from the coast near

the center of the gulf at depths 350-500 m (Fig. 2.23) and seem to be closely related to low values of the Richardson number *Ri*. The vertical shear in the across-gulf velocity is generally larger than that in the along-gulf velocity. High values of q^2 are found more frequently where the vorticity is negative, and appear to be related to the concentrations of near inertial wave energy.

In our numerical experiments we found that the circulation in the gulf is sensitive to the specification of the Coriolis parameter. These results are discussed in the appendix. In the experiments with constant Coriolis parameter f (EXP3) the circulation is more energetic than that found in the corresponding experiment with variable f (EXP2). There are no well-developed anticyclonic eddies in the central gulf with constant f and the scale of the cyclonic eddies is larger. This demonstrates that even though the gulf is relatively narrow in the east-west direction, the variation of f has an important effect on the circulation.

The propagation of remotely forced CTWs in the Gulf of California is investigated in chapter 3 and 4 using a three-dimensional primitive equation model. The evolution in the gulf of an incident CTW mode 1 with realistic time-dependent amplitude is studied for 80 days during summer 1984. The correlation between model variables and observations is reasonably good for sea level, but lower for currents. The favorable agreement between model and observations supports the importance of remote forcing in the Gulf of California. With the absence of flows produced by other forcing mechanisms, the model does not adequately represent the observed decrease in correlation of sea level fluctuations from a station at the

entrance of the gulf with sea level at other stations in the central gulf, particularly at Santa Rosalia. Incident waves propagate northward along the east side in the south gulf. At the sill, the CTWs are steered and split into two waves (Fig. 3.8). The wave that enters the north gulf contains just a small fraction of the total incident energy (<20%) and is dissipated (Fig. 3.11). The other wave turns and propagates southward along the west side with its energy appreciable reduced (Fig. 3.11 and 3.12). Although eddies are generated, the characteristics of the propagation are not significantly altered by the eddy generation. Some energy is scattered into down-slope propagating disturbances (Fig. 3.14). For elevation waves these disturbances produce relatively intense bottom currents. For depression waves, the down-slope propagating signal is weaker and more rapidly dissipated.

Nonlinear effects are found to be important for CTWs with large, but realistic amplitudes. Nonlinear advection is important in the term balance for the alongshore depth-integrated momentum equation in the large amplitude waves. Large amplitude CTWs steepen as they propagate northward along the east side of the gulf (Fig. 3.15). Some energy is lost through the generation of high frequency disturbances which appear to decrease the steepening. CTWs are also able to redistribute properties. In particular the density field is modified by the incident CTWs. The density of the water in the north is increased while that in the south is decreased (Fig. 3.17). North of the sill the mean integrated kinetic energy produced by the CTWs is small compared to that in the south, as most of the incident wave energy turns at the sill and propagates southward along the west side. The mean

integrated external kinetic energy along the west side in the south gulf is significantly reduced compared to that found in the incident waves along the east side. The CTWs that leave the gulf at the southwest corner have only a small fraction of the incident wave energy.

A primitive equation three-dimensional circulation model with realistic topography and stratification is used in chapter 4 to investigate the propagation of baroclinic coastal-trapped waves (CTWs) in the Gulf of California. The behavior of idealized single incident wave disturbances with different amplitudes and time scales is examined separately. The numerical results are consistent with the results in chapter 3 and provide new information about the evolution of CTWs in the gulf. As found in chapter 3, an incident CTW enters the gulf and propagate northward along the east side of the south gulf with no significant changes. At the sill, the wave splits and most of the wave energy is steered so that it propagates southward down-gulf along the west side. Only a small fraction of the wave energy enters the shallow north gulf where two types of behavior are found: 1) a relatively slow disturbance, with a clear but weak velocity signal that is consistent with a trapped wave, propagates northward along the east coast and eventually dissipates in the far north, 2) a very fast sea level signal that propagates and spreads over the entire northern region.

Sea level at the entrance of the gulf (Topolobampo) is well correlated (>0.9) with sea level everywhere inside the gulf (Fig. 4.2 and Fig. 4.3). Velocity correlations between Topolobampo and locations around the gulf decrease as the

wave propagates. The ratio of maximum sea level amplitudes and velocity magnitudes between the wave exiting the gulf and the incident wave is larger for elevation than for depression waves (Fig. 4.5). Most of the bottom dissipation takes place at the sill (Fig. 4.10). No significant bottom dissipation was found in the north gulf region for any amplitude or time scale of the ICTW.

Incident waves with realistic amplitudes exhibit several nonlinear properties. The propagation velocity is amplitude dependent and waves with large, but realistic, amplitudes steepen. Large amplitude waves have faster propagation velocity. A large amplitude depression wave takes almost two more days to propagate from Topolobampo to La Paz than a large amplitude elevation wave (Fig. 4.4). Steepening of the wave is observed in sea level and in velocity. In general, time series of sea level signals are relatively smooth (Fig. 4.11) and are not strong indicators of the nonlinear processes that take place. Velocity time series are a better indicator of nonlinear processes, for example, steepening is more evident in the alongshore velocity signal (Fig. 4.12). The strongest indicators of wave steepening are given by time series of the vertical displacement of isopycnals similar to those shown in Chapter 3. As the wave propagates, the isopycnal slope increases, some higher frequency fluctuations are generated and the slopes decrease before increasing again. Similar behavior is observed in the nonlinear advection terms in the vertically averaged alongshore momentum equation (Fig. 4.13). This behavior suggests that as the wave steepens and nonlinear terms become significant, partial breaking takes place and energy is dissipated smoothing the

wave. Large amplitude elevation waves generate a down-gulf countercurrent adjacent to the coast. The countercurrent is strong enough to separate the up-gulf current in the tail of the wave from the coast (Fig. 4.14). After the wave passes, the circulation consists of a down-gulf current next to the coast and an up-gulf current offshore adjacent to the down-gulf current (Fig. 4.9). The up-gulf current slowly separates from the coast and propagates offshore and vertically downward along the bottom (Fig. 4.15). Variable coastline, shelf-slope, topography, and nonlinear effects are required for the separation to take place.

Coastal-trapped waves with long time scales, or large amplitude waves of any time scale, generate eddies along the coast. The eddies have scales of 50-80 km and typically extend vertically to depths of 150 to 500 m. Elevation waves generate anticyclonic eddies, while depression waves produce cyclonic eddies. Elevation waves produce a bigger number of eddies than similar amplitude depression waves. After the wave passes, the eddies are observed to last at least 25 days. No eddy formation was observed north of the sill (Fig. 4.16).

Coastal sea level observations show large amplitude elevation waves entering the gulf. Depression waves are in general smaller. Single elevation waves in these experiments produce a density decrease along the gulf (Fig. 4.17) while depression waves increase the density. The results in Chapter 3 suggest that in the north gulf density is increased because depression waves dominate over elevation waves even though elevation waves have larger amplitude. South of the sill, however, elevation waves dominate the density flux and density is decreased.

BIBLIOGRAPHY

Allen, J. S., P. A. Newberger, and J. Frederiuk, 1995. Upwelling circulation on the Oregon continental shelf. Part 1; Response to idealized wind forcing. *J. Phys. Ocean.* **25**, 1843-1866.

Argote, M. L., A. Amador, L. F. Lavin, and J. R. Hunter, 1995. Tidal dissipation and stratification in the Gulf of California. *J. Geophys. Res.*, **100** (C8), 16103-16118.

Badan-Dangon, A., C. J. Koblinsky, and T. Baumgartner, 1985. Spring and summer in the Gulf of California: Observations of surface thermal patterns. *Oceanol. Acta*, 8, 13-22.

Beier, E., 1997. A numerical investigation of the annual variability in the Gulf of California. *J. Phys. Ocean.*, **27**, 615-632.

Beier, E. and P. Ripa, 1999. Seasonal eddies in the northern Gulf of California. *J. Phys. Ocean.*, **29**, 302-311.

Blumberg, A. F., and G. L. Mellor, 1987. A description of a three-dimensional coastal ocean circulation model. Three-Dimensional Coastal Ocean Models, Vol. **4**, N. Heaps, Ed., *Amer. Geophys. Union*, 1-16.

Bray N. A., 1988a. Thermohaline Circulation in the Gulf of California. *J. Geophys. Res.*, **93**, 4993-5020.

Bray N. A., 1988b. Water Mass Formation in the Gulf of California. *J. Geophys. Res.*, **93**, 9223-9240.

Brink, K. H., and D. C. Chapman, 1987. Programs for computing properties of coastal-trapped waves and wind-driven motions over the continental shelf and slope, 2d ed., WHOI Tech. Rep. 87-24, Woods Hole Oceanographic Institution, Woods Hole, MA., 119 pp.

Brink, K. H., 1989. Energy conservation in coastal-trapped wave calculations. *J. Phys. Ocean.*, **19**, 1011-1016.

Carbajal, N., 1993. Modeling of the circulation in the Gulf of California. Ph. D. Thesis, *Institute fur Meerskunde.* Hamburg, 186 pp.

Castro, R., M. F. Lavin, and P. Ripa, 1994. Seasonal heat balance in the Gulf of California. *J. Geophys. Res.*, **99**, 3249-3261.

Christensen., N., Jr., R de la Paz, and G. Gutierrez, 1983. A study of sub-inertial waves off the west coast of Mexico. *Deep-Sea Res.*, **30,** 835-850.

Emilsson, I., and M. A. Alatorre, 1997. Evidencias de un remolino ciclónico de mesoescala en la parte sur del Golfo de California. Contribuciones a la Oceanografía Física en México. Mon. 3. Unión Geofísica Mexicana.

Enfield, D. B., and J. S. Allen, 1983. The generation and propagation of sea level variability along the Pacific coast of Mexico. *J. Phys. Oc*ean., **13**, 1012-1033.

Figueroa, J. M., S. G. Marinone, and M. F. Lavin, 2002. Geostrophic eddies in the southern Gulf of California. Submitted to *Ciencias Marinas.*

Frederiuk, J., and J. S. Allen, 1996. Model studies of near-inertial waves in flows over the Oregon continental shelf. *J. Phys. Oc*ean., **26**, 2053-2075.

Gjevik, B., and M. A. Merrifield, 1993. Shelf sea response to tropical storms along the west coast of Mexico. *Contin. Shelf Res.*, **13**, 25-47.

Gregg, M. C., D. P. Winkel, and T. B. Sanford, 1993. Varieties of Fully Resolved Spectra of Vertical Shear. *J. Phys. Oc*ean., **23**, 124-141.

Grijalva, N., 1972. Tidal computation in the Gulf of California, *Geofísica Internacional*, **12**, 113-34.

Grimshaw, R., 1977. Nonlinear aspects of long shelf waves. Geophys. Astrophys. Fluid Dyn., **8,** 3-16.

Hendershott, M. C., and A. Speranza, 1971.Co-oscillating tides in long narrow bays; the Taylor problem revisited. *Deep-Sea Re*s., **18**, 959-980.

Holland, W. R., D. E. Harrison, and A. J. Semtner, Jr., 1983. Eddy-resolving Numerical Models of Large-Scale Ocean Circulation. In Eddies in Marine Science, edited by A. R. Robinson, pp. 379-403, Springer-Verlag, Berlin Heidelberg.

Kundu, P. K., 1976. Ekman veering observed near the ocean bottom. *J. Phys. Oc*ean., **6**, 238-242.

Kunze, E., 1985. Near-inertial wave propagation in geostrophic shear. *J. Phys. Ocean.*, **15**, 544-565.

Kunze, E., and T. B. Sanford, 1986. Near-inertial wave interactions with mean flow and bottom topography near Caryn seamount. *J. Phys. Ocean.*, **16**, 109-120.

Lavin, M. F., R. Durazo, E. Palacios, M. L. Argote, and L. Carrillo, 1997. Lagrangian observations of the circulation in the northern Gulf of California. *J. Phys. Ocean.*, **27**, 2298-2305.

Lueck, R., and T. Osborn, 1986. The dissipation of kinetic energy in a warm-core ring. *J. Geophys. Res.*, **91** (C1), 803-818.

Martinez, J. A., and J. S. Allen, 2002a. A modeling study of coastal-trapped wave propagation in the Gulf of California. Part 1, response to remote forcing. Submitted to *J. Phys. Ocean.*.

Martinez, J. A., and J. S. Allen, 2002b. A modeling study of coastal-trapped wave propagation in the Gulf of California. Part 2, response to idealized forcing. Submitted to *J. Phys. Ocean*.

Martinez, J. A., and J. S. Allen, 2002c. A modeling study of the atmospherically-forced mesoscale circulation in the Gulf of California. Submitted to *J. Phys. Ocean.*.

Mellor, G. L., 1991. User's Guide for a three Dimensional Primitive Equation, Numerical Ocean Model. Prog. In Atmos. And Ocean. Sci. 35 pp., Princeton University, Princeton, N. J.

Merrifield, M. A., and C. D. Winant, 1989. Shelf Circulation in the Gulf of California: A description of the variability, *J. Geophys. Res.*, **94** (C12), 18133-18160.

Merrifield, M. A., 1992. A comparison of long coastal-trapped wave theory with remote-storm-generated wave events in the Gulf of California. *J. Phys. Ocean.*, **22**, 5-18.

Milliff, R. F., W. G. Large, J. Morzel, G. Danabasoglu, and T. M. Chin, 1999. Ocean general circulation model sensitivity to forcing from scatterometer winds. *J. Geophys. Res.*, **104,** 11337-11358.

Mitsudera, H., and R. Grimshaw, 1990. Resonant forcing of Coastally trapped waves in a continuously stratified ocean. PAGEOPH, **133**, 635-664.

Oey, L.-Y., 1996. Simulation of Mesoscale Variability in the Gulf of Mexico: Sensitivity Studies, Comparison with Observations, and Trapped Wave Propagation. *J. Phys. Ocean.*, **26**, 145-175.

Palacios-Hernández, E., E. Beier, M. F. Lavin, and P. Ripa, 2001. The effect of the winter mixing on the circulation of the Northern Gulf of California. *J. Phys. Ocean.*, (in press).

Pegau, W. S., E. Boss, and A. Martinez, 2002. Ocean color observations of eddies in the Gulf of California during the summer. *Geophys. Res. Letters* (in press).

Petruncio, E. T., 1996. Observations and modeling of the internal tide in a submarine canyon. Ph. D. thesis. Naval Postgraduate school, Monterey, California.

Pollard, R. T., and R. C. Millard, Jr., 1970. Comparison between observed and simulated wind-generated inertial oscillations. *Deep-Sea Res.*, **17**, 813-821.

Ramp, S. R., J. McClean, C. A. Collins, A. J. Semtner, and K. A. S. Hays, 1997. Observations and modeling of the 1991-92 El Niño signal off central California. *J. Geophys. Res.*, **102** (C3), 5553-5582.

Ripa, P., 1990. Seasonal Circulation in the Gulf of California Ann. Geophys., **8**, 559-564.

Ripa, P., 1997. Towards a physical explanation of the seasonal dynamics and thermodynamics of the Gulf of California. *J. Phys. Ocean.*, **27**, 597-614.

Romea, R. D., and J. S. Allen, 1983. On vertically propagating coastal Kelvin waves at low latitudes. *J. Phys. Ocean.*, **13**, 1241-1254.

Smith, R., 1972. Nonlinear Kelvin and continental shelf waves. J. Fluid Mech., **52**, 379-391.

Spillane, M. C., D. B. Enfield, and J. S. Allen, 1987. Intraseasonal oscillations in sea level along the west coast of the Americas. *J. Phys. Ocean.*, **17**, 313-325.

Wang, D. P., 1991. Generation and propagation of inertial waves in the subtropical front. *J. Mar. Res.*, **49**, 619-633

Wilkin, J. L., and D. C. Chapman, 1990. Scattering of coastal-trapped waves by irregularities in coastline and topography. *J. Phys. Ocean.*, **20**, 396-421.